International Journal of Advances in Telecommunications Electrotechnics, Signals and Systems

a publication of the International Science and Engineering Society

Vol. 5, No. 3
2016

ISSN: 1805-5443

www.ijates.org

I J A T E S²

International Journal of Advances in Telecommunications Electrotechnics, Signals and Systems

a publication of the International Science and Engineering Society

Vol. 5, No. 3, 2016 ISSN: 1805-5443

Aims and Scope

The International Journal of Advances in Telecommunications, Electronics, Signals and Systems (IJATES²) is an all-electronic international scientific journal with the aim to bring the most recent and unpublished research and development results in the area of electronics to the scientific and technical societies, and is supported by the ISES (International Science and Engineering Society, o.s.). The journal's scope covers all the aspects of telecommunication, signal processing, theory and design of circuits and systems for electronics.

The IJATES² is ready to publish experimental and theoretical full papers and letters submitted by prospective authors. Paper submitted for publication must be written in English and must follow a prescribed format. All papers are subjected to a critical peer-review prior to publication.

The IJATES² is an open access journal which means that all content is freely available without charge to the user or his/her institution. Users are allowed to read, download, copy, distribute, print, search, or link to the full texts of the articles in this journal without asking prior permission from the publisher or the author. This journal provides immediate open access to its content on the principle that making research freely available to the public supports a greater global exchange of knowledge.

www.ijates.org

CONTENTS

Vol. 5, No. 3, 2016 ISSN: 1805-5443

Performance Evaluation of AIC Technique for Single and Multiple Primary Bands in OFDM based Cognitive Radios

Gh. Rasool Begh, and Ajaz Hussain Mir

***Abstract*—Cognitive radio has emerged as an efficient approach to address the problem of spectrum under-utilization. OFDM has been proposed as a potential candidate for the physical layer of cognitive radios due to its inherent characteristics of spectrum shaping, spectrum analysis and robustness to frequency selective fading. One of the major problems of OFDM is high Out Of Band Radiation (OOBR). This is an undesired phenomenon especially if the nearby band is occupied by primary (or licensed) user. Among the proposed techniques to overcome this problem, Active Interference Cancellation (AIC) is considered to be one of the efficient techniques. In this paper, we evaluate the performance of this technique for single and multiple primary bands in OFDM based cognitive radios. For the case of single primary band, it is shown through simulations that narrower primary bands and use of more number of cancellation carriers increases the OOBR reduction in the desired band. For the case of multiple primary bands, the AIC technique is shown to provide better OOBR reduction for larger inter primary band spacing, lesser number of primary bands and more number of cancellation carriers. We also evaluate the bandwidth efficiency for single and multiple primary bands. The bandwidth efficiency shows a linear decrease with the increase in number of cancellation carriers. Multiple primary band system has more bandwidth efficiency degradation than the single primary band system.**

***Keywords*—Cognitive Radio, OFDM, Out of Band Radiation, bandwidth efficiency.**

I. Introduction

Cognitive radio (CR) allows unlicensed users access to the licensed spectrum, provided they do not cause interference to the licensed primary users (PU) [1], [2]. The unlicensed users are termed as secondary users (SUs) and the licensed users are termed as primary users in the CR context. The secondary users need to sense the spectrum opportunities, called spectrum holes [3], for transmission. These spectrum holes can be used by the secondary users, provided they don't interfere with the primary user transmissions. To avoid interference to the PUs, the SUs should use efficient spectrum shaping techniques. OFDM provides excellent spectrum shaping features, owing to the orthognal properties of its subcarriers [4]. For example, in the simplest case, the subcarriers coinciding with the PU band can be deactivated during SU transmission, to prevent interference to the PU transmissions [4]. However, even after deactivating the subcarriers coinciding with the PU band, appreciable interference power is present in the PU band, due to high Out Of Band Radiation (OOBR) problem of the OFDM [4], [5]. To minimize the OOBR, a number of techniques have been proposed in the literature [6], [7] . These include time windowing [5], [8], Subcarrier Weighting (SW) [9], Active Interference Cancellation (AIC) [10], Adaptive Symbol Transition (AST) [11], Constellation Expansion (CE) [12] and phase adjustment technique [13]. Time windowing and AST provide smooth transition of symbol boundaries to reduce OOBR. These however, suffer from throughput loss due to symbol time extension [5], [11]. In subcarrier weighting technique, all data tones are multiplied by an optimal set of weights to minimize the OOBR. This technique, however, suffers from degradation in the bit error rate (BER) performance due to perturbation in the data tones [9]. Further this method cannot be applied to the OFDM systems using quadrature-amplitude modulation (QAM) since the detection of QAM sysmbols will be severly affected by unknown subcarrier weights [14]. In constellation expansion technique, signal points are mapped to a higher order constellation and the mapped sequence that generates minimum OOBR is chosen for transmission. This however, degrades the error performance at the receiver, as the new signal points are closer to each other than the original signal points [12]. In active interference cancellation (AIC) technique [10], few subcarriers are reserved for transmitting signals to suppress the OOBR in the PU band. These subcarriers are termed as cancellation carriers (CCs) [15], [16]. Using AIC technique, high OOBR reduction of the order of 60-80 dB can be easily achieved in the band of interest [10]. The OOBR reduction can be increased by increasing the number of cancellation tones, but this leads to a decrease in the number of effective data tones and thereby a decrease in the system throughput. Thus there is a trade off between the OOBR reduction and the bandwidth efficiency in AIC technique.

A comparison of various OOBR reduction techniques for multicarrier systems is given in [17]. The authors compare techniques like windowing, AIC, subacrrier weighting, spectral precoding, low pass filtering and filter bank based multi-carrier (FBMC) with conventional OFDM for OOBR reduction. It is shown that FBMC techniques provide the best OOBR reduction (more than 100 dB) but at the cost of high computational complexity e.g. For an overlapping factor of 4, the complexity of FBMC exceeds that of conventional OFDM by a factor of 5. On the other hand, AIC technique offers much less OOBR reduction (around 40 dB for a total of 4 cancellation carriers), but exhibits minimum computational

G.R. Begh and A.H. Mir are with the Department of Electronics and Communication Engineering, National Institute of Technology, Srinagar, J& K, India e-mail:grbegh136@yahoo.com, ahmir@rediffmail.com

Manuscript received March 7, 2016; revised August 20, 2016.

complexity among the discussed schemes [17]. Thus AIC technique is still of interest due to its low computational complexity.

In this paper, we study the trade off between bandwidth efficiency and OOBR reduction using AIC technique. We study this problem for two different cases: Single primary band cognitive system and multiple primary band cognitive system. We mainly focus on the use of AIC technique for multiple primary bands, which has been less studied in the literature.

This paper is organized as follows. In Section 2, system description is given. Simulation results and discussion are presented in Section 3. In Section 4, we draw the conclusions from the study.

II. System Description

In this study, we consider a Cognitive radio system that employs OFDM modulation with N subcarriers. The cognitive engine is assumed to detect the band(s) occupied by the primary users. The secondary users are allowed to share the spectrum with the primary user(s) subject to the condition that the PU communication is not affected. The secondary users use AIC technique to minimize the interference to the detected PU band.

The system model is shown in Fig 1. As depicted in the figure, the input data is mapped to complex constellation stream. It is then divided into *N* sub streams using serial to parallel converter. The resulting data vector is represented by $\mathbf{X} = [X_0, X_1, X_2, .X_{N-1}]^T$, where $[.]^T$ denotes transpose operation. To modulate this data vector on *N* OFDM subcarriers, an IFFT operation is performed on **X**. The discrete time OFDM signal obtained at the output of IFFT block is represented by $\mathbf{x} = [x_0, x_1, x_2, .x_{N-1}]^T$ with x_n given as

$$x_n = \frac{1}{\sqrt{N}} \sum_{k=0}^{N-1} X_k e^{j2\pi kn/N}, \quad n = 0, 1, \ldots, N-1 \tag{1}$$

In matrix form, it can be represented as

$$\mathbf{x} = F^*_{(N\times N)}\mathbf{X} \tag{2}$$

where F is (*N*×*N*) Fourier transform matrix, whose $(n,k)^{th}$ element is given as [11]

$$F_{n,k} = \frac{1}{\sqrt{N}} e^{-j2\pi kn/N}, \quad n, k = 0, 1, \ldots, N-1 \tag{3}$$

and $(.)^*$ is the conjugate operation.

The signal is then extended in time by appending the last *G* samples of the IFFT output at the beginning of each OFDM symbol. This is termed as cyclic prefix (CP). The output after adding CP is mathematically represented as

$$\mathbf{x}^{cp} = F^*_{((N+G)\times N)}\mathbf{X} \tag{4}$$

where $F_{((N+G)\times N)}$ = [A $F_{(N\times N)}$] with *A* consisting of last *G* columns of $F_{(N\times N)}$ [16].

To evaluate the signal spectrum, the time domain signal given in equation (1) is upsampled by a factor of *M* and the resulting upsampled signal is given by [11]

$$S = F_{(MN\times(N+G))}\ \mathbf{x}^{cp} \tag{5}$$

Using (4), we have

$$S = \frac{1}{N} F_{(MN\times(N+G))} F^*_{((N+G)\times N)} X \tag{6}$$
$$= \text{QX}$$

where

$$Q = \frac{1}{N} F_{(MN\times(N+G))} F^*_{((N+G)\times N)} \tag{7}$$

Assuming that a PU band with a width of *W* subcarriers is detected within the OFDM band by the cognitive engine, the SU deactivates the subcarriers corresponding to the detected band and also reserves *c* cancellation subcarriers (CCs) on the edges of the detected PU band. The interference caused by the data subcarriers in the PU band is given by [11]

$$I_P = Q_W X_W \tag{8}$$

where Q_W consists of only those rows of *Q* that correspond to the PU band and X_W is same as *X* with the subcarriers coinciding with the PU band and the *c* cancellation subcarriers turned OFF. The interference power given in equation (8) needs to be minimized by transmitting cancellation tones over *c* subcarriers on the edges of the PU band. If h is the cancellation tone vector of length *2c*, then total interference power in the PU band is

$$P_p = \|Q_I h + I_P\|^2 \tag{9}$$

where Q_I consists of only those columns of Q_W that correspond to the cancellation subcarriers.

The total interference power in equation (9) needs to be minimized and as such forms a linear least squares problem. The solution of equation (9) given in [10] is

$$h = -(Q_I^H Q_I)^{-1} Q_I^H I_P \tag{10}$$

where $(.)^H$ denotes conjugate transpose operation.

Using (8) we get

$$h = T_I X_W \tag{11}$$

where $T_I = -(Q_I^H Q_I)^{-1} Q_I^H Q_W$.

To observe the effect of cancellation carriers on OOBR reduction, we simulate an OFDM based CR system with 128 subcarriers using BPSK symbols. The primary band is assumed to span over a width of 16 subcarriers from subcarrier #61. The weights of CCs are computed using equation 10, without any constraint. The OOBR reduction achieved using one, two and three CCs is shown in Fig. 2. For comparison, the OOBR reduction achieved using conventional OFDM technique, is also shown in the figure. It is observed from the figure that a reduction of around 35 dB is achieved using single cancellation carrier (CC) and around 65 dB is achieved for three CCs case. This is quite appreciable in comparison to 20 dB achieved in carrier nulling technique (i.e. deactivating the subcarriers in the PU band). However, as depicted in Fig. 2, computing cancellation carrier weights as an unconstrained problem, results in spectrum overshoot (e.g. around 20 dB for three CCs) in the vicinity of the PU band. To overcome this problem, the complex weights of the cancellation carriers can be computed under an upper power constraint. This leads to the following constrained optimization problem:

$$h^{op} = \arg\min_h \| Q_I h + I_P \|^2, \tag{12}$$

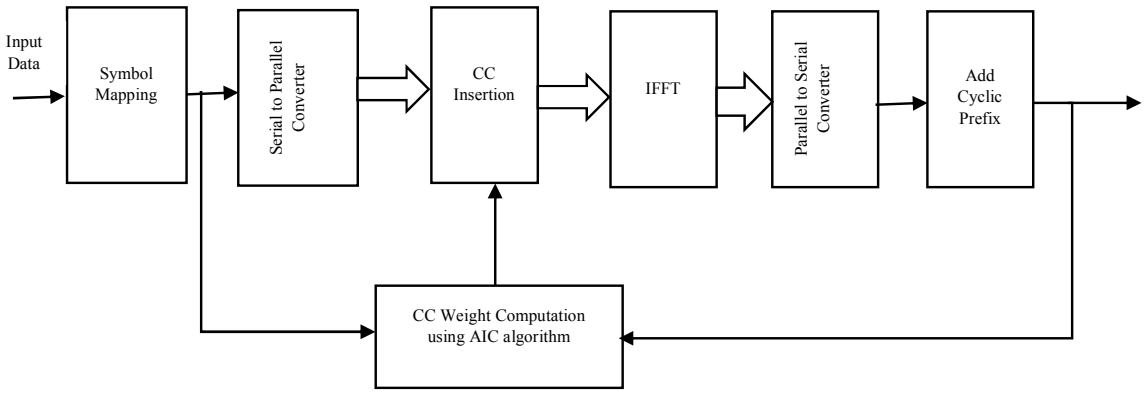

Fig. 1. Block diagram of OFDM transmitter using AIC technique for OOBR reduction

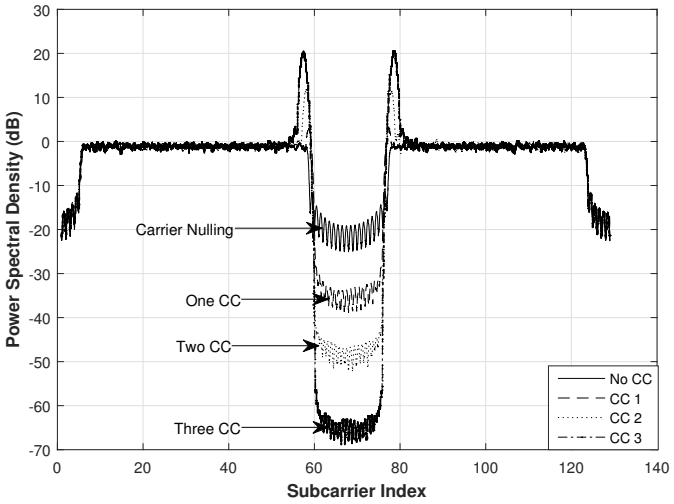

Fig. 2. OOBR Reduction using AIC technique (Unconstrained Case)

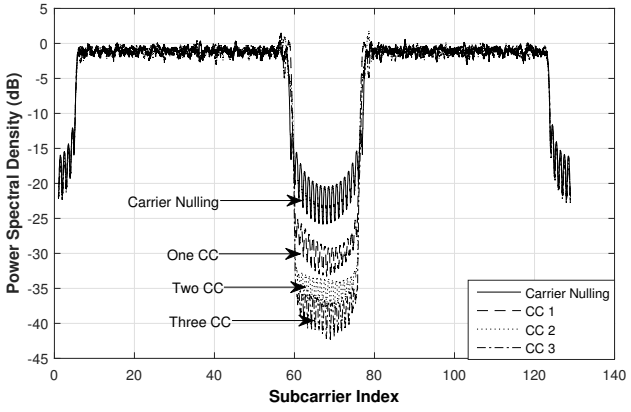

Fig. 3. OOBR Reduction using AIC technique (Constrained Case)

$$s.t. \quad |h_i|^2 \leq \alpha, \quad i = 0, 1, \ldots, 2c$$

where h^{op} represents the optimal weight vector for cancellation subcarriers with a length of $2c$ and $\alpha = E|h_i|^2$, $i = 1, 2, ...N$, is the power constraint on cancellation carriers and E represents the expectation operation. Figure 3 shows that by computing optimal weights for the cancellation tone vector, we can overcome the problem of spectrum overshoot but the overall Out Of Band Radiation (OOBR) reduction decreases in comparison to the unconstrained case of AIC technique. However, this technique still offers better reduction than the existing techniques like Adaptive symbol transition [11], Phase adjustment technique [13], windowing techniques [5], [8] and subcarrier weighting [9]. The high OOBR reduction achieved using the AIC technique forms the motivation for our study. We have considered the following two scenarios in this paper:

- Single PU band within OFDM band
- Multiple narrow PU bands within OFDM band

These scenarios are discussed in further sections of this paper.

A. Single PU band

In the single PU band case, a primary user is detected by the cognitive receiver and the secondary user (SU) refrains from transmitting in that band. To reduce the interference caused by the data subcarriers of the secondary user to the PU band, the secondary user uses AIC technique and reserves some subcarriers for interference cancellation. The amount of cancellation depends on the number of reserved subcarriers. However, increasing the number of cancellation subcarriers reduces the number of effective data subcarriers and hence reduces the bandwidth efficiency. Thus there is a trade off between OOBR reduction and bandwidth efficiency. In section III-A of the paper, we quantify this effect through simulations.

B. Multiple PU bands

In this scenario, we assume multiple narrow bands that are relatively small in comparison to the total available bandwidth of the cognitive system. This scenario is of interest, when the bandwidth of primary user is very small in comparison to the total bandwidth of the cognitive system e.g. A cognitive system can use upto three consecutive channels (18 MHz) in IEEE 802.22 standard [16]. In comparison to this cognitive system, a wireless microphone occupying a bandwidth of 200 kHz is a narrowband system. According to FCC regulations, wireless microphones can operate in both unlicensed and licensed modes [18]. When operating in licensed mode, these devices need to be protected from secondary user's transmissions. Since multiple wireless microphones can appear within

single SU band, the scenario is termed as multiple PU band scenario. To the best of our knowledge, multiple narrow PU bands scenario has not been explored much in the literature. In multiple narrow PU bands, we need to minimize interference caused by active data carriers at multiple band locations. Since in AIC technique, each PU band needs cancellation carriers at its edges, so for *M* primary bands within OFDM spectrum, we need $M * 2 * c$ cancellation carriers, where c is the number of cancellation carriers (CCs) used on each PU band edge. The effective number of data carriers available for SU's transmission, therefore reduces to $N - M*2*c - \sum_{i=1}^{M}(N_i)$ in comparison to $N - 2*c - N_P$ for single PU band case, where N_P denotes the number of subcarriers corresponding to the bandwidth occupied by PU in single band case and N_i denotes the number of subcarriers corresponding to the bandwidth occupied by i^{th} PU band. This in turn reduces the bandwidth efficiency of the cognitive system. To quantify the effect of number of CC's on bandwidth efficiency and interference reduction, simulations are performed in MATLAB. The results of these simulations are discussed in the next section.

III. SIMULATION RESULTS AND DISCUSSION

In this paper, we study the performance of Active Interference Cancellation (AIC) Technique through simulations performed in MATLAB. We assume an OFDM based Cognitive radio with 512 subcarriers. A cyclic prefix of length 64 is added to each OFDM symbol. The data subcarriers are modulated by BPSK symbols and the subcarriers in PU band(s) are deactivated. Thus the power spectral density observed in the PU band, is only due to other subcarriers and is a measure of Out Of Band Radiation (OOBR). This is termed as interference level / interference power in our study. An upsampling factor of 16 is used to find the spectrum in the PU band. The performance of the AIC technique is studied in two different scenarios.

A. Single PU band case

We consider three different widths spanning over 8,16 and 32 subcarriers, for single PU band detected within the OFDM band. The effectiveness of AIC technique in reducing the OOBR is tested by increasing the number of cancellation carriers from one to 15 on either side of the PU band. Fig. 4 shows the variation of interference level in the PU band with the number of cancellation carriers used, for different widths of the PU band. It is clear from Fig. 4 that the interference level in the PU band decreases with increase in number of cancellation carriers. However, increasing number of cancellation carriers leads to a decrease in the number of effective data carriers and hence decreases the throughput / bandwidth efficiency, thereby defeating the main objective of cognitive radios. It can also be observed from Fig. 4 that there is more reduction in narrow PU band than a wider one, if the number of cancellation carriers used is more than five. This difference is much larger for higher number of CCs used (say ten or more). This difference is attributed to the fact that the optimized weights of cancellation carriers are computed under a power constraint to overcome the spectrum overshoot near the PU band edges (as discussed in Section 2). Thus for a fixed number of cancellation carriers, interference cancellation can take place in a better manner for a narrower PU band than a wider one.

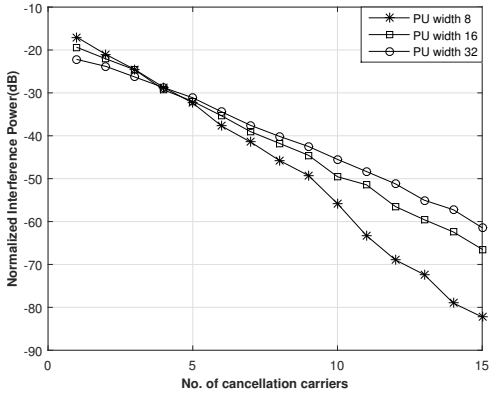

Fig. 4. Effect of number of cancellation carriers and the width of PU band on Interference power in single PU band.

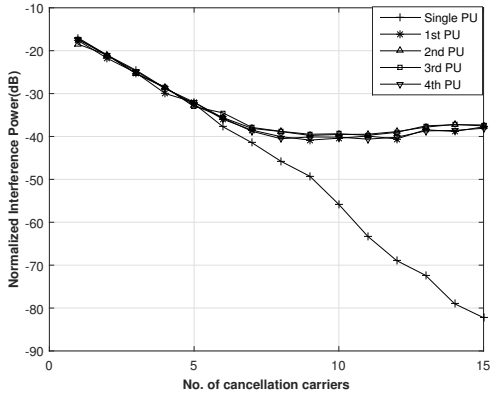

Fig. 5. Effect of number of cancellation carriers on Interference power in multiple PU bands.

B. Multiple PU bands case

In this case, we first consider 4 primary bands, separated equally from each other, and each of them spanning over a width of 8 subcarriers. Thus the total width of the multiple bands is equal to the single primary band of Section III-A. All other parameters are kept same as in single PU band case. Fig. 5 depicts a comparison of interference levels of a single PU band and each of the four multiple PU bands. It is clear that interference level in each of the multiple PU band is almost same and is thus independent of the position of detected PU band. However, the reduction in multiple PU bands is less in comparison to single PU band case especially for larger number of cancellation carriers (CC $>$10). This is attributed to the fact that increasing the number of cancellation carriers brings the CC of one PU band closer to the other PU band thereby hindering its interference cancellation capability. Further it is also observed from Fig. 5 that there is almost no improvement in interference reduction for multiple PU band case as the number of CCs is increased beyond 7.

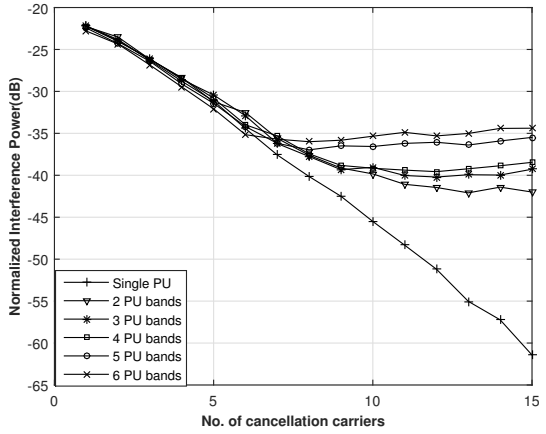

Fig. 6. Effect of number of PU bands on Interference power in multiple PU bands.

1) Effect of increasing number of PU bands: In this case, we see the variation in interference power by changing the number of detected PU bands within the OFDM spectrum. We compare the interference reduction as the number of PU bands is varied from 2 to 6. Each of these bands spans over a width of 32 subcarriers. Fig. 6 depicts a comparison of average interference power as the number PU bands is increased from 2 to 6. It is clear that the reduction of interference power in the detected PU bands decreases as the number of PU bands within OFDM spectrum increases. Thus interference cancellation behavior of AIC technique shows a decreasing trend as the number of detected PU bands increases from one to multiple PU bands. This is attributed to the fact that, increasing number of PU bands, reduces inter-PU band spacing and hence CC signals transmitted for one PU band may interfere with the other band, thereby increasing OOBR in that band.

2) Effect of inter PU band spacing: In this case, we simulate the effect of changing spacing between the detected PU bands. We consider three PU bands each of width 8 subcarriers detected within the OFDM spectrum. In this study, we have taken three inter PU band spacings-100, 75 and 50 subcarrier spacings. Effect of inter PU band spacing on interference reduction is shown in Fig. 7. It is clear from the figure that the interference reduction behaviour of AIC technique shows an upward trend as the spacing between PU bands is decreased. This is more pronounced for larger number of CCs. This can again be attributed to the fact that signals carried by CCs for one PU band cause interference to the other nearby PU bands. Thus as the inter PU band spacing is reduced, there is less suppression in the OOBR.

C. Bandwidth Efficiency

AIC technique uses *c* cancellation carriers on either side of PU band. Assuming there are *M* narrow PU bands present in the OFDM spectrum of *B* Hz, the number of effective data carriers is $N - 2M * c$. In contrast to the discussion given in section II-B, we include the subcarriers coinciding with the PU band(s), because these subcarriers are also used for data

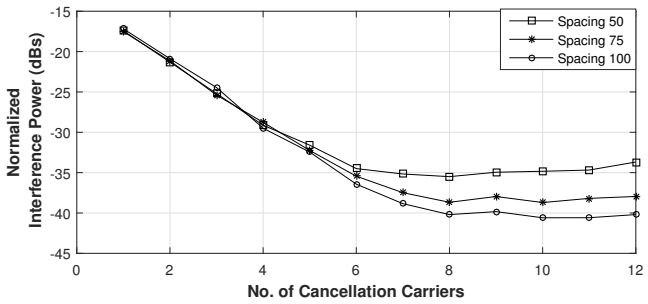

Fig. 7. Effect of inter PU band spacing on Interference power in multiple PU bands.

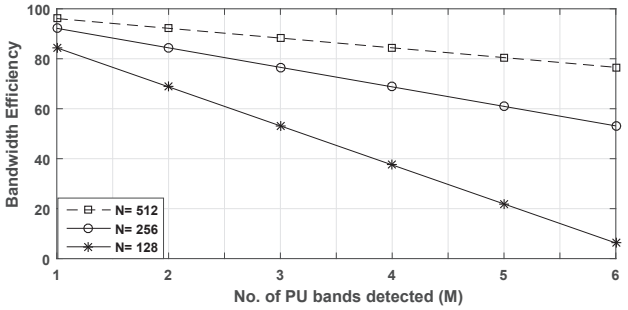

Fig. 8. Effect of number of PU bands, CCs and no. of subcarriers on bandwidth efficiency.

transmission. Thus the Useful Bandwidth for transmission is given by

$$B_u = (N - 2 * M * c) * \frac{B}{N} \tag{13}$$

where B/N is bandwidth per subcarrier. Therefore bandwidth efficiency is given by

$$\eta_b = \frac{Useful \;\; Bandwidth}{Total \;\; Available \;\; Bandwidth}$$

Using equation (13)

$$\eta_b = \{1 - \frac{(2 * M * c)}{N}\} \tag{14}$$

It is clear from Eqn (14) that the bandwidth efficiency depends on the number of PU bands, cancellation carriers and the number of subcarriers in the OFDM band. In the simulations, we fixed the number of CCs on either edge of PU band as 10. A plot of bandwidth efficiency for different values of PU bands (M) and subcarriers is shown in Fig. 8. It is clear from the Fig. 8 that there is a linear decrease in bandwidth efficiency with the number of detected PU bands. We have computed the results for three values of *N* i.e. 128, 256 & 512. It is clear from Fig. 8 that for a single PU band (i.e. $M = 1$), there is not appreciable increase in bandwidth efficiency as the value of *N* is increased from 128 to 512. Since the higher values of *N* increase the signal processing, it is better to use lower values of *N* (say $N = 128$ in our case), for single PU band. For multiple PU band case (i.e.$M > 1$) there is an appreciable increase in bandwidth efficiency in comparison to single band case ($M = 1$), especially for higher values of

M. For example, in our simulation scenario, the bandwidth efficiency increases by about 12% and 34% for $M = 1$ & $M = 2$ cases respectively, as *N* is increased from 128 to 512. This is depicted in Fig. 8. Thus for multiple PU band case, it is better to use more number of subcarriers (e.g. $N = 512$) to increase the bandwidth efficiency. This however, requires more signal processing and adds to the system complexity.

IV. Conclusion

OFDM based Cognitive radios suffer from high Out Of Band Radiation (OOBR) problem. Active interference cancellation (AIC) technique based on cancellation carriers, is one of the popular techniques to reduce OOBR. In this paper, we study the performance of this technique for single wide primary user band and multiple narrow primary user bands. For single wide primary band, the performance is compared for the cases of unconstrained and constrained computation of cancellation carrier weights. It is seen that, unconstrained computation of the weights leads to large OOBR reduction in the primary band. However, it causes spectrum overshoots in the vicinity of primary user band. A reduction of about 60dB with an overshoot of about 20 dB is obtained for three cancellation carriers on either side of PU band. Constrained computation of these weights, although removes the spectrum overshoot problem but offers much lesser reduction of about 40 dB for three cancellation carriers. Further, for single primary user band, the reduction increases with the increase in number of cancellation carriers. This however, reduces the bandwidth efficiency as the cancellation carriers do not transmit any useful data. It is also seen that OOBR reduction in wider primary bands is less in comparison to narrow primary bands for the same number of cancellation carriers. In multiple primary user bands, it is seen that much lesser reduction is achieved in comparison to the single band case for the same number of cancellation carriers. We study the effect of inter primary band spacing and the number of detected primary bands on the OOBR reduction and on the bandwidth efficiency. It is seen that there is a decrease in OOBR reduction, if the detected primary bands are closer to each other. Further it is observed that, larger the number of detected primary bands in the OFDM band, lesser is the OOBR reduction. This deterioration in performance of AIC technique for multiband case occurs due to closeness of cancellation carriers to primary bands other than their desired band. It is also observed that, there is a decrease in bandwidth efficiency with the increase in number of primary bands and with the increase in number of cancellation carriers. However, increasing the number of subcarriers in the given OFDM band has a positive effect on the bandwidth efficiency. Thus it can be used to compensate for the bandwidth efficiency loss in case of large number of primary bands but at the cost of more signal processing.

References

[1] I. F. Akyildiz, W.-Y. Lee, M. C. Vuran, and S. Mohanty, "Next generation/dynamic spectrum access/cognitive radio wireless networks: a survey," *Computer Networks*, vol. 50, no. 13, pp. 2127–2159, 2006.

[2] A. Goldsmith, *Wireless communications*. Cambridge university press, 2005.

[3] S. Haykin, "Cognitive radio: brain-empowered wireless communications," *Selected Areas in Communications, IEEE Journal on*, vol. 23, no. 2, pp. 201–220, 2005.

[4] H. Mahmoud, T. Yücek, H. Arslan *et al.*, "OFDM for cognitive radio: merits and challenges," *Wireless Communications, IEEE*, vol. 16, no. 2, pp. 6–15, 2009.

[5] T. Weiss, J. Hillenbrand, A. Krohn, and F. Jondral, "Mutual interference in ofdm-based spectrum pooling systems," in *Vehicular Technology Conference, 2004. VTC 2004-Spring. 2004 IEEE 59th*, vol. 4, May 2004, pp. 1873–1877 Vol.4.

[6] Z. You, J. Fang, and I.-T. Lu, "Out-of-band emission suppression techniques based on a generalized ofdm framework," *EURASIP Journal on Advances in Signal Processing*, vol. 2014, no. 1, pp. 1–14, 2014.

[7] X. Huang, J. A. Zhang, and Y. J. Guo, "Out-of-band emission reduction and a unified framework for precoded ofdm," *IEEE Communications Magazine*, vol. 53, no. 6, pp. 151–159, June 2015.

[8] I. Budiarjo, H. Nikookar, and L. P. Ligthart, "Cognitive radio modulation techniques," *Signal Processing Magazine, IEEE*, vol. 25, no. 6, pp. 24–34, 2008.

[9] I. Cosovic, S. Brandes, and M. Schnell, "Subcarrier weighting: a method for sidelobe suppression in ofdm systems," *Communications Letters, IEEE*, vol. 10, no. 6, pp. 444–446, 2006.

[10] H. Yamaguchi, "Active interference cancellation technique for MB-OFDM cognitive radio," in *Microwave Conference, 2004. 34th European*, vol. 2. IEEE, 2004, pp. 1105–1108.

[11] H. Mahmoud, H. Arslan *et al.*, "Sidelobe suppression in OFDM-based spectrum sharing systems using adaptive symbol transition," *Communications Letters, IEEE*, vol. 12, no. 2, pp. 133–135, 2008.

[12] S. Pagadarai, R. Rajbanshi, A. M. Wyglinski, and G. J. Minden, "Sidelobe suppression for ofdm-based cognitive radios using constellation expansion," in *Wireless Communications and Networking Conference, 2008. WCNC 2008. IEEE*. IEEE, 2008, pp. 888–893.

[13] E. H. M. Alian and P. Mitran, "A phase adjustment approach for interference reduction in ofdm-based cognitive radios," *Wireless Communications, IEEE Transactions on*, vol. 12, no. 9, pp. 4668–4679, 2013.

[14] D. Qu, Z. Wang, and T. Jiang, "Extended active interference cancellation for sidelobe suppression in cognitive radio ofdm systems with cyclic prefix," *Vehicular Technology, IEEE Transactions on*, vol. 59, no. 4, pp. 1689–1695, 2010.

[15] S. Brandes, I. Cosovic, and M. Schnell, "Reduction of out-of-band radiation in ofdm systems by insertion of cancellation carriers," *Communications Letters, IEEE*, vol. 10, no. 6, pp. 420–422, 2006.

[16] E. H. M. Alian, H. E. Saffar, and P. Mitran, "Cross-band interference reduction trade-offs in siso and miso ofdm-based cognitive radios," *Wireless Communications, IEEE Transactions on*, vol. 11, no. 7, pp. 2436–2445, 2012.

[17] W. Jiang and M. Schellmann, "Suppressing the out-of-band power radiation in multi-carrier systems: A comparative study," in *Global Communications Conference (GLOBECOM), 2012 IEEE*. IEEE, 2012, pp. 1477–1482.

[18] "Wireless michrophones." [Online]. Available: https://www.fcc.gov/general/wireless-microphones-0

Gh. Rasool Begh has done Bachelor of Engineering (B.E) in Electronics & Communication Engineering and M. Tech (Communication and Information Technology) from National Institute of Technology Srinagar (J & K) , India. He is working as Assistant Professor in the Department of E & C.E at NIT Srinagar. He has guided a number of M. Tech thesis related to OFDM, Cognitive Radios, WLANs and Security. Presently he is pursuing Ph. D in National Institute of Technology Srinagar. His areas of interest include Cognitive Radios, OFDM, MIMO and Security.

Ajaz H Mir has done his Bachelor of Engineering (B.E.) in Electrical Engineering with specialization in Electronics and Communication Engineering from REC Srinagar (J& K) India in 1982. He did his M. Tech in Computer Technology and Ph. D both from IIT Delhi in the year 1989 and 1996 respectively. He was Chief Investigator of Ministry of Communication and Information Technology, Govt. of India project: Information Security Education and Awareness (ISEA). He has been guiding PhD and M. Tech. thesis related to the area of Security and other related areas. He has a number of International publications to his credit. Presently he is working as Professor in the Department of Electronics and Communication Engineering and Dean Faculty at NIT Srinagar, Kashmir, India. His areas of interest are Biometrics, Image Processing, Security, Wireless Communication and Networks

Modeling of the Contact Center Agent‘s Work

Erik Chromy and Matej Kavacky

***Abstract*—The paper deals with the optimal sizing of the contact center. The most important part of the contact centers are their agents, therefore the modeling of their working time is also important. In the case of parameter which describes the number of handled calls during the peak hour also the other factors should be taken into account, such as time for hygienic break and time for other activities after serving of the customer. Such modified parameter can be used in Erlang C equation for calculation of optimal number of the contact center agents.**

***Keywords*—Call center, Erlang C, Quality of Service.**

I. Introduction

The contact center is dynamic technical system designed for efficient interconnection of users with request for service with operator or with systems capable of meet those needs. The principle is as follows - calling customer should be handled by one or more agents of the contact center. Every agent is trained and supported by corresponding information-telecommunication system [1]–[7].

In terms of commercial success of the contact center operators, it is important to serve customers as soon as possible and give them as much information. The main objective is to avoid that the calling customer will lost patience by long waiting and thereby avoid any unnecessary loss of interest of client for service. Contact centers are widely used in many areas: telecom operators, banking, insurance, government, education, health, tourism, etc.

The contact center consists of multiple technical components, such as:

- Private Branch eXchange (PBX), with Automatic Call Distribution (ACD) function,
- System management – system for evaluation of handled calls and monitoring of the contact center operation,
- Interactive Voice Response (IVR) [8],
- Computer Telephony Integration (CTI) [9],
- Recording system – not only for recording of the speech interaction, but also recording of agent‘s screen sequence during serving of the customer,
- Campaign manager – generates outbound calls based on customer requirement and also allows to make calling campaigns,

This article was created with the support of the Ministry of Education, Science, Research and Sport of the Slovak Republic within the KEGA agency project - 007STU-4/2016 named: Progressive educational methods in the field of telecommunications multiservice networks.

E. Chromy is with the Slovak University of Technology, Faculty of Electrical Engineering and Information Technology, Departement of Telecommunications, Ilkovicova 3, 812 19 Bratislava, Slovakia (e-mail: chromy@ut.fei.stuba.sk).

M. Kavacky is with the Slovak University of Technology, Faculty of Electrical Engineering and Information Technology, Departement of Telecommunications, Ilkovicova 3, 812 19 Bratislava, Slovakia (e-mail: kavacky@ut.fei.stuba.sk).

Manuscript received July 22, 2016, revised September 9, 2016

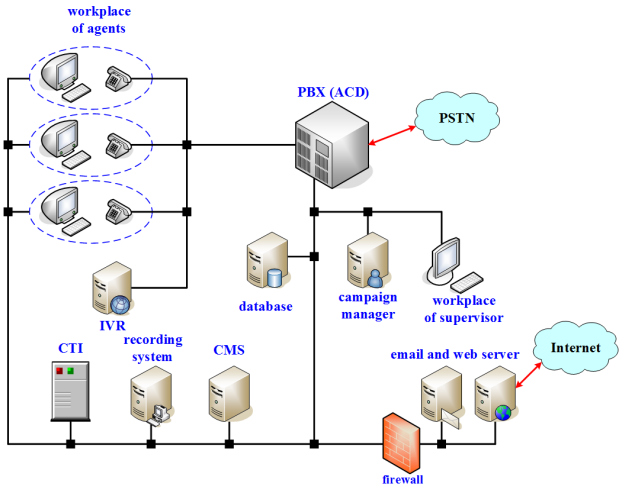

Fig. 1. Technical components of contact center

- Workplace of agent and supervisor,
- email server and
- web server.

II. Automatic Call Distribution

ACD is the basic program equipment necessary for contact center operation. It offers sophisticated and various functions of call routing, creation of queues and control of agent‘s productivity.

The task of call routing is to interconnect the calling customer with agent. Multiple important parameters should be taken into account for call routing:

- service request of the calling customer,
- profile of the agent,
- state of the agent (busy or idle),
- state of the waiting queue (number of waiting callers, average waiting time),
- system load in real-time and
- alternative resource (in case of overload).

A. Waiting Queue

The contact center represents the efficient resource usage. Therefore it is necessary to count with the situation, that in the time of call no suitable idle agent is available for the caller.

The PBX enqueues incoming calls. The required service is determined (choice of the caller in the IVR) and based on this the call is routed tothe queue for identified service. Call in the queue behaves according FIFO (First In First Out) rule. The special case occurs when the caller is marked as special. In this case the call is placed to the beginning of the queue.

Calls remain in the queue until:

- agent of the called group will become idle, or
- expiration of the optional time interval intended for caller waiting (set by manager of the contact center), or
- cancellation of call by the caller.

III. Qualitative Parameters of the Contact Center

Quality of Services (QoS) parameters important from customer's view:

- time spent for waiting for available agent,
- maximal waiting time for available agent,
- service time of request (communication with agent).

For the customer it is also important:

- to be handled by qualified agent,
- to be handled by one agent (call transfer between multiple agents is not suitable solution).

The setting of optimal number of agents is the important task for contact center manager. Therefore, he should to determine the number of agents such that customers will be satisfied with service and at the same time agents will serve the maximum customers during working time.

Following QoS parameters are important for determining the optimal number of agents [11] from the contact center manager point of view:

- the average number of calls during busy hour,
- the average number of calls waiting in the queue,
- the average waiting time of customer in the queue [10], [12], [14], [15],
- the average service time of customer by agent (this value should be decreased during contact center operation) [13],
- set of maximum waiting time of the customer for serving by agent,
- determine of percentage of incoming calls that should be connected with agent within specified time,
- the probability that all agents are occupied when customer is calling,
- the agent utilization (for determining the number of minutes when agent is active during busy hour).

IV. Estimation of the Optimal Number of Agents through Erlang C Equation

We can assume following parameters:

- upper bound for request enqueue: P_C (manager will set the probability when all agents will be occupied),
- number of requests the agent can serve during busy hour: μ,
- number of requests that are output of IVR system and are entering the service process: λ .

Erlang C equation [16]–[20] can be then stated in following form:

$$P_C(m,\frac{\lambda}{\mu}) = \frac{\dfrac{m\left(\dfrac{\lambda}{\mu}\right)^m}{m!\left(m-\dfrac{\lambda}{\mu}\right)}}{\sum\limits_{i=0}^{m-1}\dfrac{\left(\dfrac{\lambda}{\mu}\right)^i}{i!}+\dfrac{m\left(\dfrac{\lambda}{\mu}\right)^m}{m!\left(m-\dfrac{\lambda}{\mu}\right)}}. \quad (1)$$

From this equation (1) we can calculate the final number of agents *m* by iteration.

The number of agents *m* can be calculated also through equation (2) if another parameters are defined:

- Grade of Service (GoS): percentage of requests received for serving by agent until defined time AWT (Acceptable Waiting Time),
- AWT: maximal time which the request can spent in queue for available agent for defined GoS percentage.

$$GoS = 1 - P_C \cdot e^{-\mu\left(m-\frac{\lambda}{\mu}\right)AWT}. \quad (2)$$

By modification of equation (2) we have equation (3), which states the required number of contact center agents:

$$m = \frac{AWT\cdot\lambda - \ln\left(\dfrac{1-GoS}{P_C}\right)}{AWT\cdot\mu}. \quad (3)$$

Based on such stated number of agents *m* it is possible to calculate another QoS parameters of the contact center from Erlang C equation:

- occupancy of one agent in serving group:

$$\rho = \frac{\lambda}{m\cdot\mu}, \quad (4)$$

- average waiting time in serving group queue:

$$W = \frac{P_C}{\mu\left(m-\dfrac{\lambda}{\mu}\right)}, \quad (5)$$

- average number requests in service time queue:

$$Q = \lambda.W = \frac{\lambda}{\mu\left(m-\dfrac{\lambda}{\mu}\right)}\cdot P_C, \quad (6)$$

- average number of requests in service time system:

$$N = \frac{\lambda}{\mu} + Q = \frac{\lambda}{\mu} + \frac{\lambda}{\mu\left(m-\dfrac{\lambda}{\mu}\right)}\cdot P_C, \quad (7)$$

- average time which request will spent in service time system:

$$T = \frac{N}{\lambda} = \frac{1}{\mu} + W = \frac{1}{\mu} + \frac{P_C}{\mu\left(m - \frac{\lambda}{\mu}\right)}. \quad (8)$$

V. Modeling of the Working Time of Contact Center Agent

In the case of activity of contact center agent we can think about two notions: *idle time* and *administrative work*.

The notion *idle time* in the contact center system represents time dedicated for example for hygienic break. The contact center manager can set I_T minutes of working hour for such idle time. Idle times have also impact on contact center sizing. The modeling of the idle time can be done in two ways:

A. Idle Time – Shortening of the Average Service Time

If we want to preserve the original value of parameter μ (as we assume in chapter 4), representing average number of handled calls during busy hour, then we have to change average service time required for serving of one request (based on given parameter I_T - in minutes).

Then for average service rate of one request the following equation must be valid:

$$\frac{1}{\mu_{I_T}} = \frac{1}{\mu} - \frac{\frac{I_T}{60}}{\mu} = \frac{60 - I_T}{60 \cdot \mu}, \quad (9)$$

where $1/\mu_{I_T}$ represents average time (in hours) in which the request must be handled while the original value of parameter μ must be preserved. It means faster service time and also following inequality must apply:

$$\frac{1}{\mu_{I_T}} < \frac{1}{\mu}. \quad (10)$$

If the shortening of average service time is not suitable, then the number of handled calls during busy hour must be modified (decreased).

B. Idle Time – Handled Calls Decreasing

It is necessary to decrease the number of requests the one agent can serve during busy hour. It leads to increased number of agents required for serving calls. In this way the average service time of one request is not changed.

If we will assume with idle times of agent, then we must use new parameter $1/\mu_{I_T}$ in our calculations:

$$\mu_{I_T} = \frac{60 - I_T}{\frac{60}{\mu}} = \frac{\mu(60 - I_T)}{60}. \quad (11)$$

This way of calculation of optimal number of agents in contact center is preferable, because the service time is not shortened.

C. Administrative Work

The notion *administrative work* in contact center system represents activities the agent must done after every handled call. It means that customer can have request during call which the agent must handle right after the call (e.g. search for invoice or detailed record list, send e-mail, etc.). But such activity has negative impact on number of handled calls during work time of agent.

It is obvious that such activity is not required after every call, but after only percentage of calls. Therefore in the modeling of contact center processes we should also this parameter take into account. This parameter will be denoted as a_W. We must also set how much time (in minutes) the agent require for such activity in average. This parameter will be denoted as T_{a_W} (in minutes). Assumption of administrative work means that the average service time of one request for one agent will be extended (according to values of parameters a_W and T_{a_W}).

The parameter T_{a_W} can have values in the range <0, 1>.

- *0*: it means that administrative work is not assumed,
- *1*: it means that administrative work is assumed for every call.

Therefore, if we assume administrative work it is necessary to modify (before modeling) the original value of parameter μ (resp. $1/\mu$), which represents number of handled calls during busy hour and in calculations we must use new parameter μ_{a_W}:

$$\frac{1}{\mu_{a_W}} = \frac{1 + \frac{\mu \cdot a_W \cdot T_{a_W}}{60}}{\mu}, \quad (12)$$

where, $1/\mu_{a_W}$ represents average service time of call (in hours) while assuming parameters a_W and T_{a_W}.

Then the following inequality will be valid:

$$\frac{1}{\mu_{a_W}} > \frac{1}{\mu}. \quad (13)$$

The inequality (13) leads to increased number of agents required for handling calls.

Based on above assumptions we can write the final equation (14), which takes into account the idle times and administrative work of agent $\mu_{I_T+a_W}$ and modifies the original parameter μ, (resp. $1/\mu$) into following form:

$$\mu_{I_T+a_W} = \frac{\frac{\mu}{1 + \frac{\mu \cdot a_W \cdot T_{a_W}}{60}} \cdot (60 - I_T)}{60} = \frac{\mu\,(60 - I_T)}{60 + \mu \cdot a_W \cdot T_{a_W}}. \quad (14)$$

Also the following inequality will be valid:

$$\mu > \mu_{I_T+a_W}. \quad (15)$$

From equation (15) we can see that if we will assume the idle times and administrative work of agent, the average number of handled calls during busy hour will be lower than in the case when not assuming the idle times and administrative

work. Such assumption and the use of new parameter $\mu_{I_T+a_W}$ in calculations of the optimal number of agents leads to increased number of the required agents.

If we will assume the idle time and administrative work, then we can use Erlang C equation and equation for calculation of required number of agents based on GoS parameter in following modifications:

- determine the optimal number of agents using the Erlang C equation:

$$P_C\left(m, \frac{\lambda}{\mu_{I_T+a_W}}\right) = \frac{\frac{m\left(\frac{\lambda}{\mu_{I_T+a_W}}\right)^m}{m!\left(m-\frac{\lambda}{\mu_{I_T+a_W}}\right)}}{\sum_{i=0}^{m-1}\frac{\left(\frac{\lambda}{\mu_{I_T+a_W}}\right)^i}{i!} + \frac{m\left(\frac{\lambda}{\mu_{I_T+a_W}}\right)^m}{m!\left(m-\frac{\lambda}{\mu_{I_T+a_W}}\right)}}, \tag{16}$$

- determine the optimal number of agents using Erlang C equation when the parameter GoS is known:

$$m = \frac{AWT \cdot \lambda - \ln\left(\frac{1-GoS}{P_C}\right)}{AWT \cdot \mu_{I_T+a_W}}. \tag{17}$$

VI. Conclusion

In the paper we presented possibilities of modeling of working time of the contact center agent. The parameter of service time of customer we have extended with two more parameters. We took into account the idle time and time for administrative work. Based on this consideration we derived the modification of Erlang C equation for determine the optimal number of the contact center agents.

References

[1] I. Baronak and E. Chromy, *Call Center and its Evolution*, 2nd International Conference on Emerging Telecommunications Technologies and Applications and the 4th Conference on Virtual University, Kosice, Slovak Republic, 2003, pp. 85-88, ISBN 80-89066-67-4

[2] I. Baronak and E. Chromy, *The Technology of Call Center Raises the Value of the Society*. 26th International Conference Telecommunications and Signal Processing, Brno, Czech Republic, 2003, pp. 56-60, ISBN 80-214-2433-8

[3] E. Chromy and I. Baronak, *Application of Call Center*. 10th International Scientific Conference COFAX-TELEKOMUNIKACIE 2004, Bratislava, Slovak Republic, 2004, pp. 129-136, ISBN 80-967019-6-7

[4] I. Baronak and E. Chromy, *Call center client application interface*. 27th International Conference Telecommunications and Signal Processing, Brno, Czech Republic, 2004, pp. 30-37, ISBN 80-214-2684-5

[5] I. Baronak and E. Chromy, *Contact center part of modern communication infrastructure*. 3rd International Conference on Emerging Telecommunications Technologies and Applications and the Workshop Organisation and Management of Scientific, Technology and Industrial Parks, Kosice, Slovak Republic, 2004, pp. 79-83, ISBN 80-89066-85-2

[6] E. Chromy and I. Baronak, *Contribution of call center to regional development*. 5th EURASIP Conference focused on Speech and Image Processing, Multimedia Communications and Services, Smolenice, Slovak Republic, 2005, pp. 212-215, ISBN 80-227-2257-X

[7] G. Koole, *Call Center Mathematics: A Scientific Method for Understanding and Improving Contact Centers*. Departement of Mathematics, Vrije Universiteit, Amsterdam, January, 2007

[8] I. Baronak and E. Chromy, *Interactive voice response as a part of call center*. 28th International Conference Telecommunications and Signal Processing, Brno, Czech Republic, 2005, pp. 20-23, ISBN 80-214-2972-0

[9] E. Chromy and I. Baronak, *Computer Telephony Integration as a part of Call Center*. 6th RTT Conference focused on Research in Telecommunication Technology, RTT 2005, Hradec nad Moravici, Czech Republic, 2005, pp. 204 206, ISBN 80-248-0897-8

[10] G. Koole, B. Nielsen and T. Nielsen, *First in line waiting times as a tool for analyzing queueing system*. Operations Research, Vol. 80, No. 5, 2012, pp. 1258-1266, DOI: 10.1287/opre.1120.1089

[11] N. Gans, H. Shen, Y-P. Zhou, N. Korolev, A. McCord and H Ristock, *Parametric Stochastic Programming Models for Call-Center Workforce Scheduling*. Manufacturing and Service Operations Management, Vol. 17, No. 4, 2015, pp. 571-588, DOI: 10.1287/msom.2015.0546

[12] B. Legros, O. Jouini and G. Koole, *Adaptive Threshold Policies for Multi-Channel Call Centers*. IEE Transactions, Vol. 47, No. 4, 2015, pp. 414-430, ISSN: 0740-817X, DOI: 10.1080/0740817X.2014.928965

[13] A. Weerasinghe, *Optimal service rate perturbations of many server queues in heavy traffic*. Queueing Systems, Vol. 79, No. 3-4 2015, Springer US, pp. 321-363, ISSN: 0257-0130, DOI: 10.1007/s11134-014-9423-9

[14] W. Chan, G. Koole and P. Ecuyer, *Dynamic Call Center Routing Policies using Call Waiting and Agent Idle Times*. Manufacturing and Service Operations Management, Vol. 16, No. 4, 2014, pp. 544-560, DOI: 10.1287/msom.2014.0493

[15] G. Koole, B. Nielsen and T. Nielsen, T.: *Optimization of overflow policies in call centers*. Probability in the Engineering and Informational Sciences, Cambridge University Press, Vol. 29, No. 3, 2015, pp. 461-471, DOI: 10.1017/S0269964815000091

[16] E. Chromy, T. Misuth and M. Kavacky, *Erlang C Formula and Its Use In the Call Centers*. Journal AEEE - Information and Communication Technologies and Services, Vol. 9, No. 1, pp. 7-13, March 2011, ISSN 1804-3119

[17] E. Chromy, J. Diezka, M. Kovacik and M. Kavacky, *Traffic Analysis in Contact Centers*. The 11th International Conference KTTO 2011, June 22-24, Szczyrk, Poland, 2011, pp. 19-24, ISBN 978-80-248-2399-7

[18] E. Chromy, T. Misuth and A. Weber, *Application of Erlang Formulae in Next Generation Networks*. International Journal of Computer Network and Information Security (IJCNIS), Vol. 4, No. 1, February 2012, MECS Publisher, 2012, pp. 59-66, ISSN: 2074-9090 (Print), ISSN: 2074-9104 (Online)

[19] O. Jouini, G. Koole and A. Roubos, *Performance Indicators for Call Centers with Impatience*. IEE Transactions, Vol. 45, No. 3, 2013, pp. 341-354, ISSN: 0740-817X, DOI: 10.1080/0740817X.2012.712241

[20] J. Zan, J. Hasenbein and D. Morton, *Asymptotically optimal staffing of service systems with joint QoS constraints*. Queueing Systems, Vol. 78, No. 4, 2014, Springer US, pp. 359-386, ISSN: 0257-0130, DOI: 10.1007/s11134-014-9406-x

Erik Chromy was born in Velky Krtis, Slovakia, in 1981. He received the M.Sc. degree in telecommunications in 2005 from Faculty of Electrical Engineering and Information Technology of Slovak University of Technology (FEI STU) Bratislava. In 2007 he submitted PhD work. His scientific research is focused on queueing systems, contact center and admission control methods. Nowadays he works as assistant professor at the Institute of Telecommunications of FEI STU Bratislava.

Matej Kavacky was born in Nitra, Slovakia, in 1979. He received the M.Sc. degree in telecommunications in 2004 from Faculty of Electrical Engineering and Information Technology of Slovak University of Technology in Bratislava (FEI STU). In 2006 he submitted PhD. work Quality of Service in Broadband Networks. His scientific research is focused on admission control methods Nowadays he works as assistant professor at the Institute of Telecommunications of FEI STU Bratislava.

Applications, Prospects and Challenges of Silicon Carbide Junction Field Effect Transistor (SIC JFET)

Frederick O. Ehiagwina, Olufemi O. Kehinde, Lateef O. Afolabi, Hassan J. Onawola and Nurudeen A. Iromini

[1]***Abstract*—properties of Silicon Carbide Junction Field Effect Transistor (SiC JFET) such as high switching speed, low forward voltage drop and high temperature operation have attracted the interest of power electronic researchers and technologists, who for many years developed devices based on Silicon (Si). A number of power system Engineers have made efforts to develop more robust equipment including circuits or modules with higher power density. However, it was realized that several available power semiconductor devices were approaching theoretical limits offered by Si material with respect to capability to block high voltage, provide low on-state voltage drop and switch at high frequencies. This paper presents an overview of the current applications of SiC JFET in circuits such as inverters, rectifiers and amplifiers. Other areas of application reviewed include; usage of the SiC JFET in pulse signal circuits and boost converters. Efforts directed toward mitigating the observed increase in electromagnetic interference were also discussed. It also presented some areas for further research, such as having more applications of SiC JFET in harsh, high temperature environment. More work is needed with regards to SiC JFET drivers so as to ensure stable and reliable operation, and reduction in the prices of SiC JFETs through mass production by industries.**

Keywords*— *Amplifier, Boost Converter, Electromagnetic Interference, Inverter, JFET, Rectifier, SiC JFET, Silicon Carbide.

I. Introduction

Initial efforts to develop silicon carbide Junction Field Effect Transistor (SiC JFET) was in the early 1990s. However, the device' relatively low transconductance, low channel mobility and challenging fabrication process were its major drawback. Subsequently, by mid-2000s, after further research and improvement, the first prototype SiC JFET was produced [1]. SiC JFET has attractive properties such as high switching speed, low forward voltage drop and high temperature operation, which have drawn the attention of power electronics research community, who for decades developed devices based on silicon (Si). More so, many power system Engineers have been searching for alternative solutions to silicon devices in order to develop more robust equipment that requires higher power density circuits and modules. It was observed that several available power electronic devices offered by semiconductor materials were approaching their ideal performance limits with respect to capability to block high voltage, provision of low on-state voltage drop and high switching frequencies. The most promising approach was to replace Si in the fabrication of power semiconductor devices with a wider bandgap material with acceptable bulk mobility, such as SiC and gallium nitride (GaN). In this context, SiC offers great potential for the realization of high power devices owing to its attractive properties. When compared with Si materials they have ten times higher breakdown electric field; three times wider band gap - about 3 eV at 27 ^{0}C and higher thermal conductivity; and two times higher saturation velocity [2], [3]. In addition, intrinsic charge carrier concentration of SiC material is lower than the corresponding value for Si which is principally attributed to the wide band-gap of SiC [4]- [9]. Among the several polymorph of SiC, 4H- and 6H-SiC have gained the attention of researchers [4], [9], however, 4H-SiC is the most commonly used in the fabrication of SiC JFET due its preferred channel charge mobility [10].

Meanwhile, modeling of the JFET has received significant attention by researchers [2], and most of these models are derivatives of the Schockley's equation, shown in (1) [11]; I_{DS} is the drain current, I_{DSS} is drain current at saturation when pinch-off voltage, V_P is attained. The gate-to-source voltage V_{GS} , is the controlling quantity, while I_{DS} is the controlled quantity:

$$I_{DS} = I_{DSS}\left(1-\frac{V_{GS}}{V_P}\right)^2 . \quad (1)$$

Device property is parameterized by thickness, length, width and doping concentration of channel and charge mobility. And there is a need to extensively evaluate JFETs physical models, in terms of their behaviour with temperature, transfer and output characteristics, and changes in channel length [10]. The V-I characteristics of SiC JFET can effectively be modeled by the same model developed for long-channel silicon devices. This is true, although, SiC has wider band gap than Si and possesses multiple-donor levels, thus making the relationship between the impurity

Manuscript received April 29, 2016 revised June 30, 2016 revised September 10, 2016.

F. O. Ehiagwina is with the Electrical Electronics Engineering Department, Federal Polytechnic, Offa, Kwara State, Nigeria (corresponding author mobile phone: +2348051645819; e-mail: frederick.ehiagiwna@fedpoffaonline.edu.ng).

O. O. Kehinde, and L. O. Afolabi are with Electrical Electronics Engineering Department, Federal Polytechnic, Offa, Kwara State, Nigeria. (e-mail: okdecibels@yahoo.com; mrshile@yahoo.com) respectively.

H. J. Onawola and N. A. Iromini are with Computer Technology Engineering Department, Federal Polytechnic, Offa, Kwara State, Nigeria. (e-mail: honawola@yahoo.com; ajibolaforyu2003@yahoo.com) respectively.

concentration and the carrier density complex [12]. From [12], the drain current of SiC JFET is given by (2) as:

$$I_{DS}=\left(\frac{W}{L}\right)I_P^{'}\left(1+\lambda V_{DS}\right)\left[\frac{3V_{DS}}{V_P}-2\left[\left\{\frac{\left(V_{DS}-V_{GS}+V_{bi}\right)}{V_P}\right\}^{3/2}-\left\{\frac{\left(-V_{GS}+V_{bi}\right)}{V_P}\right\}^{3/2}\right]\right], \quad (2)$$

where:

W = width of channel

L = length of channel

V_{bi} = built-in voltage of the gate-channel junction

V_P = pinch-off voltage

$I_P^{'}$ = normalized pinch-off current

λ = channel length modulation parameter

Built-in voltage of the gate-channel junction V_{bi} is a function of the temperature T, doping densities in the P^+-gate N_A and n-channel N_D, and intrinsic carrier density n_i. The relationship is as shown in (3):

$$V_{bi}=\frac{KT}{q}\ln\left(\frac{N_A N_D}{n_i^2}\right), \quad (3)$$

where K and q are Boltzmann and electron charge constants respectively. Whereas, the pinch-off voltage, given in (4) depends on the depth of channel D and permittivity of the channel ε_s.

$$V_P=\frac{qN_D D^2}{2\varepsilon_s}. \quad (4)$$

Normalized pinch-off current is represented by (5) as:

$$I_P^{'}=\frac{q^2 N_D n \mu_n D^3}{6\varepsilon_s}, \quad (5)$$

where n and μ_n are the ionized carrier density in the channel and carrier mobility.

Fig. 1 shows the cross section of SiC JFET. The types and structures of the JFET is thoroughly discussed in [1], [13], and from which Fig. 2 showing a SiC JFET family tree was drawn. Operating principle of the power JFET is modulation of the channel depletion region through the applied gate-to-source voltage. If the gate-to-source voltage, V_{GS} is higher than the gate threshold voltage, the JFET begins to conduct and a current can be established in the channel. The gate threshold voltage is the boundary

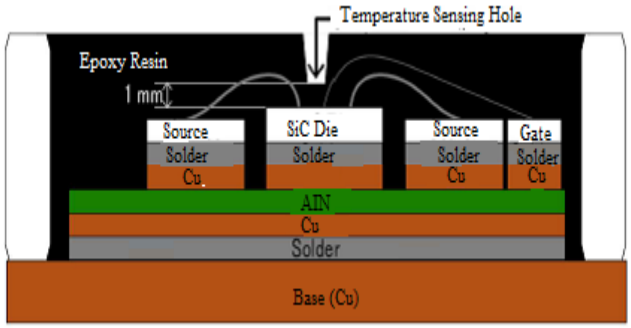

Fig. 1: A cross sectional view of SiC JFET, which was jointly developed by KEK and Sun-A corporation. The device is assembled on a 58 mm x 36 mm copper based plate and have the height of 7 mm. The size of the die is 4.16 mm x 4.16 mm, which was manufactured by SiCED (Germany) [67]

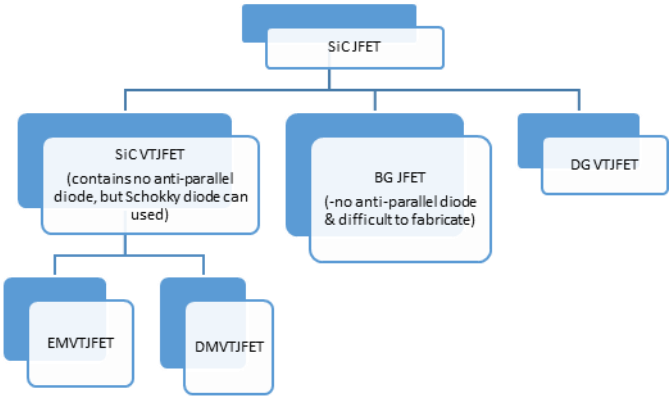

Fig. 2: SiC JFET family tree, available structures are Silicon Carbide Lateral Channel Junction Field Effect Transistor (SiC LCJFET), Silicon Carbide Vertical Trench Junction Field Effect Transistor (SiC VTJFET) - comprising of Enhancement-Mode Vertical Trench Junction Field Effect Transistor (EMVTJFET) and Depletion Mode Vertical Trench Junction Field Effect Transistor (DMVTJFET); Buried Grid Junction Field Effect Transistor (BG JFET), and Double Gate Vertical Trench Junction Field Effect Transistor (DG VTJFET)

between the conduction and the blocking area [13] with the drain current depending on the amount of the voltage barrier occurring in the channel [14].

In this paper an overview of published SiC JFET based circuit applications and evaluations is presented in Section II. While Section III highlights current challenges and suggested areas for future research with respect to SiC devices. Finally, conclusions reached are reported in Section IV.

II. OVERVIEW OF SIC APPLICATION

A. SiC JFET Application in Rectifiers and Amplifiers Circuits

Hybrid rectifiers made from Junction Barrier Schottky (JBS) rectifier and Trench JFET Schottky rectifier (TJFET), which combines the merits of Schottky rectifiers otherwise known as hot carrier diode with the advantages of PiN diode rectifiers was presented in [15]. The merits of Schottky rectifiers are better on-state and switching performance owing to the unipolar nature of Schottky diode, hence, no charges are stored and no depletion layer is formed. On the other hand, merits of PiN diode rectifiers are superior reverse leakage and breakdown characteristics, which are due to its intrinsic semiconductor layer leading to a decrease in the capacitance of the P-N region.

Furthermore, [15] measured and optimize the conductivity modulation in the hybrid rectifier. Analysis and characterization of the dynamic behaviour of a cascade rectifier base on normally-ON (N-ON) SiC JFET were carried out in [16]. Here the authors compared Si MOSFET and SiC JFET based rectifiers with Si rectifier and front-end rectifier, using boost converter incorporating power factor corrector (PFC)-used for generating ac output signals connectable to one or more loads, such as capacitive loads. It concluded that the SiC JFET based rectifier behaved poorer than the Si ultrafast diode rectifiers, in terms of reverse recovering time and current. But the recovering time of SiC JFET is lower than that of Si MOSFET, thus making SiC JFET more suitable for high speed rectification and bidirectional switch applications. Similar conclusions were reached by authors in [17], who characterized the reverse

conduction characteristics of normally-off SiC JFET using diode techniques.

A 30V supply precision operational amplifier (op-amp) designed to support industrial, instrumentation, and other application was realized using Auto-zeroing and chopping in [18] employing JFETs and Bipolar Junction Transistors (BJTs), with performance less than that of complementary metal oxide semiconductor field effect transistor (CMOS). CMOS based precision amplifier was superior because of cheaper wafer prices, reduced offset voltage, and so on. A transimpedance amplifier (TIA) based low-noise, wideband amplifier used in detecting 1064mm laser generated noise in quantum optical experiment was reported in [19]. The TIA, which conceptually, is a current-to –voltage converter and most frequently implemented using operational amplifier, performed better than single-junction field effect transistor based amplifier. Additionally, the design, development and characterization of a high gain RF amplifier for very low frequency receiver application using JFET and op-amp was presented in [20]. At 19.8 kHz, the design criteria was satisfied with a satisfactory gain of 46.003dB. Moreover, evaluation of the capability of a SiC JFETs for an induction synchrotron has been carried out. The device was operated with a repetition rate of 1 MHz, a drain–source voltage of 1 kV, and a drain current of 50 A in burst mode [21]. A synchrotron is a cyclic particle accelerator capable of generating extremely powerful x-rays. A presentation of experimental and simulation results involving an ac solid state variable current limiter circuit using 1200V SiC JFETs as an additional current limiting circuit for high power amplifiers to test power factor correction circuit was given in [22].

B. SiC JFET Application in Pulse Signal circuit

It was noted in [23] that SiC depletion mode JFET are well suited for pulse power applications as an opening switch due to their normally-ON nature. Also, the maximum avalanche energy of the device under repetitive condition was determined. The approached employed involves driving the N-ON SiC JFET has a nominal rating of 1200V/13A into punchthrough breakdown by using UIS circuit. Whereas development and description of a two-channel time-delay pulse signal generator was presented in [24]. According to [25], SiC JFET has been evaluated on an optimized double pulse circuit, where it shows switching energies four times lower than it equivalent Silicon Insulated Gate Bipolar Transistor (Si IGBT). Moreover, the performance characteristics along with the switching behaviour of a large area 6500V normally off JFETs and JBS diodes using double pulse testing at 3000V/11A with an inductive load was reported in [26], which is higher than the single 3300V application reported in [27]. However, the use of JBS diode was eliminated in [28], where a normally-off (N-OFF) SiC JFET was operated in cascode with a Si IGBT to unify the gate driver voltage and increase the switching speed of the JFET. This configuration was necessitated by the incompatibility of gate drive voltage of JFET and IGBT based FREEDM-pair, which increases the complexity and cost of the circuit. A balancing circuit that results in faster switching transients and higher operating pulse current was presented in [29]. It also reported an R-C network, which enhances the dynamic behaviour of the supercascode of SiC JFET/Si MOSFET. More so, SiC JFET/Si MOSFET cascade control methods was reported in [30].

C. SiC JFET in and Electromagnetic Interference Consideration

In [31], it was noticed that SiC based devices leads to an increased electromagnetic interference (EMI) production level. In addition, according to [31] SiC based circuits can record switching loss decrease of up to 70% in a comparison with the switching losses of Si, Si-SiC and SiC device combinations. It can pave way for the application of SiC JFET in low-voltage industrial variable-speed drives of 1200 V SiC-based devices, currently dominated by Si IGBTs and diodes. The authors in [32] reported the development of the popular 1200V/30A SiC JFET module using a half bridge topology. It consist of three-single SiC JFET chips connected in series with two parallel low voltage P-MOSFETs. This configuration help to overcome the normally-on problem of JFETs, which leads to loss of control and undesired conduction of switches. Furthermore, this may lead to shoot through current damaging the power system. This topology also makes them suitable in efficiency sensitive sections of renewable energy and uninterrupted power supply systems.

However, a non-contact signal transfer mechanism for transferring multiple signals over a rotational interface through electromagnetic means was described in [33]. The mechanism is built for space crafts. The work reported in [34], dealt with electromagnetic interference in a SiC JFET inverter. It proposed integrating small-value common-mode (CM) capacitors into the inverter so as to minimize EMI. A reduction in the CM conducted emissions was noticed, though, this approach resulted in slight increase in the system losses, system size, and poorer switching waveforms. Meanwhile, [35] proposed a method of characterizing interelectrode capacitances, which will allow for effective study of SiC JFET switching waveform during interelectrode capacitance evolution. The operating range of the JFET was optimized so as to achieve uniform gain during amplitude modulation. It benefits and limitations were discussed for space craft application. On the other hand, dv/dt control methods for a SiC JFET/Si MOSFET cascade aimed at avoiding the impairment to electromagnetic compatibility, which could result from the transient for hard commutation reaching values up to 45 KV/μs, when there is no control was reported in [30].

D. SiC JFET Application in Inverter and Boost Converter Circuit

A 10kW three phase (3 - ϕ) bidirectional on-board battery charger for use as a vehicle to grid (V2G) interface in electric vehicles was reported in [36]. It incorporated a 1200V SiC JFET, which enables the device operation at high voltage in the dc link and high switching frequency ranging between 50-150 kHz, while an IGBT boost converter serves as interface to the grid. Moreover, an evaluation of a high frequency boost converter module was reported in [37]. Whereas, in [38], a step-up oscillator configuration using a piezoelectric transformer and a JFET capable of enabling a boost dc/dc converter the moment the start-up circuit outputs enough voltage. The design of a 40kVA inverter, with an efficiency, greater than 99.5% using Si JFET was presented in [39]. The implementation involved ten 85 mΩ N-ON JFET in parallel, in each switch position, this will reduce

conduction losses. The inverter performs better than Si IGBT based inverter.

An experimental demonstration of the use of vertical SiC JFET in an inverter leg without external free-wheeling diodes was shown in [13]. This was achieved by taking advantage of the reverse conduction capability of the device. A presentation of a 3 KVA 1220v/6A with switching speed of 200 KHz all-SiC JFET current source converter, with reduced size and weight in comparison with its Si MOSFET equivalence was reported in [40]. In presenting a dc/dc boost converter, the authors in [6] compared N-ON JFET devices having a threshold voltage of 50v and -10v with BJT devices with a view of extracting the maximum performance of the devices and thereafter, choosing the optimal driving condition. It concluded that the conduction losses of both types of devices is not a function of the switching frequency. Whereas the driver loss of the BJTs seem not to be dependent on the switching frequency, the driver loss of JFET devices is proportional to the switching frequency. This comparison was repeated in a modular multilevel converter, where it was reported that SiC JFET can be used without anti-parallel diode. Hence, the body diode can be used during the switching transients to achieve an efficiency of up to 99.8%, which was achieved in a 300 MW 3.3 kV 1.2 kA SiC JFET converter. However, the choice of no anti-parallel diode is not available in Si MOSFET based devices [9].

The better efficiency of JFET over BJT is partly due to BJT requirement of a continuous base current when collector current flows. This warrants the purchase of a supply transformer for base drive circuit [41], [42]. Moreover, the authors in [9] reported dc/dc converters made of SiC JFET and SiC MOSFET with the former possessing a slightly higher efficiency of 96% as against the 95.5% of the latter, with weak frequency dependency. However, a cascode of Si MOSFET and SiC JFET possesses an efficiency of 98% at frequency range of 400 kHz to 1 MHz. The high efficiency of SiC JFET is enhanced by the absence of the Miller effect since it operates in the common-gate configuration, hence lower switching losses. On the other hand, SiC MOSFET possesses lower efficiency due to higher on-state resistance and parasitic capacitance. It is noted that a dc/dc boost converter steps up voltage while stepping down current from its supply to its load. It is a switch-mode power supply (SMPS) usually containing any of the following switches; MOSFET, IGBT or BJT. Development and testing of high frequency, high efficiency inverter using a SiC JFET power module, shown in Fig. 3 was presented in [8]. Its approach was to employ a rugged negative voltage gate drive to overcome the N-ON issue associated with JFET devices and to avoid the bridge short-through during switching on and off. The developed circuit has a turn-on and turn-off times better than that of Si IGBT based inverter. Its efficiency was higher as well.

Accordingly, the authors in [43] reported application of JFET in converters with operating temperature above 200 ^{0}C. Lateral depletion-mode 4H-SiC n-channel JFETs have been reported to have good performance at temperatures $\leq$ 600 ^{0}C, which can prove useful in environments such as fuel combustion chambers in vehicles, deep-well drilling, planetary instrumentations, and other harsh environments [44]. This was verified in [45] through demonstration of ICs based on 4H-SiC JFET integrating Hafnium ohmic contact with $TaSi_2$ interconnect with SiO_2 and SiN_4 dielectric layer

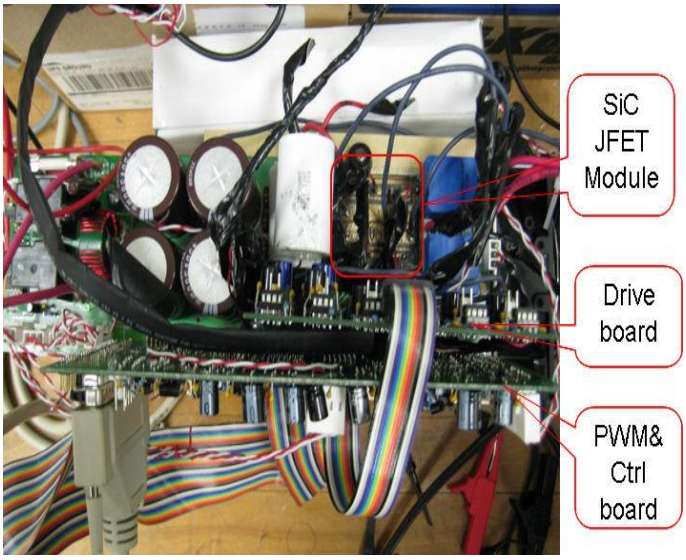

Fig. 3: SiC module based inverter circuits [8]

based on 4H-SiC JFET integrating Hafnium ohmic contact with $TaSi_2$ interconnect with SiO_2 and SiN_4 dielectric layer over about $1\mu m$ scale topology designed to withstand 1000 hours of stable electrical operation at 500 ^{0}C in the air. The research was extended further by testing the ICs at 727 ^{0}C, after 25 hours of operation little change in electrical properties was noticed due to a quick increase in device resistance [46]. However, when the IC die is attached to gold paste, it operated at 700^{0}C for about 144 hours [47]. These results are higher than that of SiC MOSFET devices with operating temperature of about 200^{0}C due to associated oxide interface problems [42]. In addition, SiC CMOS circuits tested to operate at 300 ^{0}C under probe and 540 ^{0}C when packaged was reported in [48].

E. SiC JFET Application in Short Circuit Detection

A SiC JFET with an incorporated short circuit protection was reported in [49]. Here a short circuit detection is added to a typical driver design. Furthermore, the robustness of 1200V N-ON SiC JFETs against short circuit were examined via experimental parametric analysis and 3-dimensional thermal model simulations in [50]. Merits of this report included presentation of a more accurate and realistic analysis of short circuits outside the power converter where a large stray inductance exists.

F. SiC JFET Application in Circuit Breaker

A new self-powered solid state circuit breaker (SSCB) concept using N-ON SiC JFET as the main static switch was presented in [53], [54]. When texting the suitability of SiC JFET with a N-ON recessed implanted gate vertical-channel feature for light triggered solid state circuit breaker with a 1200 V rating, [55] carried out 2.4 million pulses hard switch at a repetition rate of 10Hz from a blocking voltage of 1200 V to an on-state current of more than 13 times the rated current at 150 ^{0}C. A low inductance RLC circuit was used, in which stored energy in the capacitor is discharged in a resistor via SiC JFET. It was observed that the on-state conduction improved slightly, while blocking voltage remain the same. In principle, the SSCB is capable of interrupting current within a short duration, in the order of 10^{-6} s without arc formation and no voltage reversal is required. They are usually implemented with gate commutated turn-off thyristors and gate turn-off thyristors. The high on-state

losses of IGBT limits their usage in circuit breakers, although they have the ability of limiting current automatically [56]-[58]. This device uses power sourced from the short circuit faults to turn and hold off the SiC JFET device. Meanwhile, the authors in [59] analyzed a solid state circuit breaker incorporating an isolated dc/dc low power converter with fast-starting property serving as the protection driver. Here, short circuit is detected by sensing a rise in terminal voltage. The SiC JFET based system was able to repeatedly interrupt a fault current of up to 180A at a bus voltage of 400 VDC with an interruption time of 0.8μs. The performance of 1200 V SiC N-ON vertical JFET during unclamped inductive switching (UIS) scenario was investigated in [60] by performing UIS tests, a high stress test for characterizing the ruggedness of a device. This was used to observe the energy density. Maximum device temperature during UIS were subsequently forecasted through simulation. This also helped in understanding JFETs failure modes. A presentation of 3500V/15A power module based on SiC JFET and Schottky barrier diodes was given by [61]. The device showed a superior turn-on and turn-off of less than 15ns. It claims to be the first demonstration of SiC JFET power module at a voltage level greater than 3300 V. Meanwhile, a fully integrated six-pack power module consisting of four parallel SiC JFET and two anti-parallel Schottky diode with each module rated 1200 V 100 A, and having the capacity to withstand a temperature up to 200^0C with on-state resistance of 55mΩ. However, when implemented in a liquid cooled 3-Φ 5 kW inverter, having an efficiency of 98.5%, the coolant temperature was 95^0C. The authors also included a thermal shock test of the module assembly.

G. Miscellaneous Application of SiC JFET

Although SiC JFET is available primarily in 1200V, 1700V also exists with a current rating of up to 48A. The on-state resistance ranges from $45-127\,\text{m}\Omega$ at $27\ ^0$C, depending on whether it is N-ON- or N-OFF SiC JFET [1], [42], [51]. Moreover, the on-state resistance of 4H-SiC JFET may be up to 400 times lower than that of Si at a specific breakdown voltage. Thereby permitting its use in high current circuits with a comparatively lesser forward voltage drop [3]. The N-OFF SiC JFETs are more recent and desirable than N-ON SiC JFET [17].

An input buffer with monolithic integrated JFET in standard Bipolar-CMOS-DMOS (BCD) technologies process was presented in [52]. It further made a comparison with a buffer having P-channel MOSFET. It was observed that the JFET buffer out performs its P-channel MOSFET counterpart in terms of its low-frequency input referred noise.

An evaluation of the operation of depletion mode SiC JFET was carried out in [24] by developing a dc-dc step-down converter with realistic operating conditions. Then, the functionality of the entire system was verified through measurements. An attempt was made to address the problem of high cost militating against the large scale production and adoption of SiC power devices in [62], through a proposition of a hybrid power module using SiC JFET in parallel with Si IGBT. By so doing, it combined the merits of both transistors. The hybrid power module has a superior cost/performance figures [37], [62].

The effect of parasitic turn-on on a half-bridge with 1700V N-ON SiC JFET-containing 32 pairs of chips in parallel were tested by [63], while the effect of ion, electron and neutron radiation on the electrical properties and thermal stability of 1700 n-type 4H-SiC epilayer used in fabricating devices such JFETs were examined by [64]. The effect on device properties were analyzed by capacitance deep level transient spectroscopy (DLTS), V-I curve and C-V profiling. It further described how to reduce the effect of parasitic turn-on through a special gate-drive concept, combined with a low inductance design. Moreover, [65] presented three different ways of minimizing parasitic turn-on for a gate-drive unit level circuitry. Of the three proposed solutions, the use of active current sources and clamping can substantially reduce losses. Furthermore, [66] reported a hybrid MOSFET-JFET concept aimed at suppressing Si MOSFET parasitic capacitance effect. Conceptually, parasitic capacitance or stray capacitance exists in sections of electronic circuitry owing to proximity of components to each other. Hence, there is a need to research on device packaging and component placement. Thus, a high power discrete SiC JFET package for accelerator application having a repletion rate of 1 MHz was developed and tested in [67].

III. CURRENT CHALLENGES AND AREAS FOR FUTURE

There are still challenges that should be surmounted so as to unleash the full potentials of not just SiC JFET, but also of SiC MOSFET. This section of the paper highlights some of these and areas for future research. More work is needed so as to better appreciate the trade-off between SiC JFET switching losses and dv/dt – rate in the course of converter design [30]. Hence, further researches are needed in the area of electromagnetic interference mitigation when implementing SiC JFET in a switching circuit. Could the blocking voltage of SiC JFET be extended further? Future studies would provide the answer to this. More applications of SiC JFET in harsh, high temperature environment are expected in the future [1], [44], [68], however, according to [1] there is a need to research on the stability of the device in such environment, develop packages and other accessories that can stand such high temperature environment. For example, in a review of the development of 6H-SiC JFET by NASA for extreme temperature for application analog amplifier, digital logic gates ICs and amplifier circuits [12], reported the use of ceramic packages of Al_2O_3 and gold metallization.

In spite of the work reported in [62], which attempted to address the high cost problem of SiC materials, SiC devices are still more expensive than Si devices. Hence, there is the need to research more in the mass production of SiC JFET. Additionally, more work still needs to be done with regards to SiC JFET drivers so as to ensure stable and reliable operation. In order to fully exploit the potentials of SiC devices, researcher have went as far as developing SiC MOSFET. Some of the examples of SiC MOSFET circuit application are reported in [69]-[73]. The future will see a lot of research in the fabrication of SiC MOSFET, such as studying the reliability and stability of the oxide layer over an extended period of time [1].

IV. CONCLUSION

This review has highlighted the most advance applications of SiC JFET in the literature. Current challenges and areas for further research were discussed. More research is needed so as to facilitate the production of SiC JFET in

commercial quantity, this will bring down the prices in comparison with other switches like BJT and IGBT.

REFERENCES

[1] R. Jacek, P. Dimosthenis and N. Hans-Peter, "Silicon carbide power transistors: a new era in power electronics is initiated," *IEEE Industrial Electronics Magazine ·,* vol. 6, no. 2, pp. 17-26, 15 June 2012.

[2] E. Platania, Z. Chen, F. Chimento, A. E. Grekov, R. Fu, L. Lu, A. Raciti, J. L. Hudgins, H. A. Mantooth, D. C. Sheridan, J. Casady and E. Santi, "A physics-based model for a SiC JFET accounting for electric-field-dependent mobility," *IEEE Transactions on Industry Applications,* vol. 47, no. 1, pp. 199-211, 2011.

[3] V. Veliadis, "Silicon carbide junction field-effect transistors (SiC JFET)," *Wiley Encyclopedia of Electrical and Electronics Engineering,* pp. 1-37, 2014.

[4] F. Roccaforte, F. Giannazzo, F. Iucolano, J. Eriksson, M. Weng and V. Raneri, "Surface and interface issues in wideband gap semiconductor electronics," *Applied Surface Science,* vol. 256, no. 19, pp. 5727-5735, 2010.

[5] H. Choi, "Overview of Silicon Carbide power devices," Fairchild Semiconductor.

[6] J.-K. Lim, G. Tolstoy, D. Peftitsis, J. Rabkowski, M. Bakowski and H.-P. Nee, "Comparison of total losses of 1.2 kV SiC JFET and BJT in dc-dc converter including gate driver," *Materials Science Forum,* Vols. 679-680, pp. 649-652, March 2011.

[7] B. Wrzecionko, D. Bortis and J. W. Kolar, "A 120^0C ambient temperature forced air-cooled normally-off SiC JFET automotive inverter system," *IEEE Transactions on Power Electronics,* vol. 29, no. 5, pp. 2345-2358, May, 2014.

[8] X. Zheng and P. Sanbo, "Design and analyse of silicon carbide JFET based inverter," *WSEAS Transactions on Circuits and Systems,* vol. 11, no. 9, pp. 295-304, 2012.

[9] R. R. Devarapally, "Survey of applications of WBG devices in power electronics," Kansas, 2016.

[10] M. Lades, "Modeling and simulation of wide bandgap semiconductor devices: 4H/6H-SiC," 2000.

[11] O. A. Akpaida, O. Omoroguiwa and M. S. Okundamiya, Principles of electronic devices and circuits, 1st ed., Solozone, Ed., Benin-City, Edo-State: Stemic Publication, 2005.

[12] P. G. Neudeck, S. L. Garverick, D. J. Spry, L.-Y. Chen, G. M. Beheim, M. J. Krasowski and M. Mehrehany, "Extreme temperature 6H-SiC JFET integrated circuit technology," *Physica status solidi,* 2009.

[13] R. Ouaida, X. Fonteneau, F. Dubois, D. Bergogne, F. Morel, H. Morel and S. Oge, "SiC Vertical JFET pure diode-less inverter leg," in *Applied Power Electronics Conference and Exposition (APEC), 2013 Twenty-Eigth Annual IEEE,* Long Beach, CA, 2013.

[14] S. Bellone, L. Di Benedetto and G. Licciardo, "A model of the off-behaviour of 4H-SiC power JFET," *Solid State Electronics,* vol. 109, pp. 17-24, 2015.

[15] M. Quddus, M. Mudholkar and A. Salih, "Carrier separation technique to optimize conductivity modulation in high voltage rectifiers," in *Electron Devices and Solid-State Circuits (EDSSC), 2015 IEEE International Conference on*, 2015.

[16] A. Vazquez, A. Rodriguez, M. Fernandez, M. M. Hernando, E. Maset and J. Sebastian, "On the use of front-end cascode rectifier based on a normally-on SiC JFET and Si MOSFET," *IEEE Transaction on Power Electronics,* vol. 29, no. 5, pp. 2418-2427, May 2014.

[17] R. Shillington, P. Gaynor, M. Harrison and W. Heffernan, "Silicon carbide JFET reverse conduction characteristics and use in power converters," *IET Power Electronics,* vol. 5, no. 8, pp. 1282-1290, 2012.

[18] Y. Kusuda, "5.1A 60V auto-zero and chopper operational amplifier with 800kHz interleaved clocks and input bias-current trimming," in *Solid- State Circuits Conference - (ISSCC), 2015 IEEE International,* San Francisco, CA, 2015.

[19] H. Zhou, W. Wang, C. Chen and Y. Zheng, "A low-noise, large-dynamic-range-enhanced amplifier based on jfet buffering input and JFET bootstrap structure," *Sensors Journal, IEEE,* vol. 15, no. 4, pp. 2101-2105, April 2015.

[20] R. Putera, Kusnandar, A. Najmurrokhman, Sunubroto, Chairunnisa and A. Munir, "High gain RF amplifier for very low frequency receiver application," in *Information Technology and Electrical Engineering (ICITEE), 2014 6th International Conference on*, 2014.

[21] H. T. Keiichi Ise, K. Takaki, M. Wake, K. Okamura, K. Takayama and W. Jiang, "Development of a megahertz high-voltage switching pulse modulator using a SiC-JFET for an induction synchrotron," *IEEE Transactions on Plasma Science,* vol. 39, no. 2, pp. 730-736, 7 February 2011.

[22] W. Konrad, K. Leong, K. Krischan and A. Muetze, "A simple SiC JFET based AC variable current limiter," in *Power Electronics and Applications (EPE'14-ECCE Europe), 2014 16th European Conference on*, 2014.

[23] B. Pushpakaran, M. Hinojosa, S. Bayne, V. Veliadis, D. Urciuoli, N. El-Hinnawy, P. Borodulin, S. Gupta and C. Scozzie, "Evaluation of SiC JFET performance during repetitive pulsed switching into an unclamped inductive load," *Plasma Science, Transaction on,* vol. 44, no. 10, pp. 2968-2973, October 2014.

[24] J. Bacmaga, K. Bene, B. Pejcinovic and A. Baric, "Evaluation of the operation of depletion-mode SiC power JFET in DC-DC converter applications," in *Information and Communication Technology, Electronics and Microelectronics (MIPRO), 2014 37th International Convention on*, Opatija, 2014.

[25] A. Anthon, Z. Zhang and M. Andersen, "A high power boost converter for PV Systems operating up to 300 kHz using SiC devices," in *Electronics and Application Conference and Exposition (PEAC), 2014 International*, Shanghai, 2014.

[26] J. Hostetler, P. Alexandrov, X. Li, L. Fursin and A. Bhalla, "6.5 kV SiC normally-off JFETs - technology status," in *Wide Bandgap Power Devices and Applications (WiPDA), 2014 IEEE Workshop on*, Knoxville, TN, 2014.

[27] F. Chevaliera, G. Grossetb, D. L., D. Tourniera, D. Plansona and P. Brosselarda, "A path toward high voltage devices : 3.3 kV 4H-SiC JBS and JFET," in

HETECH 2012, Barcelone, 2012.

[28] X. Song, A. G. Huang, C. Peng and L. Zhang, "Improved 6.5kV FREEMD-Pair based on SiC JFET and Si IGBT," in *IEEE Applied Power Electronics Conference and Exposition (APEC)*, Long Beach, CA, 2016.

[29] J. Biela, D. Aggeler, D. Bortis and J. W. Kolar, "Balancing circuit for a 5-kV/50-ns pulsed-power switch based on SiC-JFET super cascode," *IEEE Transactions on Plasma Science*, vol. 40, no. 10, pp. 2554-2560, 2012.

[30] A. Daniel, C. Francisco, B. Juergen and W. K. Johann, "Dv/Dt-Control methods for the SiC JFET/Si MOSFET cascode," *IEEE Transactions on Power Electronics*, vol. 28, no. 8, pp. 4074-4082, August 2013.

[31] N. Oswald, P. Anthony, N. McNeill and B. Stark, "An experimental investigation of the tradeoff between switching losses and EMI generation with hard-switched All-Si, Si-SiC, and All-SiC device combinations," *Power Electronics, IEEE Transactions on*, vol. 29, no. 5, pp. 2393-2407, 1 May 2014.

[32] D. Domes, C. Messelke and P. Kanschat, "1st Industrialized 1200V SiC JFET module for high energy efficiency application," Infineon Technologies AG., 2011.

[33] R. Chacko, M. Ravichandran, M. Sanoop, T. Sabu, V. Sadasivan Achari and C. Joseph, "Magnetic slip ring â€" Rotary transformer based novel non-contact signal transfer mechanism for spacecraft application," in *Emerging Research Areas: Magnetics, Machines and Drives (AICERA/iCMMD), 2014 Annual International Conference on*, 2014.

[34] R. Robutel, C. Martin, C. Buttay, H. Morel, P. Mattavelli, D. Boroyevich and R. Meuret, "Design and implementation of integrated common mode capacitors for SiC-JFET inverters," *Power Electronics, IEEE Transaction on*, vol. 29, no. 7, pp. 3525-3636, 2014.

[35] K. Li, A. Videt and N. Idir, "Characteriszation method of SiC-JFET interelectrode capacitances in linear region," *IEEE Transaction on Power Electronics*, vol. 31, no. 2, pp. 1528-1540, February 2016.

[36] S. Zeljkovic, R. Vuletic, A. Miller and A. Denais, "A three phase bidirectional V2G interface converter based on SiC JFETs," in *Power Electronics and Applications (EPE'15 ECCE-Europe), 2015 17th European Conference on*, Geneva, 2015.

[37] S. Chen, J. He and K. Sheng, "High-voltage full-SiC power module: Device fabrication, testing and high frequency application in kW-level converter," in *Power Semiconductor Devices & IC's (ISPSD), 2015 IEEE 27th International Symposium on*, 2015.

[38] A. Romani, A. Camarda, A. Baldazzi and M. Tartagni, "A micropower energy harvesting circuit with piezoelectric transformer-based ultra-low voltage start-up," in *Low Power Electronics and Design (ISLPED), 2015 IEEE/ACM International Symposium on*, Rome, 2015.

[39] R. Jacek, P. Dimosthenis and N. Hans-Peter, "Design steps towards a 40-kVA SiC JFET inverter with natural-convection cooling and an efficiency exceeding 99.5%," *IEEE Transaction on Industry Applications*, vol. 49, no. 4, pp. 1589-1598, July-August 2013.

[40] T. Friedli, S. D. Round, D. Hassler and J. W. Kolar, "Design and Performance of a 200-kHz All-SiC JFET Current DC-Link Back-to-Back Converter," *IEEE Transactions on Industry Applications*, vol. 45, no. 5, pp. 1868-1878, September/October 2009.

[41] D. Peftitsis, G. Tolstoy, A. Antonopoulos, J. Rabkowski, J.-K. Lim, M. Bakowski, L. Angquist and H.-P. Nee, "High power modular multilevel converter with SiC JFETs," *IEEE Transaction on Power Electronics*, vol. 27, no. 1, pp. 28-36, 2012.

[42] F. Xu, T. J. Han, D. Jiang, L. M. Tolbert, F. F. Wang, J. Nagashima, S. J. Kim, S. Kulkarni and F. Barlow, "Development of a SiC JFET-based six-pack power module for a fully integrated inverter," *IEEE Transaction on Power Electronics*, vol. 28, no. 3, pp. 1464-1478, 2013.

[43] C. Buttay, D. Planson, B. Allard, D. Bergogne, P. Bevilaqua, C. Jouber, M. Lazar and C. Martin, "State of the art of high temperature power electronics," *Materials Science and Engineering: B*, vol. 176, no. 4, pp. 283-288, 2011.

[44] W.-C. Lien, N. Damrongplasit, J. Paredes, D. Senesky, T.-J. Liu and A. Pisano, "4H-SiC N-Channel JFET for operation in high-temperature Environments," *Electron Devices Society, IEEE Journal of the*, vol. 2, no. 6, pp. 164 - 167, November 2014.

[45] D. J. Spry, P. G. Neudeck, L. Chen, D. Lukco, C. W. Chang and G. M. Beheim, "Prolong 500^0C demonstration of 4H-SiC JFET ICs with two-level interconnect," *IEEE Electron Device Letter*, pp. 625-628, 2016.

[46] P. G. Neudeck, D. J. Spry and L.-Y. Chen, "First-order SPICE modeling of extreme-temperature 4H-SiC JFET integrated circuit," 2016.

[47] G. Tolstoy, A. K. Dutta and M. S. Islam, "Experimental duarbility testing of 4H SiC JFET integrated circuit technology at 727^0C," in *Proc. SPIE 9836 Micro-and Nanotechnology Sensors, Systems, and Applications VIII*, Maltimore, Maryland, 2016.

[48] A. Rahman, A. M. Francis, S. Ahmed, S. K. Akula, J. Holmes and A. Mantooth, "High-temperature voltage and current references in Silicon Carbide CMOS," *IEEE Transactions on Electron Devices*, vol. 63, no. 6, pp. 2455-2461, 2016.

[49] D.-P. Sadik, J. Colmenares, D. Peftitsis, G. Tolstoy, J. Rabkowski and H.-P. Nee, "Analysis of short-circuit conditions for silicon carbide power transistors and suggestions for protection," in *Power Electronics and Applications (EPE'14-ECCE Europe), 2014 16th European Conference on*, Lappeenranta, 2014.

[50] G. Kampitsis, S. Papathanassiou and S. Manias, "Comparative evaluation of the short-circuit withstand capability of 1.2 kV Silicon Carbide (SiC) power transistors in real life applications," *Microelectronics Reliability*, vol. 55, no. 12, pp. 2640-2646, 2015.

[51] X. Li, H. Zhang, P. Alexandrov and A. Bhalla, "Medium voltage power switch based on SiC JFET," in *IEEE Applied Power Electronicss Conference and Exposition (APEC)*, Long Beach, CA, 2016.

[52] K. Y. J. Hsu and T.-W. Chuang, "An input buffer with monolithic JFET in standard BCD technology for sensor applications," in *Electron Devices and Solid-State Circuits (EDSSC), 2015 IEEE International Conference on*, Singapore, 2015.

[53] Z. Miao, G. Sabui, A. Chen, Y. Li, Z. Shen, J. Wang, Z. Shuai, A. Luo, X. Yin and M. Jiang, "A self-powered ultra-fast dc solid state circuit breaker using a normally-on SiC JFET," in *Applied Power Electronics Conference and Exposition (APEC), 2015 IEEE*, Charlotte, NC, 2015.

[54] Z. J. Shen, G. Sabiu, M. Zhenyu and S. Zhikang, "Wide-bandgap solid-state circuit breakers for dc power systems: device and circuit considerations," *Electron Devices, IEEE Transaction on*, vol. 62, no. 2, pp. 294-300, February 2015.

[55] V. Veliadis, B. Steinerb, K. Lawson, S. B. Bayne, D. Urciuo, H. Li and C. Ha , "Suitability of N-ON recessed implanted gate vertical-channel SiC JFETs for optically tyriggerred 1200 V solid-sate-circuit breaker," *IEEE Journal of Emerging and Slected Topics in Power Electronics*, vol. PP, no. 99, pp. 1-1, 2016.

[56] M. Kemptkes, I. Roth and M. Gaudreau, "Solid-state circuit breaker for medium voltage dc power," in *Proceedings IEEE Electric Ship Technologies Symposium*, Alexandria, VA, 2011.

[57] C. Meyer, S. Schroder and R. W. De Doncker, "Solid-state circuit breakers and current limiters for medium-voltage systems having distributed power systems," *IEEE Transactions on Poer Electronics*, vol. 19, no. 5, pp. 1333-1340, September 2004.

[58] D. P. Sadik et al, "Short-circuit protection circuits for Silicon Carbide power transistors," *IEEE transaction on Industrial Electronics*, vol. 63, no. 4, pp. 1995-2004, April 2016.

[59] Z. Miao, G. Sabui, A. Maradkhani Roshandeh and Z. J. Shen, "Design and analysis of DC solid state circuit breakers using SiC JFET," *IEEE Journal of Emerging and Selected Topics in Power Electronics*, pp. 1-1, 2016.

[60] X. Li, A. Bhalla, P. Alexandrov and L. Fursin, "Study of SiC vertical JFET behavior during unclamped inductive switching," in *Applied Power Electronics Conference and Exposition (APEC), 2014 Twenty-Ninth Annual IEEE*, Fort Worth, TX, 2014.

[61] C. Sizhe, H. Junwei, W. Hengyu and S. Kuang, "Fabrication and testing of 3500V/15A SiC JFET based power module for high-voltage, high-frequency applications," in *Applied Power Electronics Conference and Exposition (APEC) 2015 IEEE*, Charlotte, NC, 2015.

[62] A. Huang, X. Song and L. Zhang, "6.5 kV Si/SiC hybrid power module: An ideal next step?," in *Integrated Power Packaging (IWIPP), 2015 IEEE International Workshop on*, Chicago, Il, 2015.

[63] D. Heer, R. Bayerer and D. Domes, "SiC-JFET in half-bridge configuration - parasitic turn-on at current commutation," in *PCIM Europe 2014; International Exhibition and Conference for Power Electronics, Intelligent Motion, Renewable Energy and Energy Management; Proceedings of*, Nuremberg, Germany, 2014.

[64] P. Hazdra, S. Popelka, V. Zahlava and J. Vobecky, "Radiation damage in 4H-SiC and its effect on power electronic characteristics," *Solid State Phenomena*, vol. 242, pp. 421-426, 2016.

[65] E. Velander, A. Lofgren, K. Kretschmar and H.-P. Nee, "Novel solutions for suppressing parasitic turn-on behaviour on lateral vertical JFETs," in *Power Electronics and Applications (EPE'14-ECCE Europe), 2014 16th European Conference on*, 2014.

[66] X. Ni, R. Gao, X. Song, A. Huang and W. Yu, "Development of 6kV SiC hybrid power switch based on 1200V SiC JFET and MOSFET," in *Energy Conversion Congress and Exposition (ECCE), 2015 IEEE*, 2015.

[67] K. Okamura, K. Ise, M. Wake, Y. Osawa, K. Takaki and K. Takayama, "Characterization of SiC JFET in novel packaging for 1 MHz Operation," *Materials Science Forum*, Vols. 717-720, pp. 1029-1032, May 2012.

[68] T. Singh and E. Kohn, "Harsh environment materials," in *Reference module in materials science and material engineering*, 2016.

[69] S. Hazra, A. De, L. Cheng, J. Palmour, M. Schupbach, B. Hull, S. Allen and S. Bhattacharya, "High switching performance of 1700V, 50A SiC power MOSFET over Si IGBT/BiMOSFET for advanced power conversion applications," *Power Electronics, IEEE Transactions on*, vol. PP, no. 99, p. 1, 2015.

[70] K. Chen, Z. Zhao, L. Yuan, T. Lu and F. He, "The Impact of Nonlinear Junction Capacitance on Switching Transient and Its Modeling for SiC MOSFET," *Electron Devices, IEEE Transactions on*, vol. 62, no. 2, pp. 333-338, February 2015.

[71] J. Fabre, P. Ladoux and M. Piton, "Characterization and Implementation of Dual-SiC MOSFET Modules for Future Use in Traction Converters," *Power Electronics, IEEE Transactions on*, vol. 30, no. 8, pp. 4079-4090, August 2015.

[72] K. Koiwa and J.-I. Itoh, "A Maximum Power Density Design Method for Nine Switches Matrix Converter Using SiC-MOSFET," *Power Electronics, IEEE Transactions on*, vol. 30, no. 2, pp. 1189-1202, February 2016.

[73] X. Yang, B. Lee and V. Misra, "Investigation of Lanthanum Silicate conditions on 4H-SiC MOSFET characteristics," *Electron Devices, IEEE Transactions on*, vol. 62, no. 11, pp. 3781-3785, November 2015.

Frederick Ojiemhende Ehiagwina was born in 23rd December, 1985 in Benin City, Edo state, Nigeria. He obtained his Bachelor degree in Electrical Electronics Engineering from Ambrose Alli University, Ekpoma, Edo state, Nigeria in April 2010. He did his Masters Degree in Electrical Engineering (Electronics and Telecommunication option) from the university of Ilorin, Kwara state Nigeria. His research interest include: optimization of telecommunication systems, design and characterization of

electronics system, reliability assessment of electrical and electronics systems, and renewable energy. He is currently a Lecturer III in the Federal Polytechnic, Offa, Kwara state, Nigeria. Mr. Ehiagwina has started Membership registration with IEEE. He has more that 6 conference or journal papers.

Olufemi Oluseye Kehinde obtained his Bachelor degree in Electrical and Electronics Engineering in 1992 from Abubakar Tafawa Balewa University, Bauchi, Bauchi state, Nigeria. In 2013 he had his Masters Degree in Information Technology, fron the National Open University of Nigeria, Ilorin, Study Centre. He is currently pursueing his PhD in Electronics Engineering in Atlantic International University, Hawaii, USA.
He is currently a Lecturer I in the Federal Polytechnic, Offa, Kwara state, Nigeria. Engr. Kehinde is a cooperate Member, Nigerian Society of Engineers (MNSE), a registered Member of Council for the Regulation Of Engineering in Nigeria (COREN) and Member, IEEE, where he equally belongs to Communication and Computer Society. Finally, he is a Member, Nigerian Institute of Electrical and Electronics Engineers (NIEEE).

Afolabi Lateef Olashile was born in 13th September, 1985 in Offa, Kwara state, Nigeria. He obtained his Bachelor of Engineering degree in Electrical Electronics Engineering from University of Ilorin, Ilorin, Kwara state, Nigeria in 2008. He is currently doing his Masters Degree Electrical Engineering from the university of Ilorin, Kwara state Nigeria. He is assessing the reliability values of electric pumping systems of water stations. He is currently an Assistant Lecturer in the Federal Polytechnic, Offa, Kwara state, Nigeria.
Mr. Afolabi is a Cooperate member of Nigerian Society of Engineering (MNSE). He is also a member Nigerian Institute of Management (NIM).

Onawola Hassan Jimoh obtained his First Degree in Electrical & Computer Engineering in 1995 from The Federal University of Technology, Minna (FUTMIN), Niger State, Nigeria and a Masters Degree in Information Systems from Coventry University, UK. He is a Principal Lecturer & currently Head of Department, Computer Engineering, Federal Polytechnic, Offa, Kwara State, Nigeria. Engr. H. J. Onawola is registered with a number of professional bodies such as The Council for the Regulation of Engineering in Nigeria (COREN). He is a Member, Nigeria Institute of Engineering Management (MNIEM), and Graduate Member Nigerian Institute of Safety Professionals (GMNISP). He is also corporate member Nigerian Society of Engineers and has some Publications published in reputable Journals.

Nurudeen Ajibola Iromini obtained a Higher National Diploma in Computer Science from Osun State Polytechnic, Iree, Osun State in 2003. In 2008 he obtained a Bachelor of Technology in Computer Engineering from Ladoke Akintola University, Ogbomoso, Oyo State, Nigeria. He obtained a Masters Degree in Computer Science in 2012 from the the University of Ibadan, Oyo State.

Engr. N. A. Iromini is registered The Council for the Regulation of Engineering in Nigeria (COREN).

Admission Control Methods in IMS Networks

Erik Chromy, Matej Kavacky and Lubomir Dresto

***Abstract*—In this paper we present admission control methods for IMS network. The task of RACS block is to accept or reject new connection into the network. The main goal of the admission control method is to ensure the Quality of Service not only for new connection but also for already accepted connections. We discuss and compare three admission control algorithms in the paper from the qualitative parameters point of view.**

***Keywords*—Admission Control, MBAC, IMS, Quality of Service.**

I. IP Multimedia Subsystem

IMS (IP Multimedia Subsystem) is a standardized NGN (Next Generation Network) architecture for the telecom operators in order to offer mobile and multimedia services such as IPTV (Internet Protocol Television), VoIP (Voice over Internet Protocol) and many others. The main goal of IMS is the provision of new services as well as all present and future services that can provide telecommunications network. Telecom operators can provide their services to users regardless of their location, access technology and terminals. To achieve these objectives, the IMS defines a complete architecture that enables the convergence of voice, video and data across the infrastructure based on IP protocol. This system allows interoperability between mobile and IP architecture, therefore the IMS system is independent of the access technology that supports packet-switched network such as GPRS (General Packet Radio Service), UMTS (Universal Mobile Telecommunications System), CDMA2000 (Code Division Multiple Access 2000), WLAN (Wireless Local Area Network), WiMAX (World Interoperability For Microwave Access) and DSL (Digital Subscriber Line). The older technologies such as PSTN (Public Switched Telephone Network) and GSM (Global System for Mobile Communications) are supported through the gateways. The main characteristic of the IMS architecture is the distribution of network infrastructure to the separate functions with standardized interfaces.

An important control function of NGN plays the control layer whose main goal is traffic routing, traffic acceptance or billing information provision. The control layer also controls the user traffic transmitted through the RACS (Resource and Admission Control Sub-system) component [1]-[4].

Manuscript received July 22, 2016, revised August 30.

This article was created with the support of the Ministry of Education, Science, Research and Sport of the Slovak Republic within the KEGA agency project - 007STU-4/2016 named: Progressive educational methods in the field of telecommunications multiservice networks.

E. Chromy is with the Slovak University of Technology, Faculty of Electrical Engineering and Information Technology, Departement of Telecommunications, Ilkovicova 3, 812 19 Bratislava, Slovakia (e-mail: chromy@ut.fei.stuba.sk).

M. Kavacky is with the Slovak University of Technology, Faculty of Electrical Engineering and Information Technology, Departement of Telecommunications, Ilkovicova 3, 812 19 Bratislava, Slovakia (e-mail: kavacky@ut.fei.stuba.sk).

L. Dresto is with the Slovak University of Technology, Faculty of Electrical Engineering and Information Technology, Departement of Telecommunications, Ilkovicova 3, 812 19 Bratislava, Slovakia (e-mail: lubdresto@gmail.com).

A. Resource and Admission Control Sub-system

RACS is the most important logical network element which is intended to reserve resources, access control and support for QoS (Quality of Service). RACS block is composed of PDF (Policy Decision Function) and A-RACF (Access-Resource and Admission Control Function) components. PDF implement local rules on the use of resources, it is used for example for overload protection of specific access media element and A-RACF controls the QoS network parameters.

II. Admission Control Methods

For the support of the real-time and multimedia applications, the QoS must be guaranteed in the network. The result of admission control is to accept or reject an incoming connection. The main criteria of admission control is to provide the QoS for new connection while maintaining QoS of already accepted connections [5]-[7].

AC methods can be divided into two categories: PBAC (Parameter Based Admission Control) and MBAC (Measurement Based Admission Control).

PBAC methods are applicable on total traffic characteristics such as for example peak transmission rate. Based on this focus the method determines the required network resources for all connections. MBAC methods focus on measurements of the current network traffic. This method accepts connections on the basis of measurements performed in the network [8].

The traffic characteristics of many applications are not known. In the case of small knowledge of traffic parameters, often the overstated bandwidth is allocated in order to ensure the required QoS. This leads to under utilization of network resources. Therefore the use of MBAC methods can ensure the better utilization of network resources and effective provision of the QoS.

The admission control is needed to accept new connections, respectively services. This control ensures QoS for the transmitted data. By use of admission control methods, it is possible to design a model of admission control that will ensure a certain quality of service. Created models may be used alone, or may be complementary (to achieve better QoS). The admission control of incoming flows is the most important step in order to ensure QoS. This control is provided by AC (Admission Control) methods. A key function of the AC methods is to estimate the anticipated bandwidth of incoming connection and the analysis of the current utilization of the network load, whereby it is possible to allocate a given bandwidth for connection. AC methods are mostly used for

services sensitive to delay and jitter, respectively for real-time applications.

Various admission control methods have been proposed and their difference lies mainly in various types of functionality and method of implementation. Some AC methods are based on mathematical calculations and statistical indexes and the other on traffic measurements. To ensure required QoS the AC methods should fulfill certain conditions:

- they should avoid delay by fast decision process,
- they should not affect already accepted connections and ensure QoS of requesting connection,
- they should have simple implementation into the system,
- they should effective allocate required bandwidth to data flows and efficient utilization of the link capacity.
- they should effective allocate required bandwidth to data flows and efficient utilization of the link capacity.

The use of AC methods plays a key role particularly in the field of access networks, which unlike the core networks do not have such high transmission bandwidth. The actual information about calculated bandwidth is sent to border nodes, what produces unnecessary traffic in the core network. Therefore the AC methods are applied in the access part of the network [9].

A. MBAC Methods

The MBAC methods are based on measurements of current state of output network interface or actual network state in order to make decision if the new data flow should be accepted to the network. The MBAC methods accept new data flows until measurement results reach defined values of capacity (usually recommended value is 90% of network capacity). The measurement process is needed for use of MBAC methods [10]-[12].

For measurement realization we need to know the link utilization and only minimal knowledge of connection source. Decision process of MBAC methods is based on measurement of traffic and QoS parameters. Interval measurements ensure efficient resource utilization in the case of data bursts creation or when the data transmission is slower than the peak transmission rate.

III. MBAC Algorithms

Various algorithms for admission control based on measurements have been proposed in the literature. Our paper addresses following algorithms:

- Simple Sum,
- Estimated Sum,
- Acceptance Region.

A. Simple Sum

Simple Sum is simple algorithm which ensures sufficient bandwidth for accepted flows. AC method accepts new data flow only in the case the following condition is true:

$$v + r_\alpha < C \tag{1}$$

where *v* [kbit/s] denotes the sum of reserved transmission rates, *C* [kbit/s] denotes link capacity, α is index for requesting data flow and r_α [kbit/s] denotes peak transmission rate of new data flow.

B. Estimated Sum

This algorithm samples traffic data during the defined intervals. These input samples represent the input data for prediction. After every sampling the prediction of future data transmission is done. Such prediction will be used for future connection acceptance or rejection. The decision process is based on the equation:

$$\hat{y}(n+1) + p_\alpha \leq \mu.C \tag{2}$$

where, α denotes index for requesting data flow, $\hat{y}(n+1)$ [kbit/s] denotes prediction of aggregated traffic used in next sampling *(n+1)*, p_α [kbit/s] denotes peak transmission rate of new flow, *C* [kbit/s] is link capacity, μ represents the channel utilization.

C. Acceptance Region

This algorithm [10] predicts region of maximal link utilization at the expense of packet losses. Estimation of Acceptance region can be based on the parameters such as bandwidth, switch buffer, and parameters of stack buffer filters. The calculation of acceptance region assumes Poisson distribution of incoming independent requests. The algorithm ensures that the sum of measured traffic and transmission rates of new flows will not exceed the acceptance region.

$$C(S) = \frac{1}{S}.log[1 + \frac{v}{p}(e^{Sp} - 1)] \tag{3}$$

where, *C* [kbit/s] represents estimation of bandwidth for total traffic, *v* [kbit/s] denotes average transmission rate of traffic, *p* [kbit/s] denotes peak transmission rate, *S* represents space parameter within the range (0,1).

IV. Simulations

The simulations of MBAC algorithms were performed in MATLAB environment. The principle of admission control methods is depicted in Fig. 1, where *n* represents number of data flows (Variable Bit Ratel) and the maximal link capacity is set to 1 Mbit/s (sufficient for the simulation results). The AC method accepts only such number of flows which ensures that the maximal link bandwidth will be not exceeded.

Data flows come in random times. These data flows have different requirements on network in different times. It means that the peak transmission rate of particular data flows vary during time. In our paper we assume exponential distribution with mean value (λ) set to 64 [kbit/s]. Current traffic is simulated with sample of 250 time points during which the loss parameter of particular flows is calculated.

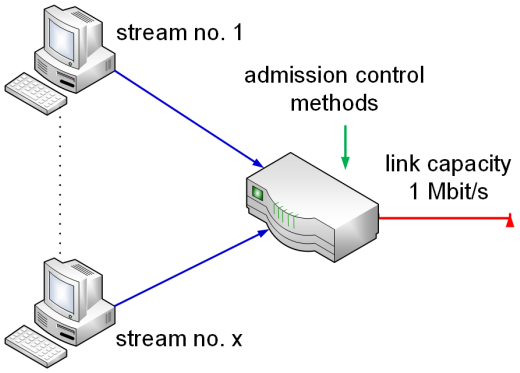

Fig. 1. Principle of admission control simulation

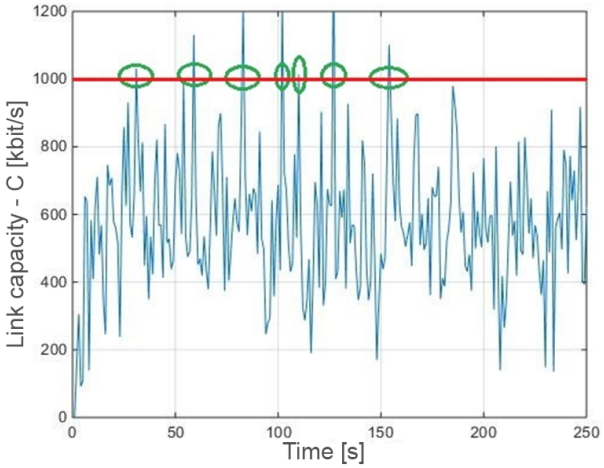

Fig. 2. Simulation results for Simple Sum algorithm

A. Simple Sum Algorithm Simulation

The Simple Sum is the simplest admission control algorithm. It accepts or rejects requesting connection according to available bandwidth. The simulation results for this algorithm are depicted in Fig. 2. The red line represents the maximal allowed link capacity and it is set to 1 Mbit/s. This value can not be exceeded by decision result. The blue curve represents the current network traffic consisting of 10 accepted data flows (i.e. on the base of simulations, the Simple Sum algorithm has accepted 10 flows). Green circles are points in which link capacity was exceeded. When the link capacity is exceeded, packet losses will occur. The main task of AC method is to ensure QoS and it is not sufficiently ensured when there are packet losses. We can see in Fig. 2 that in some time points the link utilization is only around 50% of allowed capacity. The main factor of AC method evaluation in our paper is loss. The Simple Sum algorithm reached 3% loss.

B. Estimated Sum Algorithm Simulation

Estimated Sum algorithm makes decision of acceptance or rejection of requesting connection based on estimation of the future traffic while uses only part of link capacity. In our simulation this part of link capacity was set to 90% of total link capacity (brown line in Fig. 3). The red line represents the maximal allowed link capacity. Blue curve represents the

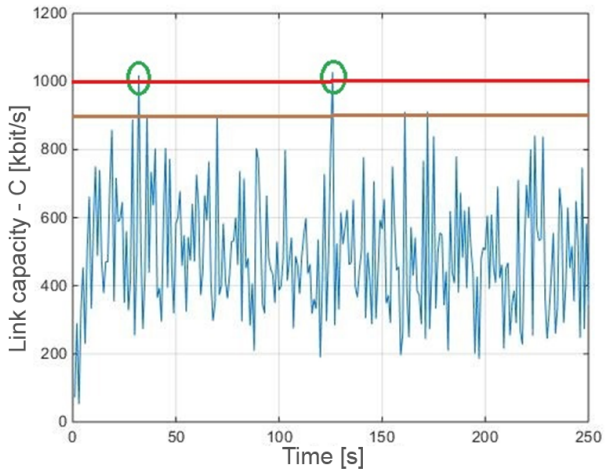

Fig. 3. Simulation results for Estimated Sum algorithm

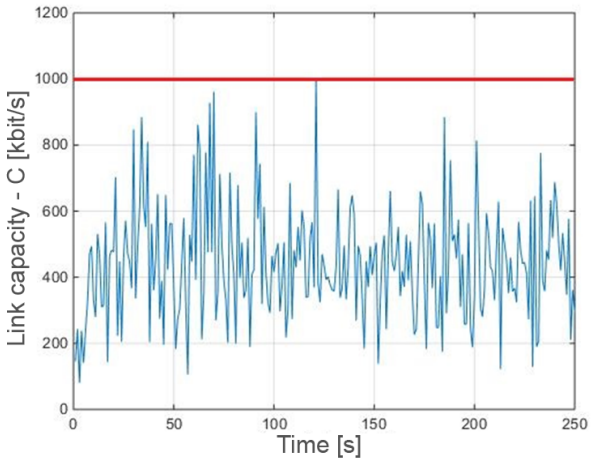

Fig. 4. Simulation results for Acceptance Region algorithm

current traffic consisting of 9 data flows accepted by Estimated Sum algorithm. Green circles are points in which available link capacity was exceeded. The Estimated Sum algorithm accepted 1 less connection than Simple sum algorithm, but the loss is only 1%. From this point of view the Estimated Sum algorithm is better for admission control than Simple Sum algorithm.

C. Acceptance Region Algorithm Simulation

Simulation results for Acceptance Region algorithm are depicted in Fig. 4. Compared to Simple Sum and Estimated Sum algorithms this algorithm is more complicated because more input parameters are used. Decision process of this algorithm is based on area of maximal link utilization at the expense of data loss. Space parameter S within the range (0,1) is set to 0,5 due to most precise measurement. Red line represents the maximal allowed link capacity. Blue curve represents the current traffic consisting of 8 data flows accepted by this algorithm. It is the smallest number of accepted connections from performed simulations, but data loss is zero, therefore sufficient QoS is ensured.

V. DISCUSION

Performed simulations demonstrate the field of admission control methods in IMS networks. Selected algorithms accept or reject connections into the network on the basis of different ways and methods. From the simulation results we can see that for given link capacity particular algorithms accept different number of connections while each of them aims to ensure some level of QoS. But not all of them can achieve the sufficient level of QoS. In our paper we have observed data loss as main parameter for comparison of simulated admission control algorithms.

The Simple Sum algorithm has accepted 10 data flows at the loss of 3%. Estimated Sum algorithm has accepted 9 data flows at the loss of 1%. The best algorithm from loss point of view appears the Acceptance Region with 8 accepted data flows and zero loss. Therefore only this last algorithm has achieved the required QoS in proposed network.

VI. CONCLUSION

The admission control in IMS network is actual and perspective research subject today. The RACS block is network component in which admission control methods should be implemented. There is not any actual standard with recommendation which AC method should be preferred for the particular services.

In our paper we have observed three admission control algorithms. These algorithms are not used for IPTV or VoIP traffic. In our simulations we have observed these methods in general - the input flow with variable bit rate character was used. In the future work detailed analysis of selected AC methods for particular services will be performed.

REFERENCES

[1] ETSI Standard, ETSI ES 282 003 V1.1.1(2006-06): *Telecommunications and Internet converged Services and Protocols for Advanced Networking (TISPAN); Resource and Admission Control Sub-system (RACS); Functional Architecture*

[2] H. Zeng, Y. Gao and Y. Xia, *On NGN Architecture And Evolution Strategy*, Innovations in NGN: Future Network and Services, 2008. K-INGN 2008. First ITU-T Kaleidoscope Academic Conference, 2008, pp. 337-342, ISBN: 978-92-61-12441-0

[3] H. Allouch and M. Belkasmi, *Design of distributed IMS by classification and evaluation of costs for secured architecture*, Innovative Computing Technology (INTECH), 2012 Second International Conference on. 2012, pp. 291-296, ISBN: 978-1-4673-2678-0

[4] M.A. Qadeer and A.H. Khan, *IMS Network Architecture*, International Conference on Future Computer and Communication, 2009, ICFCC 2009, pp. 329-333, ISBN: 978-0-7695-3591-3

[5] E. Chromy, M. Jadron, M. Kavacky and S. Klucik, *Admission Control in IMS Networks*, Advances in Multimedia, vol. 2013, Article ID 918930, 7 pages, 2013, ISSN:1687-5680 (Print),ISSN:1687-5699 (Online), DOI:10.1155/2013/918930

[6] A.W. Moore, *Measurement- Based Management of Network Resources*, A dissertation submitted for the degree of Doctor Philosophy of University Cambridge, June, 2001

[7] E. Chromy, M. Weber and T. Behul, *Admission Control Methods and Quality of Service*, Workshop of the 12th International Conference KTTO 2012, November, 2012, Malenovice, Czech Republic, pp. 36-40, ISBN 978-80-248-2810-7

[8] L. Yuan-Cheng and T. Sheng-Fu, *Unfairness of Measurement-based Admission Controls in a Heterogeneous Environment*, 8th International Conference on Parallel and Distributed Systems, ICPADS 2001, June, 2001, Kyongju City, pp. 667-674, ISBN: 0-7695-1153-8, DOI: 10.1109/ICPADS.2001.934882

[9] S. Jamin, S.J. Shenker and P.B. Danzig, *Comparision of Measurement-based Admission Control Algorithms for Controlled-Load Service*, INFOCOM '97, 16th Annual Joint Conference of the IEEE Computer and Communications Societies. Driving the Information Revolution, April, 1997, Kobe, pp. 973-980, ISBN: 0-8186-7780-5, DOI: 10.1109/INFCOM.1997.631035

[10] S. Jamin and S. Shenker, *Measurement-based Admission Control Algorithms for Controlled-load Service: A Structural Examination*, Michigan: University of Michigan, 1997, Technical Report.CSE-TR-333-97

[11] M. Egyhazy and Y. Liang, *Predicted Sum: A Robust Measurement-Based Admission Control with Online Traffic Prediction*, IEEE Communications Letters, 2007, Vol.11, Issue 2, pp.204-206, ISSN: 1089-7798, DOI: 10.1109/LCOMM.2007.061127

[12] S.Y. Yerima, *Implementation and Evaluation of Measurement-based Admission Control Schemes within a Converged networks QoS Management Framework*, International Journal of Computer Networks & Communications (IJCNC) Vol.3, No. 4, July, 2011, DOI: 10.5121/ijcnc.2011.3410

Erik Chromy was born in Velky Krtis, Slovakia, in 1981. He received the M.Sc. degree in telecommunications in 2005 from Faculty of Electrical Engineering and Information Technology of Slovak University of Technology (FEI STU) Bratislava. In 2007 he submitted PhD work. His scientific research is focused on queueing systems, contact center and admission control methods. Nowadays he works as assistant professor at the Institute of Telecommunications of FEI STU Bratislava.

Matej Kavacky was born in Nitra, Slovakia, in 1979. He received the M.Sc. degree in telecommunications in 2004 from Faculty of Electrical Engineering and Information Technology of Slovak University of Technology in Bratislava (FEI STU). In 2006 he submitted PhD. work Quality of Service in Broadband Networks. His scientific research is focused on admission control methods Nowadays he works as assistant professor at the Institute of Telecommunications of FEI STU Bratislava.

Lubomir Dresto was born in Ilava, Slovakia, in 1991. He received the M.Sc. degree in telecommunications in 2016 from FEEIT STU in Bratislava. His scientific research is focused on admission control methods.

Performance Analysis of Quantized Feedback JLS Precoder in CoMP transmission

Yasmine Fahmy

***Abstract*—Joint Processing (JP) in Coordinated Multi-Point (CoMP) transmission allows user data to be jointly processed by several interfering base stations to achieve high performance and large capacity gain. This is achieved by making use of timing advance mechanisms; to ensure that the desired signals from the cooperating cells reach the mobile station at exactly the same time. The Joint Leakage Suppression (JLS) precoder is a suitable linear precoding scheme in this scenario. In this paper, JLS performance analysis is considered under real assumptions such as the presence of asynchronous reception of the interfering signals and the effect of the finite capacity backhaul links. The effect of quantizing the feedback channel on the sum rate is derived, and a tight upper bound of the rate loss due to quantization is obtained. Simulation results are provided to validate these results.**

***Keywords*—CoMP transmission, JLS precoder, asynchronous interference, quantized feedback.**

I. Introduction

Coordinated Multi-Point transmission/reception (CoMP) has been considered by the 3^{rd} Generation Partnership Project (3GPP) as a candidate technique for LTE-Advanced systems [1], [2]. CoMP has been proposed to increase the average cell throughput and the cell edge user throughput in both the uplink and downlink [3]. Several precoding schemes can be used to support CoMP transmission and achieve these objectives. Among these schemes is the Dirty Paper Coding (DPC) scheme [4], [5], which achieves the capacity of MU-MIMO downlink channel, however, its complexity stands up against its practical implementation. Other non-linear precoding techniques including Tomlinson-Harashima precoding [6], or multi-user detection in Mobile Stations (MSs) [7] are approaching such capacity, but they still suffer from prohibitive complexity. Therefore, there is great interest in linear precoding designs. Such linear precoding schemes have shown adequate performance. For example, the Zero Forcing (ZF) precoder only loses about 1.26 dB compared to DPC when having 10 transmit antennas and 5 receive antennas [8].

Joint processing transmission requires sharing the data stream of the MS among all cooperative BSs, in addition to the Channel State Information (CSI) and the propagation delay information from each BS to each MS to allow timing advance mechanisms to be used. However, such feedback requires infinite backhaul capacity. Practically, the backhaul has limited rate, and therefore each BS should consider quantizing the shared information with other cooperating BSs. Typically, CSI is quantized and shared first in joint processing transmission, then only a sub-stream of user data or a quantized version of the antenna signals is shared among the base stations, which allows partial interference cancellation [9]. In [10], the impact of quantized and delayed CSI on the average achievable rate is derived. Accurate approximations on the expected sum rate of CoMP systems with imperfect CSI are also given.

Advancing the signal from each BS in the cooperative set to reach the intended user at exactly the same time, results in asynchronous reception of these signals at other users. This opened the way for different precoding schemes that can account for the problem of asynchronous interference.

Taking the ZF precoder that can achieve the ergodic sum capacity in limit of large number of active users [11], it can no longer cancel all the interference in the presence of asynchronous interference, except under severe limitations, where the number of antennas of all users must be less than the number of transmit antennas in each BS [12]. In [13], a new MMSE design was investigates in CoMP system. The proposed scheme is robust to the asynchronous interference and the channel quantization errors. Joint Leakage Suppression (JLS) was proposed in [14] to minimize the co-channel interference (CCI) instead of canceling it out completely. This technique aims at maximizing the Signal to Leakage plus Noise Ratio (SLNR) for all users simultaneously. Where, compared to zero-forcing precoding, JLS method can minimize the asynchronous interference without imposing any conditions on the relation between the number of transmit and receive antennas. Moreover, it avoids noise enhancement.

In this paper, the finite rate feedback-JLS precoder is presented where a tight upper bound for the rate loss due to channel quantization is derived in two different scenarios; the synchronous interference scenario, and the more realistic scenario of asynchronous interference. The rate loss of other precoders has been studied in the literature for multi-cell systems. In [15] and [16], the rate loss, as a function of the quantization error when using generalized eigenvector beamforming in a rate-limited environment, is studied. However, the expression derived for the rate loss is kept as a function of the quantization error of both the desired and interfering channel vectors, while this quantization error has not been analyzed. This quantization error analysis differs in case of multi-cell MIMO than the case of single-cell MIMO, and that is what will be presented in the following section. Moreover, no analysis has been carried out for the JLS precoder before. As explained earlier, this precoder is a practical choice for the implementation of the multi-cell MIMO in the presence of asynchronous interference.

Manuscript received March 10, 2016; revised September 28, 2016.

Y. Fahmy is with Electronics and Communication department, Cairo University, Egypt, e-mail: yfahmy@cws-cufe.org.

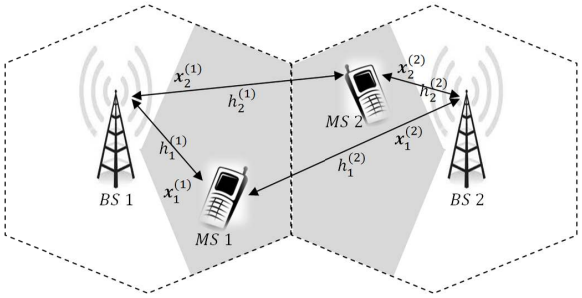

Fig. 1. System Model

The rest of this paper is organized as follows. Section II presents the asynchronous interference systems model, then the design criteria of the JLS precoder is given. In section III, the JLS rate is derived. Section IV presents the analysis of the quantization error of the random vector quantizer in the MU-CoMP network, then the rate loss due to feedback quantization is presented, in the synchronous idealized scenario. The proof is then extended to the more realistic case of asynchronous interference. Section V presents the simulation results, verifying the analytical results obtained for the rate loss, under both scenarios. Finally, Section VI concludes the paper.

II. Asynchronous Interference System Model

The system model considers a MU-CoMP network [1] where B Base Stations (BSs), having N_T antennas each, cooperate together to send data to K Mobile Stations (MSs), with N_R antennas each. The cooperative BSs together transmit L_k data streams to MS k, where the transmit vector from BS b to MS k is linearly precoded by the $N_T \times L_k$ matrix $\boldsymbol{T}_k^{(b)}$. If $\boldsymbol{s}_k(m)$ is the zero-mean data vector, of size $L_k \times 1$ at time m meant for MS k, then the transmit vector from BS b to MS k is $\boldsymbol{x}_k^{(b)}(m) = \boldsymbol{T}_k^{(b)} \boldsymbol{s}_k(m)$. The data vector has normalized power such that $E\left[\boldsymbol{s}_k(m)\boldsymbol{s}_k(m)^\dagger\right] = \mathbf{I}_{L_k}$, where $\mathbf{I}_{L_k}$ is the identity matrix of size L_k and $[.]^\dagger$ is the Hermitian transpose. Data vectors for different users are independent of each other, i.e., $E\left[\boldsymbol{s}_k(m)\boldsymbol{s}_l(m)^\dagger\right] = \mathbf{0}$, for $k \neq l$. A linear modulation with a unit energy baseband signature waveform $g(t)$ of duration T_s is used. The system model is shown in Fig. 1.

Assume that $\boldsymbol{h}_k^{(b)}$ is the $N_R \times N_T$ baseband matrix representation of the channel from BS b to MS k, having complex Gaussian elements. Different links are assumed to be independent of each other and undergo frequency-flat Rayleigh fading. Also, block fading channel model with large enough coherence time is used, such that the channel fading remains the same over the duration in which $\boldsymbol{T}_k^{(b)}$ is used.

In order to guarantee simultaneous reception of $\left\{\boldsymbol{x}_k^{(b)}(m)\right\}_{b=1}^{B}$ at MS k, each BS b advances the transmission time of $\boldsymbol{x}_k^{(b)}(m)$ by $\triangle\tau_k^{(b)} = \tau_k^{(b)} - \tau_k^{(b_k)}$ such that all $\left\{\boldsymbol{x}_k^{(b)}(m)\right\}_{b=1}^{B}$ arrive with the same delay $\tau_k^{(b_k)}$, where b_k is the closest BS to MS k. The equivalent received baseband signal at MS k is

$$\boldsymbol{r}_k(t) = \sum_{m=0}^{\infty}\left(g(t-mTs-\tau_k^{(b_k)})\boldsymbol{H}_k\boldsymbol{x}_k(m)\right) + \boldsymbol{n}_k(t) + \sum_{\substack{j=1\\ j\neq k}}^{K}\sum_{b=1}^{B}\sum_{m=0}^{\infty}\left(g(t-mTs-\tau_k^{(b)}+\triangle\tau_j^{(b)})\boldsymbol{h}_k^{(b)}\boldsymbol{x}_j^{(b)}(m)\right),$$

where $\boldsymbol{n}_k(t)$ is the additive white Gaussian noise vector with zero mean and variance N_0. $\boldsymbol{H}_k$ is the $N_R \times BN_T$ composite channel matrix of user k defined as $\boldsymbol{H}_k = [\boldsymbol{h}_k^{(1)}, \ldots, \boldsymbol{h}_k^{(B)}]$, and $\boldsymbol{x}_k(m)$ is the composite data matrix, defined as $\boldsymbol{x}_k(m) = [\boldsymbol{x}_k^{(1)}(m)^\dagger, \ldots, \boldsymbol{x}_k^{(B)}(m)^\dagger]^\dagger$.

In the asynchronous interference case, when the received signal is passed through a filter matched to $g(t-mTs-\tau_k^{(b_k)})$, the resulting signal is given by

$$\begin{aligned}\boldsymbol{y}_k(m) &= \boldsymbol{H}_k\boldsymbol{T}_k\boldsymbol{s}_k(m) + \boldsymbol{n}_k(m)\\ &+ \sum_{\substack{j=1\\ j\neq k}}^{K}\sum_{b=1}^{B}\boldsymbol{h}_k^{(b)}\boldsymbol{T}_j^{(b)}(m)\boldsymbol{i}_{jk}^{(b)}(m),\end{aligned} \quad (1)$$

where $\boldsymbol{i}_{jk}^{(b)}(m)$ is the asynchronous interference arising from two consecutive symbols with indices $m_{jk}^{(b)}$ and $m_{jk}^{(b)}+1$ at MS k from the signal transmitted by BS b for MS j.

The statistical characteristics of the asynchronous interference are $E[\boldsymbol{i}_{jk}^{(b)}(m)] = \mathbf{0}$ and

$$E[\boldsymbol{i}_{j_1k}^{(b_1)}(m)\boldsymbol{i}_{j_2k}^{(b_2)}(m)^\dagger] = \begin{cases}\mathbf{0} & j_1 \neq j_2 \neq k\\ \beta_{jk}^{(b_1,b_2)}\boldsymbol{I}_{l_j} & j_1 = j_2 = j \neq k\\ \boldsymbol{I}_{l_j} & j_1 = j_2 = j = k\end{cases}$$

where the asynchronous interference correlation $\beta_{jk}^{(b_1,b_2)}$ is given in [12].

III. JLS Precoder Performance

The goal of the JLS precoder [14] is to jointly optimize the transmitter precoding matrices $\boldsymbol{T}_k$ to maximize the SLNR, subject to the following two constraints: first, $Tr\{\boldsymbol{T}_k^\dagger\boldsymbol{T}_k\} \leq P_k^{tx}$, where P_k^{tx} is the transmitted power to MS k, for $1 \leq k \leq K$. This uniform per-MS power constraint, $P_k^{tx} = P_T$, for all k, ensures "power fairness" for different users. Even though, the per-BS power constraint makes more physical sense, the advantage of the MS-specific power constraint is that it is more amenable to analytically tractable solutions. The second design constraint we have is that $B.N_T \geq \sum_{k=1}^{K} L_k$.

The SLNR is defined as the ratio between the power of the desired signal at MS k and the sum of noise power plus total interference power (leakage) due to MS k at all other MSs. From which the SLNR, for the idealized synchronous case, was given in [14] by

$$\mathrm{SLNR}_k = \frac{P_k^{tx}\cdot Tr\left(\boldsymbol{Q}_k^\dagger\boldsymbol{H}_k^\dagger\boldsymbol{H}_k\boldsymbol{Q}_k\right)}{Tr\left(\boldsymbol{Q}_k^\dagger\left(N_0N_R\boldsymbol{I}_{BN_T} + P_k^{tx}\tilde{\boldsymbol{H}}_k^\dagger\tilde{\boldsymbol{H}}_k\right)\boldsymbol{Q}_k\right)} \quad (2)$$

where $\boldsymbol{Q}_k = \frac{1}{\sqrt{P_k^{tx}}}\boldsymbol{T}_k$ and

$\tilde{\boldsymbol{H}}_k = [\boldsymbol{H}_1\, \boldsymbol{H}_2 \cdots \boldsymbol{H}_{k-1}\, \boldsymbol{H}_{k+1} \cdots \boldsymbol{H}_K]$ represents all the channels except the channel of the intended user k.

While the SLNR was calculated in the case of asynchronous interference in [12] as

$$\mathrm{SLNR}_k = \frac{P_k^{tx} \cdot Tr\left(\boldsymbol{Q}_k^\dagger \boldsymbol{H}_k^\dagger \boldsymbol{H}_k \boldsymbol{Q}_k\right)}{Tr\left(\boldsymbol{Q}_k^\dagger \left(N_0 N_R \boldsymbol{I}_{BN_T} + P_k^{tx} \sum_{\substack{j=1 \\ j \neq k}}^{K} \boldsymbol{W}_{kj}\right) \boldsymbol{Q}_k\right)} \quad (3)$$

where

$$\boldsymbol{W}_{kj} = \begin{bmatrix} \beta_{kj}^{(1,1)} \boldsymbol{h}_j^{(1)^\dagger} \boldsymbol{h}_j^{(1)} & \dots & \beta_{kj}^{(1,B)} \boldsymbol{h}_j^{(1)^\dagger} \boldsymbol{h}_j^{(B)} \\ \beta_{kj}^{(2,1)} \boldsymbol{h}_j^{(2)^\dagger} \boldsymbol{h}_j^{(1)} & \dots & \beta_{kj}^{(2,B)} \boldsymbol{h}_j^{(2)^\dagger} \boldsymbol{h}_j^{(B)} \\ \vdots & \ddots & \vdots \\ \beta_{kj}^{(B,1)} \boldsymbol{h}_j^{(B)^\dagger} \boldsymbol{h}_j^{(1)} & \dots & \beta_{kj}^{(B,B)} \boldsymbol{h}_j^{(B)^\dagger} \boldsymbol{h}_j^{(B)} \end{bmatrix}.$$

Let

$$\boldsymbol{Y}_k = \frac{P_k^{tx}}{N_0} \boldsymbol{H}_k^\dagger \boldsymbol{H}_k$$

and

$$\boldsymbol{Z}_k = N_R \boldsymbol{I}_{BN_T} + \frac{P_k^{tx}}{N_0} \sum_{\substack{j=1 \\ j \neq k}}^{K} \boldsymbol{W}_{kj},$$

then (3) is simplified to

$$\mathrm{SLNR}_k = \frac{Tr\left(\boldsymbol{Q}_k^\dagger \boldsymbol{Y}_k \boldsymbol{Q}_k\right)}{Tr\left(\boldsymbol{Q}_k^\dagger \boldsymbol{Z}_k \boldsymbol{Q}_k\right)} \quad (4)$$

In order to get more insights into the behavior of the JLS precoder, we will consider the practical case of having one receiving antenna at the MSs ($N_R = 1$ and consequently $L_k = 1$). This case is also mathematically tractable and will result in a closed form solution of the rate loss.

A. *Maximum* SLNR

Assume the case of $L_k = 1$, $\boldsymbol{Q}_k$ is a vector of size $N_T \times 1$ and since $\boldsymbol{Y}_k$ is Hermitian and $\boldsymbol{Z}_k$ is positive definite with real diagonal elements, equation (4) can be further simplified to take the form of a generalized Rayleigh quotient [17], where $\mathrm{SLNR}_k = \frac{\boldsymbol{Q}_k^\dagger \boldsymbol{Y}_k \boldsymbol{Q}_k}{\boldsymbol{Q}_k^\dagger \boldsymbol{Z}_k \boldsymbol{Q}_k}$.

Define $\boldsymbol{C}$ as the Cholesky decomposition of the matrix $\boldsymbol{Z}_k = \boldsymbol{C}^\dagger \boldsymbol{C}$ and $\boldsymbol{D} = \boldsymbol{C}^{\dagger^{-1}} \boldsymbol{Y}_k \boldsymbol{C}^{-1}$, the SLNR can be simplified to the Rayleigh Quotient $R(\boldsymbol{D}, \boldsymbol{CQ}_k) = \frac{(\boldsymbol{CQ_k})^\dagger \boldsymbol{D} (\boldsymbol{CQ_k})}{(\boldsymbol{CQ_k})^\dagger (\boldsymbol{CQ_k})}$, where $|\boldsymbol{CQ}_k| = 1$. This Rayleigh quotient reaches its maximum value of $\lambda_{\max}$ (the maximum eigenvalue of the matrix $\boldsymbol{D}$) when $\boldsymbol{CQ}_k = \boldsymbol{v}_{\max}$, which is the corresponding eigenvector of the matrix $\boldsymbol{D}$.

Starting by $\boldsymbol{DCQ}_k = \lambda_{\max} \boldsymbol{CQ}_k$, we get $\boldsymbol{Z}_k^{-1} \boldsymbol{Y}_k \boldsymbol{Q}_k = \lambda_{\max} \boldsymbol{Q}_k$, then $\boldsymbol{Q}_k$ is the eigenvector of the matrix $\boldsymbol{Z}_k^{-1} \boldsymbol{Y}_k$ corresponding to its largest eigenvalue.

The maximum SLNR can then be given at this $\boldsymbol{Q}_k$ as

$$\begin{aligned} &\max(\mathrm{SLNR}_k) = \max(R(\boldsymbol{D}, \boldsymbol{CQ}_k)) \\ &= (\boldsymbol{CQ_k})^\dagger \boldsymbol{D} (\boldsymbol{CQ_k}) = \boldsymbol{Q}_k^\dagger \boldsymbol{Y}_k \boldsymbol{Q}_k = \lambda_{\max} \end{aligned} \quad (5)$$

It is worth noting that at this maximum condition $|\boldsymbol{H}_k \boldsymbol{Q}_k|^2 = \frac{N_0}{P_k^{tx}} \lambda_{\max}$ and $\boldsymbol{Q}_k^\dagger \boldsymbol{Z}_k \boldsymbol{Q}_k = 1$ then

$$\boldsymbol{Q}_k^\dagger \Big(N_R \boldsymbol{I}_{BN_T} + \frac{P_k^{tx}}{N_0} \sum_{\substack{j=1 \\ j \neq k}}^{K} \boldsymbol{W}_{kj} \Big) \boldsymbol{Q}_k = 1$$

at $N_R = 1$

$$\boldsymbol{Q}_k^\dagger \boldsymbol{Q}_k + \frac{P_k^{tx}}{N_0} \boldsymbol{Q}_k^\dagger \sum_{\substack{j=1 \\ j \neq k}}^{K} \boldsymbol{W}_{kj} \boldsymbol{Q}_k = 1$$

from the orthonormality condition $\boldsymbol{Q}_k^\dagger \boldsymbol{Q}_k = 1$, then

$$\boldsymbol{Q}_k^\dagger \sum_{\substack{j=1 \\ j \neq k}}^{K} \boldsymbol{W}_{kj} \boldsymbol{Q}_k = 0$$

Using the definition of $\boldsymbol{W}_{kj}$, this equation can be expanded to

$$\sum_{\substack{j=1 \\ j \neq k}}^{K} \sum_{b_i=1}^{B} \sum_{b_l=1}^{B} \beta_{jk}^{(b_i,b_l)} \boldsymbol{Q}_k^{(b_l)\dagger} \boldsymbol{h}_j^{(b_l)\dagger} \boldsymbol{h}_j^{(b_i)} \boldsymbol{Q}_k^{(b_i)} = 0 \quad (6)$$

Given the quantized channel $\hat{\boldsymbol{H}}_j$, the precoding vector $\boldsymbol{Q}_k$ is calculated to satisfy

$$\sum_{\substack{j=1 \\ j \neq k}}^{K} \sum_{b_i=1}^{B} \sum_{b_l=1}^{B} \beta_{jk}^{(b_i,b_l)} \boldsymbol{Q}_k^{(b_l)\dagger} \hat{\boldsymbol{h}}_j^{(b_l)\dagger} \hat{\boldsymbol{h}}_j^{(b_i)} \boldsymbol{Q}_k^{(b_i)} = 0 \quad (7)$$

as a design criterion.

B. *Maximum achievable Rate*

The JLS rate is given as a function of P, the SNR per MS, in [12] as

$$R_{JLS}(P) \quad =$$

$$KE_H \left[\log_2 \left| \boldsymbol{I}_{N_R} + \boldsymbol{\phi}_{k,JLS}^{-1} \boldsymbol{H}_k \boldsymbol{T}_{k,JLS} \boldsymbol{T}_{k,JLS}^\dagger \boldsymbol{H}_k^\dagger \right| \right] \quad (8)$$

where the expectation $E_H[.]$ is held over the channel H and $\boldsymbol{\phi}_k$ is the covariance of noise plus interference for MS k. It is given by

$$\boldsymbol{\phi}_{k,JLS} =$$

$$\sum_{\substack{j=1 \\ j \neq k}}^{K} \sum_{b_i=1}^{B} \sum_{b_l=1}^{B} \beta_{jk}^{(b_i,b_l)} \boldsymbol{h}_k^{(b_i)} \boldsymbol{T}_{j,JLS}^{(b_i)} \boldsymbol{T}_{j,JLS}^{(b_l)\dagger} \boldsymbol{h}_k^{(b_l)\dagger} + N_0 \boldsymbol{I}_{N_R}$$

For $N_R = 1$ and given that $\boldsymbol{H}_k \boldsymbol{T}_k \boldsymbol{T}_k^\dagger \boldsymbol{H}_k^\dagger = |\boldsymbol{H}_k \boldsymbol{T}_k|^2 = P_k^{tx} |\boldsymbol{H}_k \boldsymbol{Q}_{k,JLS}|^2$ and $P = \frac{P_k^{tx}}{N_0}$, $R_{JLS}(P)$ reduces to

$$R_{JLS}(P) = KE_H \left[\log_2 \left(1 + \frac{P |\boldsymbol{H}_k \boldsymbol{Q}_{k,JLS}|^2}{1 + P \cdot \gamma_{k,JLS}} \right) \right] \quad (9)$$

where

$$\gamma_{k,JLS} = \sum_{\substack{j=1 \\ j\neq k}}^{K} \sum_{b_i=1}^{B} \sum_{b_l=1}^{B} \beta_{jk}^{(b_i,b_l)} \boldsymbol{h}_k^{(b_i)} \boldsymbol{Q}_{j,JLS}^{(b_i)} \boldsymbol{Q}_{j,JLS}^{(b_l)\dagger} \boldsymbol{h}_k^{(b_l)\dagger}$$

For perfect channel knowledge, $\gamma_{k,JLS} = 0$ from (7), then

$$R_{JLS}(P) = KE_H\left[\log_2\left(1 + P|\boldsymbol{H}_k \boldsymbol{Q}_{k,JLS}|^2\right)\right]. \quad (10)$$

IV. Quantized feedback JLS Precoder

In the available literature, scalar quantization, vector quantization (VQ) and matrix quantization have all been used to quantize CSI. It is now well established in the single data stream case that projecting the MIMO channel to an appropriate vector channel yields better performance than full channel scalar quantization with the same feedback overhead [18]. In the case of the single data stream case, the MIMO channel is projected to a vector channel. This was proved to yield better performance than full channel scalar quantization providing the same feedback overhead [18]. This has led to considerable research in VQ, which reduces the feedback overhead by allocating bits in the proper vector direction. For the case of having multiple data streams, the channel matrix is projected to the appropriate channel vector using one of the combining schemes proposed in the literature, for example eigen-based combining [19], quantization based combining [20], and maximum expected signal combining [21]. In the multi user case, we can apply the same principle of VQ to each user channel individually. The vector quantization is performed using a quantization codebook that is known at the BSs. And since the optimal vector quantizer for this problem is not known in general, Random Vector Quantizer (RVQ) is used [22]. Quantization schemes require a measure of the distance between the two vectors, where two commonly used measures are the chordal and euclidean distances. Since the former ensures a higher inner product between the original and quantized channel, in the limited feedback scenario [23], it is the one used in this paper.

A. Random Vector Quantization Error Analysis

In VQ, n feedback bits are sent as the channel index to the master cell or other cooperating BSs. A quantization codebook $\mathbf{C}$ consisting of 2^n N_T-dimensional unit norm vectors $\mathbf{C} = \{w_1, \ldots, w_{2^n}\}$ is used. Each of the codewords is independently drawn from the isotropic distribution on the N_T-dimensional unit sphere. We analyze the performance by averaging over the distribution of all choices of such codebooks.

Defining d as the chordal distance between the channel vector and its quantized version [24] allows it to be used as the magnitude of quantization error. The average value of the quantization error of the composite channel vector $\boldsymbol{H}_k$, of size $1 \times BN_T$, can be proved from the quantization errors of its consisting channel vectors $\boldsymbol{h}_k^{(b)}$ for $b = 1, \ldots, B$ as

$$\begin{aligned} d &= \sin^2\left(\angle(\boldsymbol{H_k}, \hat{\boldsymbol{H}}_{\boldsymbol{k}})\right) = 1 - \left(\frac{|\boldsymbol{H_k}\hat{\boldsymbol{H}}_{\boldsymbol{k}}^{\dagger}|^2}{\|\boldsymbol{H_k}\|^2.\|\hat{\boldsymbol{H}}_{\boldsymbol{k}}\|^2}\right) \\ &= 1 - \left(\frac{|\sum_{b=1}^{B} \boldsymbol{h}_k^{(b)} \hat{\boldsymbol{h}}_k^{(b)\dagger}|^2}{\|\boldsymbol{H}_k\|^4}\right) \end{aligned} \quad (11)$$

since both the channel and the quantized vectors have the same gain, and

$$\cos^2\left(\angle(\boldsymbol{H_k}, \hat{\boldsymbol{H}}_{\boldsymbol{k}})\right) = \left(\frac{|\sum_{b=1}^{B} \boldsymbol{h}_k^{(b)} \hat{\boldsymbol{h}}_k^{(b)\dagger}|^2}{\|\boldsymbol{H}_k\|^4}\right)$$

By defining $a_b = \cos\big(\angle\big(\boldsymbol{h}_k^{(b)}, \hat{\boldsymbol{h}}_k^{(b)}\big)\big)$, we can define the quantity α as follows:

$$\begin{aligned} \alpha &= \|\boldsymbol{H}_k\|^4 \cdot \cos^2\left(\angle(\boldsymbol{H_k}, \hat{\boldsymbol{H}}_{\boldsymbol{k}})\right) \\ &= \sum_{j=1}^{B}\sum_{l=1}^{B} a_{b_j} a_{b_l} \|\hat{\boldsymbol{h}}_k^{(b_j)}\|^2 \|\hat{\boldsymbol{h}}_k^{(b_l)}\|^2 \end{aligned} \quad (12)$$

And by taking the expectation of both sides, we get

$$\begin{aligned} E(\alpha) &= E\Big(\|\boldsymbol{H}_k\|^4\Big) \cdot E\Big(\cos^2\left(\angle(\boldsymbol{H_k}, \hat{\boldsymbol{H}}_{\boldsymbol{k}})\right)\Big) \\ &= E\Big(\sum_{j=1}^{B}\sum_{l=1}^{B} a_{b_j} a_{b_l} \|\hat{\boldsymbol{h}}_k^{(b_j)}\|^2 \|\hat{\boldsymbol{h}}_k^{(b_l)}\|^2\Big) \end{aligned} \quad (13)$$

where we used here the fact that the angle between two vectors is independent of the values of their norm. Finally,

$$E(\alpha) = \sum_{i=1}^{B} E\big(a_{b_i}^2\big) \cdot E\Big(\|\hat{\boldsymbol{h}}_k^{(b_i)}\|^4\Big)$$

$$+ 2\sum_{j=1}^{B}\sum_{l=j+1}^{B} E\big(a_{b_j}\big)E\big(a_{b_l}\big)E\big(\|\hat{\boldsymbol{h}}_k^{(b_j)}\|^2\big)E\big(\|\hat{\boldsymbol{h}}_k^{(b_l)}\|^2\big). \quad (14)$$

In [25] the error performance of the RVQ scheme has been analyzed in the case of point to point MISO systems, and the expected quantization error has been bounded by the following bounds

$$\big(\tfrac{N_T-1}{N_T}\big)2^{\frac{-n}{N_T-1}} < E\Big[\sin^2\big(\angle\big(\boldsymbol{H_k}, \hat{\boldsymbol{H}}_{\boldsymbol{k}}\big)\big)\Big] < 2^{\frac{-n}{N_T-1}} \quad (15)$$

therefore the lower bound of each of the terms $E\big(a_{b_j}^2\big)$ is given by

$$E\big(a_{b_j}^2\big) = E\Big(\cos^2\big(\angle\big(\boldsymbol{h}_k^{(b_j)}, \hat{\boldsymbol{h}}_k^{(b_j)}\big)\big)\Big) \geq 1 - 2^{\frac{-n}{N_T-1}}, \quad (16)$$

while $E\big(a_{b_j}\big) = 0$ as the codebook vectors are isotropically distributed in the 2^n dimensional space, then the channel vector can be mapped to a certain vector or the one in the opposite direction with the same probability.

To get $E\Big(\|\hat{\boldsymbol{h}}_k^{(b_i)}\|^2\Big)$, we use the fact that the squared norm of a vector consisting of r Gaussian i.i.d. random variables, each with zero mean and variance σ^2, is a chi-squared distribution with r degrees of freedom. The norm of each channel vector, as well as the quantized one, is the summation of two independent chi-squared random variables, one for the real part of the vector and one for the imaginary

part. Each part has N_T degrees of freedom, and variance $\frac{L_k^{(b_i)}}{2}$, where $L_k^{(b_i)}$ is the path loss of the channel between BS $b_{(i)}$ and MS k.

Then

$$E\Big(\|\hat{\boldsymbol{h}}_k^{(b_i)}\|^2\Big) = \frac{L_k^{(b_i)}}{2}N_T + \frac{L_k^{(b_i)}}{2}N_T = L_k^{(b_i)}N_T$$

$$\begin{aligned} Var\Big(\|\hat{\boldsymbol{h}}_k^{(b_i)}\|^2\Big) &= 2N_T\big(\frac{L_k^{(b_i)}}{2}\big)^2 + 2N_T\big(\frac{L_k^{(b_i)}}{2}\big)^2 \\ &= N_T\big(L_k^{(b_i)}\big)^2 \end{aligned}$$

and hence

$$\begin{aligned} E\Big(\|\hat{\boldsymbol{h}}_k^{(b_i)}\|^4\Big) &= Var\Big(\|\hat{\boldsymbol{h}}_k^{(b_i)}\|^2\Big) + E^2\Big(\|\boldsymbol{h}_k^{(b_i)}\|^2\Big) \\ &= (L_k^{(b_i)})^2(N_T + N_T^2). \end{aligned} \quad (17)$$

Then substituting in (14), we find that

$$E(\alpha) \geq (N_T + N_T^2)(1 - 2^{\frac{-n}{N_T-1}})\sum_{i=1}^{B}(L_k^{(b_i)})^2. \quad (18)$$

Since $\|\hat{\boldsymbol{H}}_k\|^2 = \sum_{i=1}^{B}\|\hat{\boldsymbol{h}}_k^{(b_i)}\|^2$, then the norm $\|\hat{\boldsymbol{H}}_k\|^2$ has a mean value of $E(\|\hat{\boldsymbol{H}}_k\|^2) = N_T \cdot \sum_{i=1}^{B} L_k^{(b_i)}$, and variance given by $Var(\|\hat{\boldsymbol{H}}_k^{(b_i)}\|^2) = N_T \cdot \sum_{i=1}^{B}(L_k^{(b_i)})^2$, then

$$E(\|\hat{\boldsymbol{H}}_k\|^4) = N_T \cdot \sum_{i=1}^{B}(L_k^{(b_i)})^2 + (N_T \cdot \sum_{i=1}^{B} L_k^{(b_i)})^2$$

By substituting with this value and the value of $E(\alpha)$ in (13), the value of $E\Big(\cos^2\big(\angle(\boldsymbol{H_k}, \hat{\boldsymbol{H}}_{\boldsymbol{k}})\big)\Big)$ is bounded by

$$E\Big(\cos^2\big(\angle(\boldsymbol{H_k}, \hat{\boldsymbol{H}}_{\boldsymbol{k}})\big)\Big) \geq$$

$$\frac{(N_T + N_T^2)(1 - 2^{\frac{-n}{N_T-1}})\sum_{i=1}^{B}(L_k^{(b_i)})^2}{N_T \cdot \sum_{i=1}^{B}(L_k^{(b_i)})^2 + N_T^2 \cdot (\sum_{i=1}^{B} L_k^{(b_i)})^2}$$

which can be reduced to the following form, in the case of having equal path losses,

$$E\left(\cos^2\left(\angle(\boldsymbol{H_k}, \hat{\boldsymbol{H}}_{\boldsymbol{k}})\right)\right) \geq \frac{B(N_T + N_T^2)(1 - 2^{\frac{-n}{N_T-1}})}{BN_T + B^2N_T^2}.$$

Therefore the mean value of the distance d is bounded by

$$\begin{aligned} E(d) &= E\left(\sin^2\left(\angle(\boldsymbol{H_k}, \hat{\boldsymbol{H}}_{\boldsymbol{k}})\right)\right) \\ &\leq 1 - \frac{B(N_T + N_T^2)(1 - 2^{\frac{-n}{N_T-1}})}{BN_T + B^2N_T^2} \\ &\leq 1 - \frac{(1 + N_T)}{(1 + BN_T)}(1 - 2^{\frac{-n}{N_T-1}}) \end{aligned} \quad (19)$$

This is the upper bound of the quantization error resulting from random vector quantization when using chordal distance as the decision metric. This bound is used to find the rate loss in the next subsection.

B. Rate Loss due to Quantization

To quantify the performance degradation when the feedback channel is quantized in case of the JLS precoder, we define the rate gap $\triangle R(P)$ to be the difference between the per mobile throughput achieved by perfect CSIT-based JLS and finite-rate feedback-based JLS as

$$\triangle R(P) = \frac{1}{K}\left[R_{JLS}(P) - R_{FB}(P)\right] \quad (20)$$

The JLS rate, $R_{JLS}(P)$, is given by equation (10), while the quantized feedback rate of the JLS precoder can be given by

$$R_{FB}(P) = KE_{H,w}\left[\log_2\left(1 + \frac{P|\boldsymbol{H}_k\boldsymbol{Q}_{k,FB}|^2}{1 + P \cdot \gamma_{k,FB}}\right)\right] \quad (21)$$

where the expectation $E_{H,w}[.]$ is held over the channel H and the quantization codebook vectors w, and

$$\gamma_{k,FB} = \sum_{\substack{j=1 \\ j \neq k}}^{K}\sum_{b_i=1}^{B}\sum_{b_l=1}^{B}\beta_{jk}^{(b_i,b_l)}\boldsymbol{h}_k^{(b_i)}\boldsymbol{Q}_{j,FB}^{(b_i)}\boldsymbol{Q}_{j,FB}^{(b_l)\dagger}\boldsymbol{h}_k^{(b_l)\dagger}.$$

Then,

$$\begin{aligned} \triangle R(P) &= E_H\left[\log_2\left(1 + P|\boldsymbol{H}_k\boldsymbol{Q}_{k,JLS}|^2\right)\right] \\ &- E_{H,w}\left[\log_2\left(1 + \frac{P|\boldsymbol{H}_k\boldsymbol{Q}_{k,FB}|^2}{1 + P \cdot \gamma_{k,FB}}\right)\right] \end{aligned} \quad (22)$$

Due to the use of the precoder, which tries to enhance the signal power and minimize the interference terms, the interference term $P \cdot \gamma_{k,FB}$ is much less than the received signal power $P|\boldsymbol{H}_k\boldsymbol{Q}_{k,FB}|^2$. The rate gap, $\triangle R(P)$, can then be bounded as

$$\begin{aligned} \triangle R(P) \leq\ & E_H\left[\log_2\left(1 + P|\boldsymbol{H}_k\boldsymbol{Q}_{k,JLS}|^2\right)\right] \\ & - E_{H,w}\left[\log_2\left(1 + P|\boldsymbol{H}_k\boldsymbol{Q}_{k,FB}|^2\right)\right] \\ & + E_{H,w}\left[\log_2\left(1 + P \cdot \gamma_{k,FB}\right)\right]. \end{aligned} \quad (23)$$

This bound is valid taking into consideration the fact that $\gamma_{k,FB}$ is positive real and $\log(\cdot)$ is an increasing function.

Recall that the distribution of an isotropically random vector (which is the Rayleigh fading channel in our case) is not affected by multiplication with a unitary matrix [26]. It is the mathematical way to capture the notion that the vector is equally likely to point in any direction in the N_T dimensional vector space. Using this result, $E_H[\log_2(1 + P|\boldsymbol{H}_k\boldsymbol{Q}_{k,JLS}|^2)] = E_{H,w}[\log_2(1 + P|\boldsymbol{H}_k\boldsymbol{Q}_{k,FB}|^2)]$. Then, $\triangle R(P) \leq E_{H,w}[\log_2(1 + P \cdot \gamma_{k,FB})]$. Using Jensen's inequality [27] the rate loss becomes bounded by

$$\triangle R(P) \leq \log_2(1 + E_{H,w}[P \cdot \gamma_{k,FB}]) \quad (24)$$

1) Synchronous Interference Rate Loss: In case of having synchronous interference, $\beta_{jk}^{(b_i,b_l)} = 1 \,\forall b_i, b_l$, then

$$\begin{aligned}\gamma_{k,FB} &= \sum_{\substack{j=1\\ j\neq k}}^{K}\sum_{b_i=1}^{B}\sum_{b_l=1}^{B}\boldsymbol{h}_k^{(b_i)}\boldsymbol{Q}_{j,FB}^{(b_i)}\boldsymbol{Q}_{j,FB}^{(b_l)\dagger}\boldsymbol{h}_k^{(b_l)\dagger}\\ &= \sum_{\substack{j=1\\ j\neq k}}^{K}|\boldsymbol{H}_k\boldsymbol{Q}_{j,FB}|^2\end{aligned}$$

and inequality (24) then becomes

$$\triangle R(P) \leq \log_2(1+E_{H,w}[P\sum_{\substack{j=1\\ j\neq k}}^{K}|\boldsymbol{H}_k\boldsymbol{Q}_{j,FB}|^2]) \qquad (25)$$

which is reduced to the following form, since all the mobile users' channels are independently quantized,

$$\triangle R(P) \leq \log_2(1+(K-1)\cdot P\cdot E_{H,w}(|\boldsymbol{H}_k\boldsymbol{Q}_{j,FB}|^2))$$

And since $E\left(\|\boldsymbol{H}_k\|^2\right) = N_T\cdot(L_k^{(1)}+\cdots+L_k^{(B)})$ where $L_k^{(b)}$ is the path loss coefficient of the channel between BS b and MS k, then

$$\triangle R(P) \leq$$

$$\log_2\Big(1+(K-1)P\sum_{b=1}^{B}L_k^{(b)}N_T E_{H,w}(|\overline{\boldsymbol{H}}_k\boldsymbol{Q}_{j,FB}|^2)\Big) \qquad (26)$$

where $\overline{\boldsymbol{H}}_k = \frac{\boldsymbol{H}_k}{\|\boldsymbol{H}_k\|}$ is the normalized composite channel vector.

Using RVQ to quantize the channel of each BS $\boldsymbol{h}_k^{(b)}$, then MS k has a composite quantized channel vector of $\hat{\boldsymbol{H}}_k = [\hat{\boldsymbol{h}}_k^{(1)},\ldots,\hat{\boldsymbol{h}}_k^{(B)}]$. $\overline{\boldsymbol{H}}_k$ can be considered as the sum of two vectors, one in the direction of the quantized vector, and the other is isotropically distributed in the null space. Then

$$\overline{\boldsymbol{H}}_k = \sqrt{1-d}\hat{\boldsymbol{H}}_k + \sqrt{d}\boldsymbol{S},$$

where $d = \sin^2(\theta) = 1-|\overline{\boldsymbol{H}}_k\hat{\boldsymbol{H}}_k^{\dagger}|^2$ is the magnitude of the quantization error and $\boldsymbol{S}$ is a unit norm vector isotropically distributed in the null space of $\hat{\boldsymbol{H}}_k$.

The product of $\overline{\boldsymbol{H}}_k$ and $\boldsymbol{Q}_{j,FB}$ is then given by

$$\begin{aligned}|\overline{\boldsymbol{H}}_k\boldsymbol{Q}_{j,FB}|^2 &= (1-d)\,|\hat{\boldsymbol{H}}_k\boldsymbol{Q}_{j,FB}|^2 + (d)\,|\boldsymbol{S}\boldsymbol{Q}_{j,FB}|^2\\ &= d|\boldsymbol{S}\boldsymbol{Q}_{j,FB}|^2\end{aligned}$$

In case of having synchronous interference, (7) is reduced to

$$\sum_{\substack{j=1\\ j\neq k}}^{K}|\hat{\boldsymbol{H}}_k\boldsymbol{Q}_{j,FB}|^2 = 0$$

therefore, the vector $\boldsymbol{Q}_{j,FB}$ is isotropically distributed in the BN_T-1 dimensional null space of $\hat{\boldsymbol{H}}_k\,\forall k\neq j$. And since $\boldsymbol{S}$ is also i.i.d. isotropic vector in the BN_T-1 dimensional null space of $\hat{\boldsymbol{H}}_k$, therefore the term $|\boldsymbol{S}\boldsymbol{Q}_{j,FB}|^2$ is beta distributed as $\beta\,(1, BN_T-2)$ random variable [28], having a mean value of $\frac{1}{BN_T-1}$. Accordingly, the mean value of $|\overline{\boldsymbol{H}}_k\boldsymbol{Q}_{j,FB}|^2$ is given by

$$\begin{aligned}E_{H,w}(|\overline{\boldsymbol{H}}_k\boldsymbol{Q}_{j,FB}|^2) &= E(d|\boldsymbol{S}\boldsymbol{Q}_{j,FB}|^2)\\ &= E(d)\cdot E(|\boldsymbol{S}\boldsymbol{Q}_{j,FB}|^2)\\ &= E(\sin^2(\theta))\cdot\frac{1}{BN_T-1}\end{aligned}$$

where the expectation of the quantization error has been proved in (19). By substituting these results in (26), we can find that the rate loss is upper bounded by the following bound

$$\begin{aligned}\triangle R(P) \leq \log_2\Big(1+(K-1)P\frac{\sum_{b=1}^{B}L_k^{(b)}N_T}{BN_T-1}\\ \cdot\big(1-\frac{(1+N_T)}{(1+BN_T)}(1-2^{\frac{-n}{N_T-1}})\big)\Big)\end{aligned} \qquad (27)$$

2) Asynchronous Interference Rate Loss: To simplify the analysis and without loss of generality, we consider the case of having 2 BSs to get the rate loss of the JLS precoder in case of the presence of the more realistic scenario of Asynchronous interference. We have

$$\gamma_{k,FB} = \sum_{\substack{j=1\\ j\neq k}}^{K}\sum_{b_i=1}^{2}\sum_{b_l=1}^{2}\beta_{jk}^{(b_i,b_l)}\boldsymbol{h}_k^{(b_i)}\boldsymbol{Q}_{j,FB}^{(b_i)}\boldsymbol{Q}_{j,FB}^{(b_l)\dagger}\boldsymbol{h}_k^{(b_l)\dagger}$$

since $\beta_{jk}^{(b_i,b_l)} = \beta_{jk}^{(b_l,b_i)}$, then

$$\begin{aligned}\gamma_{k,FB} &= \sum_{\substack{j=1\\ j\neq k}}^{K}\Big(\beta_{jk}^{(b_i,b_i)}|\boldsymbol{h}_k^{(b_i)}\boldsymbol{Q}_{j,FB}^{(b_i)}|^2\\ &+ \beta_{jk}^{(b_l,b_l)}|\boldsymbol{h}_k^{(b_l)}\boldsymbol{Q}_{j,FB}^{(b_l)}|^2\\ &+ 2\beta_{jk}^{(b_i,b_l)}Real\left\{\boldsymbol{Q}_{j,FB}^{(b_l)\dagger}\boldsymbol{h}_k^{(b_l)\dagger}\boldsymbol{h}_k^{(b_i)}\boldsymbol{Q}_{j,FB}^{(b_i)}\right\}\Big)\end{aligned}$$

hence,

$$\begin{aligned}E_{H,w}(\gamma_{k,FB}) = \sum_{\substack{j=1\\ j\neq k}}^{K}E_{H,w}\Big(\beta_{jk}^{(b_i,b_i)}|\boldsymbol{h}_k^{(b_i)}\boldsymbol{Q}_{j,FB}^{(b_i)}|^2\Big)\\ +E_{H,w}\Big(\beta_{jk}^{(b_l,b_l)}|\boldsymbol{h}_k^{(b_l)}\boldsymbol{Q}_{j,FB}^{(b_l)}|^2\Big)\\ +2E_{H,w}\Big(\beta_{jk}^{(b_i,b_l)}Real\left\{\boldsymbol{Q}_{j,FB}^{(b_l)\dagger}\boldsymbol{h}_k^{(b_l)\dagger}\boldsymbol{h}_k^{(b_i)}\boldsymbol{Q}_{j,FB}^{(b_i)}\right\}\Big)\end{aligned}$$

And since $\boldsymbol{h}_k^{(b_i)}$ and $\boldsymbol{h}_k^{(b_l)}$ are mutually independent isotropically distributed random vectors in the vector space $\mathbb{C}^{N_T}$, having zero mean each, then

$$E_{H,w}\Big(\boldsymbol{Q}_{j,FB}^{(b_l)\dagger}\boldsymbol{h}_k^{(b_l)\dagger}\boldsymbol{h}_k^{(b_i)}\boldsymbol{Q}_{j,FB}^{(b_i)}\Big) = 0,$$

therefore,

$$E_{H,w}(\gamma_{k,FB}) =$$

$$\sum_{\substack{j=1\\ j\neq k}}^{K}E_{H,w}\Big(\beta_{jk}^{(b_i,b_i)}|\boldsymbol{h}_k^{(b_i)}\boldsymbol{Q}_{j,FB}^{(b_i)}|^2+\beta_{jk}^{(b_l,b_l)}|\boldsymbol{h}_k^{(b_l)}\boldsymbol{Q}_{j,FB}^{(b_l)}|^2\Big)$$

Since $E\left(\beta_{jk}^{(b_i,b_i)}\right) = E\left(\beta_{jk}^{(b_l,b_l)}\right)$, then

$$E_{H,w}(\gamma_{k,FB}) = (K-1)\cdot\overline{\beta_{jk}^{(b_i,b_i)}} \cdot E_{H,w}\Big(|\boldsymbol{h}_k^{(b_i)}\boldsymbol{Q}_{j,FB}^{(b_i)}|^2 + |\boldsymbol{h}_k^{(b_l)}\boldsymbol{Q}_{j,FB}^{(b_l)}|^2\Big) = (K-1)\cdot\overline{\beta_{jk}^{(b_i,b_i)}}\cdot E_{H,w}\Big(|\boldsymbol{H}_k\boldsymbol{Q}_{j,FB}|^2\Big)$$

where $\boldsymbol{H}_k = [\boldsymbol{h}_k^{(1)},\ldots,\boldsymbol{h}_k^{(B)}]$ and $\boldsymbol{Q}_k = [\boldsymbol{Q}_k^{(1)\dagger},\ldots,\boldsymbol{Q}_k^{(B)\dagger}]^\dagger$

Using the same argument as in the case of synchronous interference, $\overline{\boldsymbol{H}}_k$ can then be expressed as $\overline{\boldsymbol{H}}_k = \sqrt{1-d}\hat{\boldsymbol{H}}_k + \sqrt{d}\boldsymbol{S}$. The expectation of the product of $\overline{\boldsymbol{H}}_k$ and $\boldsymbol{Q}_{j,FB}$ is then given by

$$E_{H,w}\Big(|\overline{\boldsymbol{H}}_k\boldsymbol{Q}_{j,FB}|^2\Big) = E_{H,w}\Big((1-d)\,|\hat{\boldsymbol{H}}_k\boldsymbol{Q}_{j,FB}|^2\Big) + E_{H,w}\Big(d|\boldsymbol{S}\boldsymbol{Q}_{j,FB}|^2\Big) \quad (28)$$

From the design criteria (7)

$$E_{H,w}\Big(\sum_{\substack{j=1\\ j\neq k}}^{K}\sum_{b_i=1}^{B}\sum_{b_l=1}^{B}\beta_{jk}^{(b_i,b_l)}\boldsymbol{Q}_k^{(b_l)\dagger}\hat{\boldsymbol{h}}_j^{(b_l)\dagger}\hat{\boldsymbol{h}}_j^{(b_i)}\boldsymbol{Q}_k^{(b_i)}\Big) = 0$$

$$(K-1)\cdot\overline{\beta_{jk}^{(b_i,b_i)}}\cdot E_{H,w}\Big(|\hat{\boldsymbol{H}}_k\boldsymbol{Q}_{j,FB}|^2\Big) = 0$$

$$E_{H,w}\Big(|\hat{\boldsymbol{H}}_k\boldsymbol{Q}_{j,FB}|^2\Big) = 0, \quad (29)$$

then (28) reduces to

$$E_{H,w}\Big(|\overline{\boldsymbol{H}}_k\boldsymbol{Q}_{j,FB}|^2\Big) = E_{H,w}\,(d)\,E_{H,w}(|\boldsymbol{S}\boldsymbol{Q}_{j,FB}|^2).$$

Since the term $|\boldsymbol{S}\boldsymbol{Q}_{j,FB}|^2$ is a beta $(1, BN_T-2)$ random variable, then its mean value is $\frac{1}{BN_T-1}$, and $E_{H,w}\,(d) = 1-\frac{1+N_T}{1+BN_T}(1-2^{\frac{-n}{N_T-1}})$, then the rate loss in (10) becomes,

$$\triangle R(P) \leq \log_2\Big(1+(K-1)P\overline{\beta_{jk}^{(b_i,b_i)}}E_{H,w}(|\boldsymbol{H}_k\boldsymbol{Q}_{j,FB}|^2)\Big) = \log_2\Big(1+(K-1)P\overline{\beta_{jk}^{(b_i,b_i)}} \cdot N_T\sum_{b=1}^{B}L_k^{(b)}E_{H,w}(|\overline{\boldsymbol{H}}_k\boldsymbol{Q}_{j,FB}|^2)\Big)$$

therefore

$$\triangle R(P) \leq \log_2\Big(1+(K-1)P\frac{\sum_{b=1}^{B}L_k^{(b)}N_T}{BN_T-1} \cdot\overline{\beta_{jk}^{(b_i,b_i)}}\cdot\big(1-\frac{(1+N_T)}{(1+BN_T)}(1-2^{\frac{-n}{N_T-1}})\big)\Big), \quad (30)$$

where the average value of $\beta_{jk}^{(b_i,b_i)} = \rho^2(\delta_{jk}^{(b_1)})+\rho^2(\delta_{jk}^{(b_1)}-T_s)$. Using rectangular pulse shape with unit energy, $\rho(\delta_{jk}^{(b_1)}) = \frac{1}{T_s}(T_s-|\delta_{jk}^{(b_1)}|)$. It can be easily shown that $E(\rho^2(\delta_{jk}^{(b_1)})) = E(\rho^2(\delta_{jk}^{(b_1)}-T_s)) = 1/3$.

To conclude, the rate loss $\triangle R(P)$ given by (27) for the case of synchronous interference and (30) for the more general case of asynchronous interference shows the effect of quantizing the channel state information on the system performance.

It is clear from both equations, that the rate loss is an increasing function of the SNR (P). This means that the throughput of the limited feedback-based JLS system is bounded if the SNR is taken to infinity. In other words, the system with a fixed number of feedback bits is interference-limited at high SNR.

It was shown in [29] that, in case of single-cell MIMO networks $B=1$, the rate loss tends to zero when the number of feedback bits grows to infinity. This same conclusion can be deduced from (27) and (30) by setting $B=1$ and $n\to\infty$. It was also shown that the number of feedback bits per mobile must be increased linearly with the SNR (in decibels) in order to achieve the full multiplexing gain. On the contrary, from (27) and (30) when $B\neq 1$, it is clear that the rate loss does not tend to zero when the number of feedback bits grows to infinity and subsequently increasing the number of bits in case of MU-MIMO CoMP networks does not achieve the full multiplexing gain. This is due to the fact that optimizing the codeword choice for each BS channel separately does not imply that the global channel vector, which comprises the channels of all cooperating BSs for a certain user, is accurately quantized.

V. Simulation Results

To verify the analytical results, we simulate the downlink of an urban micro-cellular network using the 3GPP TR 25.996 channel model. The channel is assumed to be frequency selective and varying slowly in the time domain with a coherence time of 15 ms, for a mobile station with a velocity of 10 m/sec. The system model consists of two cells, each with 1 BS and 1 MS. The inter-BS distance is 500 m. The MSs are uniformly distributed in a limited cell area around each BS from $^{-\pi}/_{3}$ to $^{\pi}/_{3}$ radians and at a distance that is at least 150m from each BS. The path-loss coefficient for all the BS-MS channels is 2.0 (free-space propagation) up to a distance of 30 m, and increases to 3.7 thereafter [30]. Using the MSs locations' distribution, described earlier and we consider $N_T=3$, $N_R=1$, $B=2$ and $K=2$.

The theoretical upper bound on the rate loss, given by (27), is compared to the simulated rate loss at different feedback bits in Fig 2. The simulated rate loss is lower than the upper bound primarily due to the use of Jensen's inequality. This result is repeated for the case of asynchronous interference, given by (30), in Fig 3. The rate loss in case of asynchronous environment is smaller than that in synchronous, the performance degradation in asynchronous case due to channel quantization is less. This is clear from the theoretical upper bounds given in (27) and (30), where the term $\overline{\beta_{jk}^{(b_i,b_i)}}$ in the asynchronous rate loss upper bound is always less than or equal 1.

Another important result can be concluded from Fig. 4 and Fig 5, that is increasing the number of quantization bits does not result in a linear performance enhancement. This is clear when we compare the enhancement achieved when the number of quantization bits increases from 3 to 5 and the one achieved when the number of bits increases from 5 to 10. Hence, increasing the number of feedback bits to infinity does not lead to a rate loss that tends to zero. This behavior is in contrast to the conventional single-cell MIMO case, where increasing the

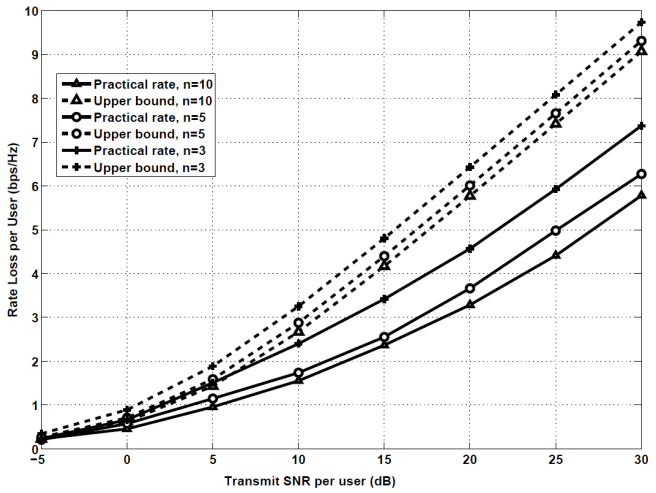

Fig. 2. Theoretical upper bound of rate loss and simulated one at 3, 5, and 10 feedback bits in an idealized synchronous environment.

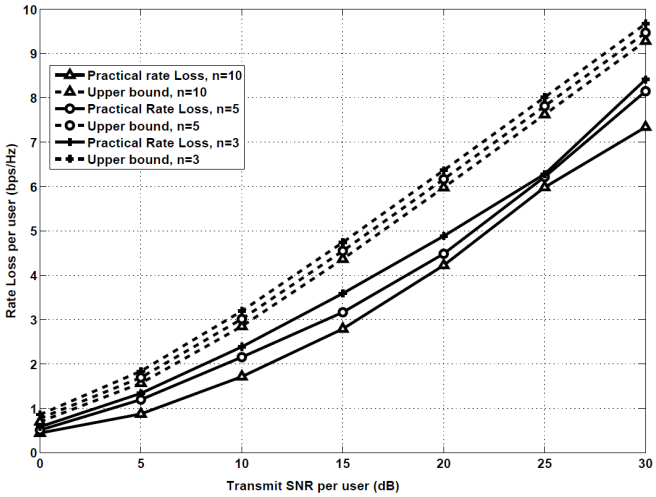

Fig. 3. Theoretical upper bound of rate loss and simulated one at 3, 5, and 10 feedback bits in asynchronous environment.

number of quantization bits to infinity guaranties a rate loss of zero.

VI. Conclusion

In this paper we considered the finite rate feedback JLS precoder used in CoMP transmission as it is a suitable linear precoding scheme for the asynchronous interference case, that inevitably exists in the cooperative data transmission scenarios. We analyzed its performance in the case of finite capacity backhaul links. Random Vector Quantization has been used as the vector quantization technique to quantize the channel state. The rate loss due to this quantization is derived in both cases, the synchronous interference case and the asynchronous interference case. Finally simulation results verified the upper bounds derived for the case of finite feedback-JLS precoding scheme.

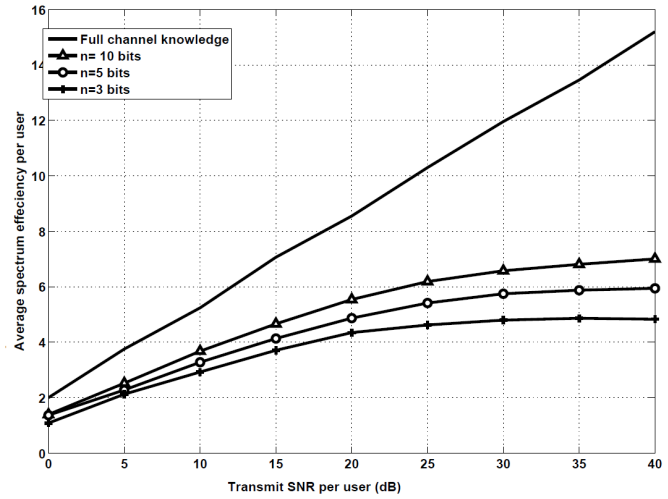

Fig. 4. Average Spectrum efficiency per user in case of using infinite channel feedback and finite feedback with 3, 5, and 10 feedback bits in an idealized synchronous environment.

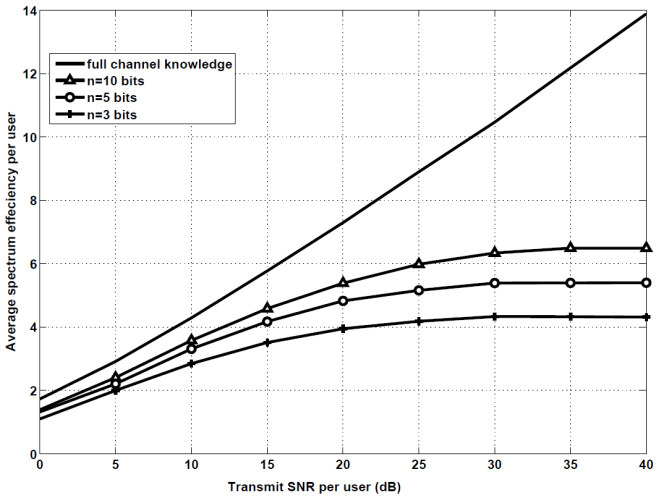

Fig. 5. Average Spectrum efficiency per user in case of using infinite channel feedback and finite feedback with 3, 5, and 10 feedback bits in asynchronous environment.

References

[1] Technical Specification Group Radio Access Network; Evolved Universal Terrestrial Radio Access (E-UTRA); Further advancements for E-UTRA physical layer aspects, TR 36.814. (9.0.0), 3rd Generation Partnership Project (3GPP), March 2010.

[2] D. Lee et al., Coordinated multipoint transmission and reception in LTE-advanced: deployment scenarios and operational challenges, *IEEE Communications Magazine*, vol. 50, no. 2, pp. 148-155, Feb. 2012.

[3] M. Sawahashi, Y. Kishiyama, A. Morimoto, D. Nishikawa, and M. Tanno, Coordinated multipoint transmission/reception techniques for lte-advanced [coordinated and distributed MIMO], in *Wireless Communications, IEEE*, Vol.17, pp.26-34, June 2010.

[4] N. Jindal and A. Goldsmith, Dirty-paper coding versus TDMA for MIMO broadcast channels, *Information Theory, IEEE Transactions on*, Vol.51, pp.1783-1794, May 2005.

[5] S. Shamai and B. Zaidel, Enhancing the cellular downlink capacity via co-processing at the transmitting end, in *Vehicular Technology Conference*, 2001. VTC 2001 Spring. IEEE VTS 53rd, Vol. 3, pp. 1745 -1749 vol. 3, 2001.

[6] C. Windpassinger, R. Fischer, T. Vencel, and J. Huber, Precoding in

multiantenna and multiuser communications, *Wireless Communications, IEEE Transactions on*, Vol. 3, pp. 1305 - 1316, July 2004.
[7] H. Dai, A. Molisch, and H. Poor, Downlink capacity of interference-limited MIMO systems with joint detection, *Wireless Communications, IEEE Transactions on*, Vol. 3, pp. 442 - 453, March 2004.
[8] J. Lee and N. Jindal, High snr analysis for MIMO broadcast channels: Dirty paper coding versus linear precoding, *Information Theory, IEEE Transactions on*, Vol. 53, pp. 4787 -4792, Dec. 2007.
[9] O. Simeone, O. Somekh, Y. Bar-Ness, and U. Spagnolini, Uplink throughput of TDMA cellular systems with multicell processing and amplify-and-forward cooperation between mobiles, *Wireless Communications, IEEE Transactions on*, Vol. 6, pp. 2942-2951, Aug. 2007.
[10] D. Jaramillo-Ramrez, M. Kountouris and E. Hardouin, Coordinated Multi-Point Transmission With Imperfect CSI and Other-Cell Interference, *IEEE Transactions on Wireless Communications*, vol. 14, no. 4, pp. 1882-1896, April 2015.
[11] H. Bahrami and T. Le-Ngoc, A capacity achieving precoding scheme based on partial channel information for broadcast MIMO systems, in *Wireless Communications and Networking Conference*, 2007. WCNC 2007. IEEE, pp. 1045 -1050, March 2007.
[12] H. Zhang, N. Mehta, A. Molisch, J. Zhang, and H. Dai, Asynchronous interference mitigation in cooperative base station systems, *Wireless Communications, IEEE Transactions on*, Vol. 7, pp. 155 -165, Jan. 2008.
[13] J. Tang et al., Robust MMSE Design With Asynchronous Interference Mitigation in Cooperative Base Station Systems, *Wireless Personal Communications*, Volume 78, Issue 2, pp 889-903, Sep. 2014
[14] M. Sadek, A. Tarighat, and A. Sayed, A leakage-based precoding scheme for downlink multi-user MIMO channels, *Wireless Communications, IEEE Transactions on*, Vol. 6, pp. 1711 -1721, May 2007.
[15] R. Bhagavatula, R. Heath, and B. Rao, Limited feedback with joint CSI quantization for multicell cooperative generalized eigenvector beamforming, in *Acoustics Speech and Signal Processing (ICASSP), 2010 IEEE International Conference on*, pp. 2838-2841, March 2010.
[16] R. Bhagavatula and R. Heath, Sum-rate maximizing beamforming in multicell systems with limited feedback, in Signals, Systems and Computers, *2009 Conference Record of the Forty-Third Asilomar Conference on*, pp. 1838 -1842, Nov. 2009.
[17] http://planetmath. org/encyclopedia/RayleighQuotient. html
[18] D. J. Love and R. Heath, Feedback techniques for MIMO channels, in *MIMO System Technology for Wireless Communications*, pp. 113146, edition 1: CRC Press, March 2006.
[19] F. Boccardi, H. Huang, and M. Trivellato, Multiuser eigenmode transmission for MIMO broadcast channels with limited feedback, in *Signal Processing Advances in Wireless Communications*, 2007. SPAWC 2007. IEEE 8th Workshop on, pp. 1 -5, June 2007.
[20] N. Jindal, Antenna combining for the MIMO downlink channel, *Wireless Communications, IEEE Transactions on*, Vol. 7, pp. 3834 -3844, Oct. 2008.
[21] M. Trivellato, H. Huang, and F. Boccardi, Antenna combining and codebook design for the MIMO broadcast channel with limited feedback, in *Signals, Systems and Computers*, 2007. ACSSC 2007. Conference Record of the Forty-First Asilomar Conference on, pp. 302 -308, Nov. 2007.
[22] W. Santipach and M. Honig, Asymptotic performance of MIMO wireless channels with limited feedback, in *Military Communications Conference*, 2003. MILCOM 2003. IEEE, Vol. 1, pp. 141 - 146 Vol. 1, Oct. 2003.
[23] J. Roh and B. Rao, Transmit beamforming in multiple-antenna systems with finite rate feedback: a VQ-based approach, *Information Theory, IEEE Transactions on*, Vol. 52, pp. 1101 -1112, March 2006.
[24] J. Conway, R. Hardin, and N. Sloane, Packing lines, planes, etc. : Packings in grassmannian spaces, *Experimental Mathematics*, Vol. 5, no. 2, p. 139-159, 1996.
[25] C. K. Au-Yeung and D. J. Love, On the performance of random vector quantization limited feedback beamforming in a MISO system, *Wireless Communications, IEEE Transactions on*, Vol. 6, pp. 458-462, Feb. 2007.
[26] S. Jafar and A. Goldsmith, Isotropic fading vector broadcast channels:the scalar upper bound and loss in degrees of freedom, *Information Theory, IEEE Transactions on*, Vol. 51, pp. 848 - 857, March 2005.
[27] J.L.W.V. Jensen, Sur les fonctions convexes et les inégalités entre les valeurs moyennes, *Acta Math.*, Vol. 30: 175, 1906.
[28] http://planetmath. org/encyclopedia/BetaRandomVariable. html
[29] M. Kountouris, R. de Francisco, D. Gesbert, D. Slock, and T. Salzer, Multiuser diversity-multiplexing tradeoff in *MIMO broadcast channels with limited feedback, in Signals, Systems and Computers, 2006*. ACSSC06. Fortieth Asilomar Conference on, pp. 364-368, Oct.29-Nov.1 2006.
[30] Technical Specification Group Radio Access Network; Spatial channel model for Multiple Input Multiple Output (MIMO) simulations, TR 25.996. (6.1.0), 3rd Generation Partnership Project(3GPP), Sept. 2003.

Yasmine Fahmy received the B. Sc with Honors from Cairo University in 1999 where she graduated as top of her class, the MSc. in 2001, and the PhD. in 2005, all in telecommunications, and all from the faculty of Engineering at Cairo University. She was appointed as a teaching assistant, at Cairo University, from September 1999 to September 2005. She is presently an associate professor at the Electronics and Communications Department, Faculty of Engineering, Cairo University, Egypt. Her current field of interest includes wireless communication and modern coding techniques. Since 2009, she has been with the Center of Wireless Studies (CWS), Cairo University.

Hierarchical mask creation for intelligent image coding using saliency maps

R. Vargic and J. Polec

***Abstract*—In this paper we analyze basic mask creation methods for intelligent image coding using saliency maps. For saliency maps based image coding we use specific extension of SPIHT algorithm called SM SPIHT related to region of interest encoding but extending this approach further, ending with individual weight of importance for each pixel in image using the form of saliency map. This approach is proved to be effective. In this article we analyze impact of different basic hierarchical mask creation methods, which have impact on error separation between salient and not salient parts of the image. The results indicate that proposed mask creation method outperforms JPEG2000 based mask tree creation method.**

***Keywords*—saliency, wavelet, image compression, hierarchical mask, SPIHT.**

I. Introduction

In recent years, saliency information in video and image, its presence and exploitation is attracting the attention not only in image and video compression area but also in human computer interaction (HCI) and multimodal interfaces area, where the saliency can be one of inputs influencing the HCI. In the static image compression area, the wavelet based approaches are among the most successful. Well-known references are SPIHT [1] (Set Partitioning In Hierarchical Trees) and standardized JPEG 2000 algorithm [2]. Both of them were extended for classical region of interest (ROI) oriented coding. In classical ROI encoding one or more ROIs get certain advantage in sense of their bit budget over non-ROI areas but as the number of ROIs increases, the efficiency of the process decreases.

The SM SPITH method [3] [4] takes in account the individual significance of each pixel of the image in the encoding/decoding process. The significance information is expressed in the form of saliency map (SM). The "intelligence" of this approach lies in the generalization of ROI approach: first - describe what is important (significant) in the image with as much freedom as possible, second - encode the image accordingly, i.e. allocate from available bit budget more bits for more important pixels. The original SM SPIHT method was also extended to JPEG 2000 [5].

The paper focuses on detail, how the SM is embedded in the encoding process in original SM SPIHT in the form of hierarchical mask and what are the limits of the approach.

The paper is divided in four sections, first we discuss in more detail the differences between ROI and SM approach, then we explain in deep the steps in the SM SPIHT approach followed by details regarding the mask tree creation methods. Lastly the performance results are presented and discussed.

II. Region oriented coding and saliency maps

In the classical ROI coding one or more regions are defined and their importance is stated.

In JPEG 2000 there are defined 2 different ROI methods [2], maxshift and general scaling. In maxshift approach, spectral coefficients belonging to particular ROI are shifted in the sense of bit planes clearly over the other coefficients. Based on their value the decoder can distinguish them from other coefficients (and shift them back) so there is no need to encode the ROI shape information. The general scaling approach shifts the spectral coefficients belonging to particular ROI only particularly, so they overlap in value with other coefficients and encoding of the ROI shape is needed to distinguish into which group the particular coefficient belongs and shift the ROI coefficients back.

There are several extensions of these concepts [6] [7] [8] but none of them handles the significance of each image pixels separately in the sense of significance map. This approach can be simulated by many ROIs with different shift, but as the number of ROIs increases, the efficiency of the process decreases.

The aims of the proposed method are to possibly and effectively take in account the individual significance of each pixel of the image. The significance information of the pixels of the evaluated image is expressed in the form of SM, which is 8-bit gray scale image with the same dimensions as the evaluated image. Its pixel values contain the importance of the corresponding pixels of the evaluated image (0=no importance, ..., 255=highest importance).

III. Details of SM SPIHT approach

The SM SPIHT algorithm [3] [4] addresses the key question "how to pass to the encoder the side information about importance" of the particular pixels using the saliency map. The basis is the well-known and recognized SPIHT [1] algorithm, coupled with biorthogonal discrete wavelet transform (DWT) and famous 9/7 tap filter known as bior4.4 in the Matlab community (the filter pair has four zero moments in both, decomposition and reconstruction parts of

Manuscript received August 5, 2016; revised October 10, 2016.

This paper was partly supported by the Slovak Research Grant Agency VEGA under grant No. 1/0625/14 and grant No. 1/0789/15.

Radoslav Vargic works at Department of Telecommunications at Slovak Technical University in Bratislava. Tel: +421 2 60291415; e-mail: Radoslav.vargic@stuba.sk.

Jaroslav Polec works at Department of Telecommunications at Slovak Technical University in Bratislava. Tel: +421 2 60291409; e-mail: jaroslav.polec@stuba.sk

doi: 10.11601/ijates.v5i3.191

corresponding filter bank). The DWT uses nonstandard decomposition, i.e. one decomposition level to low pass (L) subband and high pass (H) subband is applied on each row, then in each column resulting in the LL, LH, HL and HH subbands. The decomposition is then repeated only on the LL subband. The basic steps in the the wavelet based SPIHT encoding algorithm are:

1. 2D DWT with nonstandard decomposition using 9/7 filter is performed
2. SPIHT encoding of the spectrum including arithmetic encoding of the resulting stream is performed

As in EBCOT (Embedded Block Coding with Optimized Truncation) in JPEG 2000 uses SPIHT bit plane coding, so the significance of the coefficients is given by his value. The significance information for the encoder and decoder in the SM SIPHT is provided as side information. The saliency map for the decoder is encoded using separate SPIHT path as normal image. The whole SM SPIHT process in encoding and decoding phase is depicted in Fig. 1.

In the encoding phase the saliency map has to be prepared e.g. as in [3] [4]. After that it is needed the saliency mask encoding and immediate back-decoding, to have the same information in image encoder as in the decoder. From the decoded saliency mask, the mask tree is derived. The derivation of the mask tree is the main topic of this article and will be separately discussed in the next chapter.

The form of hierarchical saliency mask (HSM) has to have the same form as the subbands in 2D nonstandard wavelet spectrum. This particular form of the hierarchical mask is important from the viewpoint that all spectral coefficients that influence the same pixel in the reconstructed image, shall reflect the importance of that pixel. The correspondence of the particular coefficients to the same spatial location is well known feature of the 2D nonstandard decomposition spectral structure.

The mask tree is applied to the image spectrum before the encoder starts the bit plane encoding process of the spectral coefficients. We shift the spectral coefficients $SC(i,j)$ depending on their significance (0-255) expressed in the form of saliency map HSM(i,j) in the using the formula

$$SC(i,j)_{new} = \frac{SC(i,j)_{old}}{1 + str\,\frac{255 - HSM(i,j)}{255}}, \qquad (1)$$

where the *str* is configurable strength parameter in the range 0 - 255. When strength is set to 0, the SM SPIHT algorithm is equivalent to normal SPIHT algorithm. When strength is set do 255, then the least significant coefficients are divided by 256, so they are shifted 8 bit planes lower. After the spectrum is masked, it can be encoded using the original SPIHT algorithm.

In the decoder the hierarchical mask tree shall be constructed and the weights created using the saliency mask shall be applied using the following reverse formula to approximate the original spectrum values

$$SC(i,j)_{new} = SC(i,j)_{old}\left(1 + str\,\frac{255 - HSM(i,j)}{255}\right). \qquad (2)$$

Fig. 1. Schematic picture of whole SM SPIHT encoding and decoding process

After that the inverse DWT can be applied to spectrum to finally get the decoded image.

IV. HIERARCHICAL MASK CREATION

There are many options how to create the hierarchical mask, with respect which sub band levels shall be suppressed and which amplified. In the SM SPIHT approach [3], [4] the hierarchical mask was prepared using the averaging mask with following rules:

1) *mask pixels in the lower subband N were created by averaging the corresponding 4 pixels in the subband N+1, i.e. as if the Haar low pass filter would be used.*
2) *the same mask dynamic (values 0-255) was preserved across the sub bands.*
3) *all the 3 spatial tree orientations were handled equally*

We refer to this mask tree creation method as Method A (MA). In optimal conditions the mask image can be delivered to the decoder losslessly (of course bigger bit budget would be needed). We refer to this case as MA LSM (MA with Lossless Saliency Mask).

The second considered basic method for hierarchical mask creation is inspired by the method used JPEG 2000 [9] (Part 2, Annex K). Here for both ROI based methods it is important to know, which spectral coefficient influences the ROI and which not. The rule is simple: Select all spectral coefficients that could have non zero influence to the ROI.

The implementation rule is straightforward: Perform the inverse 2D discrete wavelet transform back – doing all operations in reversed order, including order of steps in lifting scheme and directions of arrows in lifting scheme steps, …). Note:

1) This (rather complicated) kind of implementation implements the question "given the set of spatial points, by which set of spectral points is affected by that set of spatial points in the inverse DWT process?"
2) If we would just simply use forward transform of the saliency map, we would get the answer for the following questions: "given the set of spatial points, which set of spectral points in the DWT process it affects"?

These questions are not same and also the sets of spectral coefficients are not same. We can illustrate the difference by the example on Fig. 2.

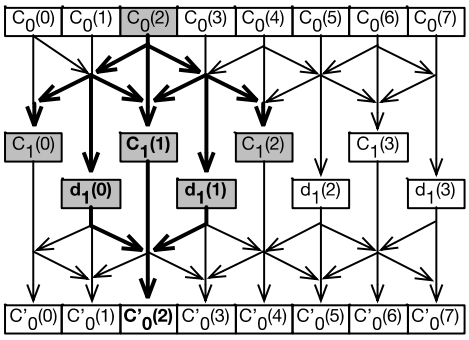

Fig. 2. Example of typical liftings steps in the DWT and inverse DWT. One can see that coefficient $c_0(2)$ affects 5 spectral coefficients, but in inverse DWT it is reconstructed from (affected by) only 3 spectral coefficients.

In JPEG 2000 conveys the resulting hierarchical mask just the binary information - which spectral coefficients could be needed and which not. In the saliency map approach this is not sufficient as the typical example are slowly changing values in the Saliency map. Resulting HSM has to be smooth as well, extending the binary information (important/not important) to how important the particular spectral coefficient is. This can be basically achieved by filtering using, where the 9/7 filters have the filter coefficients set equally to 1/7 in the case of 7 tap and 1/9 in the case of 9 tap filter. We refer to this mask creation method as Method B (MB).

From this method we derive also the MB LSM variant as it was the case in Method A.

In case we use lossless mask and the original saliency mask has binary form (not smooth), then we can use binary form of HSM and use exact the algorithm as in JPEG2000 (and abandon the filtering approach in MB). We refer to this method as MBO (MB optimized). Again – this method is applicable only for binary valued SM images and LSM mask has to be used. If the lossy mode for saliency mask in connection with MBO would be used, then even small nonzero values in non ROI area after mask reconstruction would indicate nonzero saliency and MBO declares them as significant. So we do not consider pure MBO method here.

We do not consider any further mask tree creation methods. In the next chapter pre provide performance results of abovementioned methods and outline the needed properties of another optimized method.

V. Results and Discussion

In this article we do not concentrate on situations with typical smooth saliency mask, they were evaluated in [3][4][5]. We concentrate on the border case, where the saliency mask has binary form – i.e. ROI with sharp edges exist. The best method shall have the best separation between the error in ROI compared to error in whole image.

a) Original Lena image b) very simple saliency map

Fig. 3. Image and saliency map used for experiments, a) Lena image b) very simple saliency map (equal to circular ROI in the Lena's face)

We compare the performance of all abovementioned masking methods. The experiments were performed using Lena image and typical circle shaped ROI as depicted on Fig. 3. We evaluated MSE and PSNR differences of the compressed image for the whole image and also taking in account she saliency information using the weighted MSE in the form:

$$MSE_{SM} = \frac{\sum_{i,j} \left(x(i,j) - \hat{x}(i,j) \right)^2 SM(i,j)}{\sum_{i,j} SM(i,j)}, \qquad (3)$$

where $x_{i,j}$ and $\hat{x}_{i,j}$ are pixels of the original and reconstructed image and $SM_{i,j}$ the pixels of the saliency map image. We apply this formula for the MSE computation in the ROI. The PSNR measure is derived from MSE using formula:

$$PSNR = 10 \log_{10} \frac{255^2}{MSE}. \qquad (4)$$

The result obtained for the method MA and its lossless variant MA LSM are depicted on Fig. 4. Both variants of MA method start to penalize the ROI at strength 10. Moreover, despite the expectation, the sharp saliency mask (available in the LSM mode) generally decreases the performance of the MA method then increasing the strength parameter.

The optimal strength value for the setup seems to be 7. The PSNR in ROI area is approximately the highest and by further increasing the strength the overall PSNR falls down.

The result obtained for the MB method its variants are depicted on Fig. 5. MB LSM and MB variants start to penalize the ROI at strength 10. The optimized variant continues to exploit the saliency of the ROI further. This leads us to important conclusion that the decrease of the performance in the ROI area at higher strengths is caused by low pass filtering during the hierarchical mask creation. The mask shape deformed and increasing the strength of the

process does not yield better results anymore (this explains also drop of the overall PSNR in the method A). The performance of the MBO LSM method is the best for the ROI area, however bigger strengths have to be used and we pay with heavy drop of the overall PSNR, so strength above 15 should be avoided.

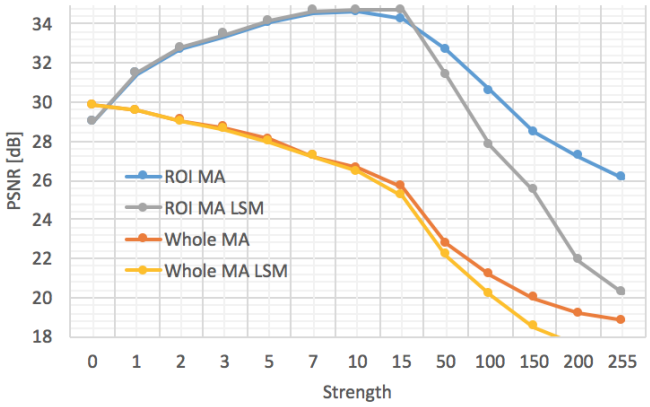

Fig. 4. Performance of the MA and MA LSM methods on Lena image compressed at 0.1 Bpp using different strength parameter. In MA is the mask lossy compressed to 0.01 Bpp. PSNR achieved in the ROI (weighted formula for MSE used) and in whole image can be compared.

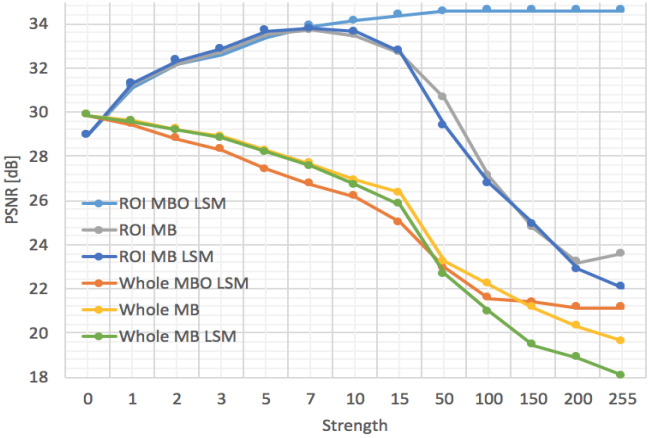

Fig. 5. Performance of the MB method and its variants on Lena image compressed at 0.1 bpp using different strength parameter. In MB is the mask lossy compressed to 0.01 bpp. PSNR achieved in the ROI (weighted formula for MSE used) and in whole image can be compared.

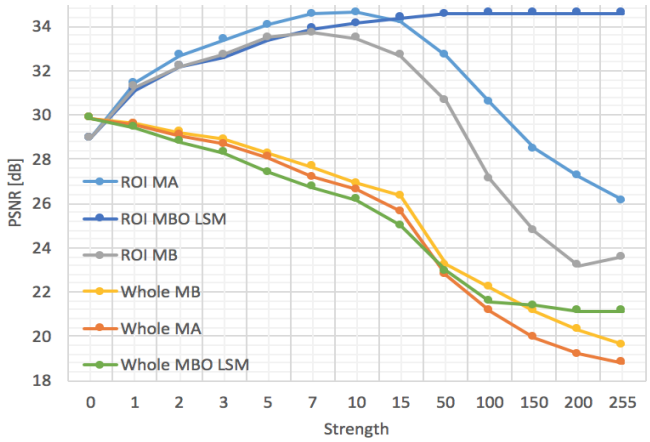

Fig. 6. Performance comparison of the MA and MB methods on Lena image compressed at 0.1 bpp using different strength parameter. In the lossy variants is the mask lossy compressed to 0.01 bpp.

Finally, the comparison of the best variants of MA and MB are given in the Fig. 6. As we can see, in the interesting part of the graph (strength <= 15) the MA clearly outperforms the MB methods – taking the same overall PSNR, the PSNR in the ROI is better for MA. Even more, the MA very slightly outperforms MBO LSM in the absolute PSNR achieved in the ROI. This leads us to important statement that is proven at least for tested image and bitrates: The JPEG 2000 algorithm makes sure that all spectral coefficients that could affect the ROI are taking in account, however this approach does not assure best performance from the rate/distortion sense. Simple averaging with as the MA method could achieve significantly better results.

Some representative results of compression are given in Fig. 7. All masking method enhance the facial area as expected. At strength = 7 the MA and MB perform visually similar, the 0,85 PSNR difference in the ROI is not visible. With strength set to maximum 255 the overall degradation is more visible in the MB than in MB LSM. Note, that though the MB method (as the MA method) has low PSNR in the face area, the facial details are preserved very good, there is notable only low pass distortion.

a) original image b) 0.1bpp, strength=0

a) 0.1bpp, MA, strength=7 b) 0.1bpp MB, strength=7

c) 0.1bpp MB, strength=255 d) 0.1bpp, MBO LSM, strength=255

Fig. 7. Examples of performance comparison of the presented mask creation methods using the mask from Fig. 5b, 0.1 bpp as target bitrate for the image and various strengths.

VI. CONCLUSION

In the presented contribution we demonstrate the performance of the selected basic hierarchical mask creation methods. The geometric/averaging principle is compared to "take all, that can have influence on" (JPEG 2000) principle. As the results show, the JPEG 2000 ROI approach can be outperformed in the rate/distortion sense by even simple averaging method. When the primary stress is really on the ROI area and overall PSNR is not important measure, there is probably space to further enhance the averaging method to better keep the ROI shape and do not drop down at strengths 7-15.

REFERENCES

[1] A. Said, and W. A. Pearlman, A new Fast and Efficient Image Codec Based on Set Partitioning in Hiererchical Trees, *IEEE Transactions on Circuits and Systems for Video Technology*, Vol. 6, June 1996

[2] A. P. Bradley and F. W. M. Stentiford, JPEG 2000 and region of interest Coding, DICTA2002, 21-22. January 2002, Melbourne

[3] R. Vargic and J. Polec, Intelligent image coding using saliency map extended PSIHT algorithm, In *INES 2015: 19th International conference on intelligent engineering systems*. Bratislava, Slovakia. September 3-5, 2015. Danvers : IEEE, 2015, pp. 69-72.

[4] R. Vargic, J. Kučerová, J. Polec, Wavelet based image coding using saliency map, SPIE *Journal of Electronic Imaging*, Vol. 25, No. 6, 061610 (Nov/Dec 2016), published online

[5] R. Vargic, and Kačur, Image coding using saliency maps based on JPEG 2000, Redžúr 2016, *10th International workshop on multimedia and signal processing*. Bratislava, Slovakia. May 24, 2016.

[6] M. Penedo, W. A. Pearlman, P. G. Tahoces, M. Souto, J. J. Vidal, Region-Based Wavelet Coding Methods for Digital Mammography, *IEEE transactions on medical imaging*, Vol. 22, No. 10, October 2003, pp. 1288-1296.

[7] K. Martin, R. Lukac, K. N. Plataniotis, SPIHT-Based Coding of the Shape and Texture of Arbitrarily Shaped Visual Objects, *IEEE transaction on circuits and systems for video technology*, Vol. 16, No. 10, October 2006

[8] P. G. Tahoces, J. R. Varela, M. J. Lado, M. Souto, Image compression: Maxshift ROI encoding options in JPEG2000, *Computer Vision and Image Understanding*, Vol. 109, pg.139-145, 2008.

[9] JPEG 2000 image coding system: Extensions, ISO/IEC 15444-2:2004, International standard.

R**adoslav Vargic** was born in 1972 in Myjava. He has received the Ing and PhD Degree from Slovak Technical University in Bratislava in years 1995 and 1999 respectively. From that time, he works at Department of Telecommunications at Slovak Technical University in Bratislava. His research interests are wavelets and multimedia processing.

Jaroslav Polec was born in 1964 in Trstená, Slovakia. He received the Ing and PhD degrees in telecommunication engineering from the Faculty of Electrical Engineering and Information Technology, Slovak University of Technology in 1987 and 1994, respectively. Since 1997 he has been associate professor and since 2007 professor at the Institute of Telecommunications of the Faculty of Electrical Engineering and Information Technology, Slovak University of Technology and since 1998 at the Department of Applied Informatics, Faculty of Mathematics, Physics and Informatics of the Comenius University. His research interests include Automatic Repeat Request (ARQ), channel modelling, image coding, interpolation and filtering.

Performance Estimation of the Mtd64-ng DNS64 Implementation

Gábor Lencse

***Abstract*—DNS64 and NAT64 are IPv6 transition technologies enabling IPv6 only clients to communicate with IPv4 only servers. Mtd64-ng is a novel DNS64 implementation, being a successor of MTD64. In this paper, the performance of mtd64-ng is compared with that of MTD64 and BIND. The details of the measurements are fully disclosed. It is found that under heavy load conditions mtd64-ng can answer six times as many "AAAA" record requests per second than BIND. Mtd64-ng fixed two issues of MTD64 and also outperformed its predecessor by answering 46% more "AAAA" record requests per second under heavy load conditions.**

***Keywords*—BIND, DNS, DNS64, IPv6 transition, MTD64, mtd64-ng, performance comparison**

I. Introduction

The DNS64 [1] IPv6 transition technology (together with NAT64 [2]) enables clients having only IPv6 addresses to communicate with servers having only IPv4 addresses. Several free software [3] (also called open source [4]) DNS64 implementations exist. The stability and performance of BIND, TOTD, PowerDNS and Unbound were examined and compared in [5]. Two of them (BIND and PowerDNS) are multithreaded, thus they can benefit from the current multi-core CPUs, whereas the other two ones are single-threaded. A novel DNS64 implementation, namely MTD64 (Multi-Threaded DNS64) was developed at the Department of Networked Systems and Services, Budapest University of Technology and Economics [6]. The novelty of this implementation is that it starts a new thread for each request and therefore it can inherently utilize the computing power of all cores of a multi-core CPU. Its performance was compared to that of BIND and it was found that MTD64 seriously outperformed BIND concerning the number of answered "AAAA" record requests per second [7].

However, MTD64 is vulnerable to DoS (Denial of Service) attack by design: an attacker can force MTD64 to start a high number of threads, which may exhaust the memory of the computer. Therefore, MTD64 has been redesigned and re-implemented as mtd64-ng by Daniel Bakai [8]. The new design contains a thread pool of a fixed size (which is a configuration parameter), thus it spares the extra work of starting and terminating threads. In addition to that, mtd64-ng has a full object oriented design, whereas MTD64 was written mostly in C to achieve higher speed (C++ was used for convenient thread handling plus a class was used for storing the configuration parameters) [9]. MTD64 had another problem: memory leaking was experienced during its performance testing. This problem is fully eliminated in mtd64-ng by using the RAII idiom (Resource Acquisition Is Initialization) [10]. The most important design and implementation details of mtd64-ng can be found in the developer documentation of mtd64-ng [11].

The aim of this paper is to check whether mtd64-ng kept the high performance of MTD64 after its redesign and reimplementation. For this purpose, the performances of mtd64-ng, MTD64 and BIND are measured and compared using a similar test setup to that of [9].

Manuscript received July 28, 2016, revised October 1, 2016.

G. Lencse is with the Department of Networked Systems and Services, Budapest University of Technology and Economics, 2 Magyar tudósok körútja, H-1117 Budapest, Hungary (phone: +36-20-775-82-67; fax: +36-1-463-3263; e-mail: lencse@hit.bme.hu).

doi: 10.11601/ijates.v5i3.176

II. Method for Testing

A. Overview

The principles of the DNS64 testing method were laid down in [12]. In short, a high number of queries for "AAAA" records (IPv6 addresses) are sent to the DNS64 server. The requests contain different domain names which have only "A" records (IPv4 addresses) and no "AAAA" records. Therefore, the DNS64 server needs to synthesize them. It happens as follows. When the DNS64 server receives an "AAAA" record request for a particular domain name then first, it asks the normal DNS system for an "AAAA" record of the given domain name. Since it receives an empty answer, second, it sends an "A" record request to the DNS system for the same domain name. Now it receives a valid answer and it synthesizes a so-called *IPv4 embedded IPv6 address* using the prefix, which was set in its configuration file and embeds the 32 bits of the "A" record (IPv4 address). Finally it returns the synthesized IPv6 address.

The testing method has been improved over time. Originally, bash shell scripts were applied using the standard Linux host command. As its default behavior, it also requested an "MX" record [13]. Then, the request for the "MX" record was eliminated in order to focus on the "AAAA" record only [14]. Next, the shell script was partially rewritten in C to be able to provide high enough load for testing multi-core CPUs [5]. After that, the whole test program was implemented in C [15], which was named **`dns64perf`**. This program has added another factor of freedom: the user may set the number of threads to be able to tune the intensity of the load, however the number of sent queries was still

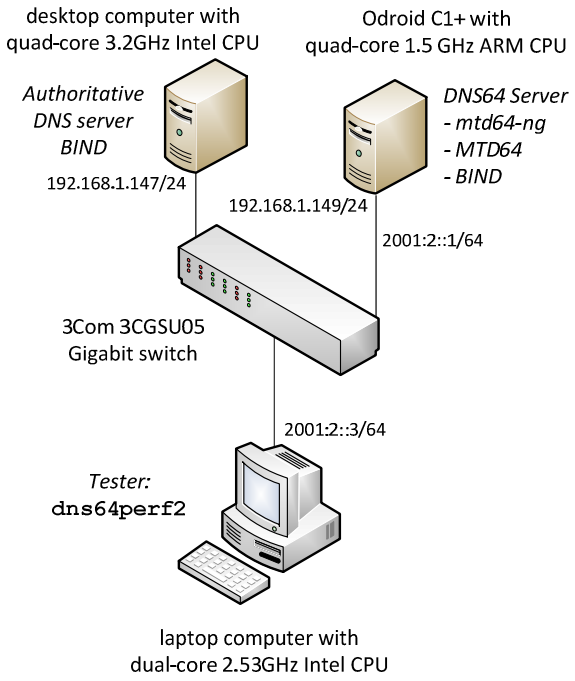

Fig. 1. Topology of the test network

fixed. Finally, this program was modified to be able to tune the number of sent queries and the second version of the program was used in our before mentioned paper for testing the performance of MTD64 [7]. The operation of the **dns64perf** program and its changes in the second version (**dns64perf2**) are well documented in [15] and in [7], respectively. Therefore, now we give only a short summary of the testing method.

B. Namespace

The **n1-n2-n3-n4.dns64perf.test** independent namespace is used, where n1, n1, n3 and n4 are integers in the [0, 255] interval. The elements of the namespace are mapped by a local authoritative DNS server to the n1.n2.n3.n3 IPv4 addresses.

C. Measurement Program Details

An *experiment* is composed of the queries for "AAAA" records of 256 different domain names. The 256 queries are sent by *n* threads, were *n* must be a power of 2 (e.g. 1, 2, 4, 8, 16, etc.) and each thread sends 256/*n* number of queries sequentially in a way that the next query can be sent after receiving the reply for the current one. Thus parameter *n* can be used to tune the intensity of the load. The execution time of an experiment is measured and printed to the standard output of the program (in milliseconds). Whereas the old version of the program (**dns64perf**) always performed exactly 256 experiments, **dns64perf2** has a further parameter: *b*, and it executes *b**256 number of experiments (to be able to perform longer tests continually).

D. Test Setup and Measurements

The topology of the test network is shown in Fig. 1. The three DNS64 implementations were executed by an Odroid C1+ single board computer (see top right) to be able to produce high enough load by the laptop computer (see at the bottom). The authoritative DNS server was a modern desktop computer to avoid being a bottleneck (see top left).

The measurements were performed using different parameters. First, the optimal value for the number of *working threads* of mtd64-ng was determined by executing a series of measurements using 1, 2, 4, 8, 16, 32, 64 or 128 working threads and generating the possible highest load by the **dns64perf2** program using 32 threads in it. Then the number of working threads of mtd64-ng was set fixed to the value that resulted in the best performance of mtd64-ng, and the performances of the three DNS64 implementations were compared under different load conditions produced by using different number of threads in the **dns64perf2** test program. Besides the execution time of the **dns64perf2** program, also the CPU utilization of the DNS64 server was measured to give more insight into the behavior of the three DNS64 implementations. Finally, MTD64 and mtd64-ng were tested against memory leaking by executing extremely long tests.

The measurements were carried out by several scripts disclosed in the next subsection.

E. Measurement Scripts

The "main" measurements were performed by the following bash script:

```
#!/bin/bash
#Paramaters:
server=2001:2::1  # IPv6 addr. of the DNS64 server
dns64=mtd64-ng    # DNS64 server (set manually)
b=4               # the length of the measurement

for (( i=0; i<6; i++ ))
do
  nth=$((2**i));  # number of threads
  ssh $server ./stats $dns64 $nth &
  sleep 1
  ./dns64perf2 $i $b $nth 1 $server > \
    odroid-${dns64}-$nth
  ssh $server killall dstat
  sleep 5
done
```

As it can be seen, variable **i** took the values from 0 to 5 that is the number of threads were: 1, 2, 4, 8, 16 and 32.

The above script started the **stats** script on the DNS64 server to log the CPU utilization using the **dstat** Linux command. The contents of the **stats** script was:

```
#!/bin/bash
nice -n 10 dstat -c --output \
  dns64-stats-$1-$2.dstat > /dev/null
```

Before the execution of the "main" measurements, we needed to optimize the number of working threads to be set in the configuration file of mtd64-ng. For this purpose, the modified version of the first script was used:

```
#!/bin/bash
#Paramaters:
server=2001:2::1  # IPv6 addr. of the DNS64 server
dns64=mtd64-ng    # DNS64 server (set manually)
b=4               # the length of the measurement

for (( i=0; i<8; i++ ))
```

```
do
  nth=$((2**i));  # No.of mtd64-ng working threads
  ssh -l root $server ./set-mtd64-ng-wth $nth
  ssh $server ./stats $dns64 $nth &
  sleep 1
  ./dns64perf2 0 $b 32 1 $server > \
    odroid-${dns64}-$nth
  ssh $server killall dstat
  sleep 5
done
```

During the optimization process, the number of threads used in **dns64perf2** was always 32 (see its third parameter) to ensure the highest possible load. Variable **nth** (taking the values 1, 2, 4, 8, 16, 32, 64, 128) denoting the number of *working threads* was set in the configuration file of mtd64-ng by the **set-mtd64-ng-wth** script:

```
#!/bin/bash
killall mtd64-ng
cd /etc
cp mtd64-ng.conf.core mtd64-ng.conf
echo "num-threads $1" >> mtd64-ng.conf
mtd64-ng
```

The script for testing memory leaking was much simpler than the above measurement scripts. It executed only one but very long test, achieving it by using 255 for the value of **b**, and thus performing 255*256*256 "AAAA" queries. Its content was:

```
#!/bin/bash
#Paramaters:
server=2001:2::1  # IPv6 addr. of the DNS64 server
dns64=mtd64-ng    # DNS64 server (set manually)
b=255             # length of the measurement

ssh $server ./memstat $dns64 &
sleep 1
./dns64perf2 0 $b 32 1 $server > \
  odroid-${dns64}-mem
ssh $server killall pidstat
```

The above script started the **memstat** script on the DNS64 server to log the memory utilization using the **pidstat** Linux command. The contents of the **memstat** script was:

```
#!/bin/bash
nice -n 10 pidstat -h -r -p $(pidof $1) 1 | \
  grep $1 > dns64-mem-stats-$1
```

For the repeatability of our measurements, we provide configuration details in the following subsections.

F. Hardware and Software Parameters

1) Authoritative DNS Server

Desktop computer with: 3.2GHz Intel Core i5-4570 CPU (4 cores, 6MB cache), 16GB 1600MHz DDR3 SDRAM, 250GB Samsumg 840 EVO SSD, Realtek RTL8111F PCI Express Gigabit Ethernet NIC; Debian 8.2 GNU/Linux operating system, 3.2.0-4-amd64 kernel, BIND 9.9.5-9+deb8u3-Debian

2) DNS64 server

Odroid C1+ single board computer with: 1.5GHz quad-core ARM Cortex A5 CPU (4 cores, 512kB cache), 1GB DDR3 SDRAM, 16GB Kingston micro SD card, 1000BaseTX Ethernet NIC; Ubuntu 14.04.4 LTS GNU/Linux operating system, 3.10.80-131 armv7l kernel, BIND 9.9.5-3ubuntu0.8-Ubuntu, MTD64 from [16], mtd64-ng from [8].

3) Tester

Dell Latitude E6400 series laptop with: 2.53GHz Intel Core2 Duo T9400 CPU (2 cores, 6MB cache), 4GB 800MHz DDR2 SDRAM, 250GB Samsumg 840 EVO SSD, Intel 82567LM Gigabit Ethernet NIC; Debian 8.2 GNU/Linux operating system, 3.2.0-4-amd64 kernel, **dns64perf2** from [17].

4) Switch

3CGSU05 5-port 3Com Gigabit Ethernet switch.

G. Authoritative DNS Server Configuration

1) BIND settings

The **/etc/bind/named.conf.local** file contained the following settings:

```
zone "dns64perf.test" {
        type master;
        file "/etc/bind/db.dns64perf.test";
};
```

2) Zone file

The **db.dns64perf.test** zone file was generated by the following bash script:

```
#!/bin/bash
cat > db.dns64perf.test << EOF

\$ORIGIN dns64perf.test.
\$TTL    86400
@  IN  SOA  localhost. root.localhost. (
        2016012901     ; Serial
            604800     ; Refresh
             86400     ; Retry
           2419200     ; Expire
             86400 )   ; Negative Cache TTL
;
@       IN      NS      localhost.

EOF

for a in {0..6} # to provide independent namespace
do
  for b in {0..10} # see parameter b of dns64perf2
  do
    for c in {0..255}
    do
      echo '$'GENERATE 0-255 $a-$b-$c-$ \
        IN A $a.$b.$c.$ >> db.dns64perf.test
    done
  done
done
echo "" >> db.dns64perf.test
```

The memory leaking tests required only single but much larger namespace. Therefore, the **for** cycle for **a** was omitted (the value of **a** was set to 0) and the value of **b** was running from 0 to 255, thus the size of the namespace was 256^3=16M.

H. DNS64 Server Configuration

1) BIND

The **/etc/bind/named.conf.options** file contained the following settings:

```
options {
        directory "/var/cache/bind";
        forwarders { 192.168.1.147; };
        forward only;
        dns64  2001:db8::/96 { };
```

TABLE I. DNS64 PERFORMANCE OF MTD64-NG AS A FUNCTION OF THE NUMBER OF WORKING THREADS, USING ALWAYS 32 THREADS IN DNS64PERF2

1	No. of working threads in **mtd64-ng**		1	2	4	8	16	32	64	128
2	Execution time of 256	average	82.53	53.05	37.18	29.37	27.40	36.89	36.79	36.93
3	queries (ms)	std. dev.	2.35	0.80	0.60	0.84	2.49	3.84	3.78	3.90
4	No. of served queries per sec. (q/s)		3102	4826	6885	8716	9342	6940	6959	6933

TABLE II. DNS64 PERFORMANCE OF BIND

1	Number of threads used in **dns64perf2**		1	2	4	8	16	32
2	Execution time of 256 queries (ms)	average	517.60	291.78	183.20	165.99	163.01	166.32
3		standard deviation	34.78	28.46	6.63	14.95	11.14	8.48
4	Number of served queries per second (query/sec)		495	877	1397	1542	1570	1539
5	DNS64 server CPU utilization (%)	average	34.55	52.45	82.42	90.45	92.32	93.03
6		standard deviation	8.20	2.58	1.90	3.59	2.73	2.28

TABLE III. DNS64 PERFORMANCE OF MTD64

1	Number of threads used in **dns64perf2**		1	2	4	8	16	32
2	Execution time of 256 queries (ms)	average	125.81	75.25	50.54	42.15	40.62	40.30
3		standard deviation	2.69	1.24	11.47	2.56	5.57	1.80
4	Number of served queries per second (query/sec)		2035	3402	5066	6073	6302	6353
5	DNS64 server CPU utilization (%)	average	23.43	39.28	61.44	76.58	87.22	88.45
6		standard deviation	2.76	1.12	3.03	1.19	1.95	1.39

TABLE IV. DNS64 PERFORMANCE OF MTD64-NG USING 16 WORKING THREADS

1	Number of threads used in **dns64perf2**		1	2	4	8	16	32
2	Execution time of 256 queries (ms)	average	117.20	67.65	44.80	34.90	30.74	27.56
3		standard deviation	0.65	0.97	1.21	1.07	2.29	2.62
4	Number of served queries per second (query/sec)		2184	3784	5714	7335	8328	9289
5	DNS64 server CPU utilization (%)	average	20.63	34.64	51.89	67.18	76.93	83.87
6		standard deviation	1.15	0.92	0.69	0.87	1.14	1.43

```
        dnssec-validation no;
        auth-nxdomain no
        listen-on-v6 { any; };
};
```

We note that dnssec validation was switched off for the fair comparison with the two other DNS64 implementations.

2) MTD64

The **settings.conf** file contained the following settings:

```
nameserver 192.168.1.147
dns64-prefix 2001:db8::/96
debugging no
timeout-time-sec  1
timeout-time-usec 0
resend-attempts   1
response-maxlength  512
```

3) Mtd64-ng

The **/etc/mtd64-ng.conf** file contained the following settings:

```
nameserver 192.168.1.147
dns64-prefix 2001:db8::/96
debugging no
timeout-time  1.0
resend-attempts   1
response-maxlength  512
port 53
num-threads 16 # for the "main" measurements
```

III. RESULTS

A. Number of Working Threads for Mtd64-ng

The measurement results of the experiment series for determining the optimal number of working threads of mtd64-ng are presented in Table I. The first row specifies the number of working threads used in mtd64-ng. The average and the standard deviation of the execution time of an experiment (256 queries) are shown in rows 2 and 3, respectively. The number of the replied "AAAA" record queries per second (N) is shown in row 4, which was calculated according to (1), where T denotes the average execution time of one experiment (resolution of 256 "AAAA" record queries) specified in milliseconds.

$$N = \frac{256 \frac{query}{exp} * 1000 \frac{ms}{s}}{T \frac{ms}{exp}} \quad (1)$$

As it was expected, first, the number of server requests per second increased with the number of working threads. It reached its maximum value at 16 working threads and then it showed degradation up to 128 working threads. Therefore, the number of working threads was set to 16 for the following experiments and all three DNS64 implementations were tested under the same conditions.

B. Performance Comparison

The performance measurement results are presented in identical tables for all three DNS64 implementations: Table II, Table III and Table IV contain results of BIND, MTD64 and mtd64-ng, respectively. In each table, the first row specifies the number of threads used in **`dns64perf2`**. The number of threads is used for setting higher and higher loads, but we note that doubling the number of threads does not result in exactly double intensity of the load. The average and the standard deviation of the execution time of an experiment (256 queries) are shown in rows 2 and 3, respectively. The number of served queries per second was calculated according to (1) and it is given in row 4. The average and the standard deviation of the CPU utilization of the DNS64 server computer are displayed in rows 5 and 6, respectively. (100% denotes the aggregated CPU capacity of the four cores.) We note that the CPU utilization was calculated as subtracting the idle time percentage from 100%. (See [5] for the justification of this method.)

Our most important result is that mtd64-ng has seriously outperformed BIND at any load conditions by answering 4-6 times higher number of queries than BIND (it was 2184 vs. 495 at 1 thread and 9289 vs. 1539 at 32 threads.) The performance of mtd64-ng was similar to that of MTD64 under low load (1 thread) and the difference increased with the increase of the load: mtd64-ng significantly outperformed MTD64 under high load (it was 9289 q/s vs. 6353 q/s at 32 threads).

The observation of the CPU utilization values gives a deeper understanding of the behavior of the three DNS64 implementations. BIND used visibly more computing power (34.55%) at 1 thread than MTD64 (23.43%) or mtd64-ng (20.63%). BIND could increase its performance until its CPU utilization approached 90% at 8 threads, and then neither the number of served queries nor the CPU utilization could significantly grow. MTD64 needed significantly less CPU power and its performance showed similar saturation at 16 – 32 threads (6302q/s – 6353q/s). As the CPU utilization of mtd64-ng was even lower it could significantly increase its performance even during the 16 – 32 threads change (8328q/s – 9289q/s).

C. Discussion

As for the question why both MTD64 and mtd64-ng could seriously outperform BIND, we can mention multiple reasons. First of all, our measurement method eliminates the possible performance gain of caching. Whereas this aspect of our testing method complies with the requirements of the relevant Internet Draft [18], the measurement method impairs the measured performance of DNS64 implementations that use caching as they waste a significant amount of CPU cycles with maintaining their caches (without any possible performance gain). Another factor can be that both MTD64 and mtd64-ng are simple and tiny thus their working sets [19] better fit into the L1 or L2 cache of the CPU of the DNS64 server than that of BIND, thus they can be executed faster than BIND.

Our results definitely show that mtd64-ng not only kept the high performance of MTD64 but even significantly outperformed it. We identify one of the reasons as the usage of a thread pool: thus no thread creation is necessary for the processing of every single new requests. Since the processing of "AAAA" record requests does not require much computation but only constructing and sending two requests (first, for an "AAAA" record and, after an empty answer, for an "A" record) to the authoritative DNS server and synthesizing the reply and sending it back to the client, the thread creation overhead may be significant. We also consider that mtd64-ng has a better quality source code than MTD64, which may also result in higher performance.

D. Memory Leaking and Vulnerability to DoS Attacks

As for the memory leaking tests, on the one hand, MTD64 showed so high memory leaking that the test could not be fully performed, because MTD64 was unable to respond (in time) and the **`dns64perf2`** ran out of available sockets. On the other hand, mtd64-ng showed no memory leaking at all: both VSS (virtual set size) and RSS (resident set size) were constant during the measurements. Thus mtd64-ng proved to be totally free of memory leaking.

MTD64 starts a separate thread for every single request and thus it is susceptible to the kind of DoS attacks where the memory of the DNS64 server is exhausted by sending too many "AAAA" record requests per second. Using a fixed sized thread pool, mtd64-ng is no more susceptible to this kind of DoS attack.

IV. Conclusion

We conclude that mtd64-ng, the successor of MTD64 fixed the memory leaking and vulnerability to DoS attacks issues of MTD64 and also significantly outperformed it. We plan to test and develop this promising DNS64 implementation further.

References

[1] M. Bagnulo, A. Sullivan, P. Matthews and I. Beijnum, "DNS64: DNS extensions for network address translation from IPv6 clients to IPv4 servers", IETF RFC 6147, April 2011.

[2] M. Bagnulo, P. Matthews and I. Beijnum, "Stateful NAT64: Network address and protocol translation from IPv6 clients to IPv4 servers", IETF RFC 6146, April 2011.

[3] Free Software Fundation, "The free software definition", [Online]. Available: http://www.gnu.org/philosophy/free-sw.en.html

[4] Open Source Initiative, "The open source definition", [Online]. Available: http://opensource.org/docs/osd

[5] G. Lencse, S. Répás, "Performance analysis and comparison of four DNS64 implementations under different free operating systems", *Telecommun. Systems*, in press, DOI: 10.1007/s11235-016-0142-x

[6] G. Lencse and A. G. Soós, "Design of a tiny multi-threaded DNS64 server", in *Proc. 38th Internat. Conf. on Telecommunications and Signal Processing (TSP 2015)*, Prague, 2015, pp. 27–32. DOI: 10.1109/TSP.2015.7296218

[7] G. Lencse, "Performance analysis of MTD64, our tiny multi-threaded DNS64 server implementation: Proof of concept", *Internat. J. of Adv. in Telecommun., Electrotechn., Signals and Systems*, vol. 5, no 2, pp. 116–121, DOI: 10.11601/ijates.v5i2.166

[8] D. Bakai, "Mtd64-ng: A lightweight C++11 DNS64 server", source code, [Online]. Available: https://github.com/bakaid/mtd64-ng

[9] G. Lencse, A. G. Soós, "Design, implementation and testing of a tiny multi-threaded DNS64 server", *Internat. J. of Adv. in Telecommun.,*

Electrotechn., Signals and Systems, vol. 5. no. 2, pp. 68–78, DOI: 10.11601/ijates.v5i2.129

[10] B. Stroustrup, The C++ Programming Language, 3rd ed. Addison-Wesley Longman. Reading Mass. USA.

[11] D. Bakai, "mtd64-ng: A lightweight C++11 DNS64 server" developer documentation, [Online]. Available: https://github.com/bakaid/mtd64-ng/tree/master/doc

[12] G. Lencse and G. Takács, "Performance analysis of DNS64 and NAT64 solutions", *Infocommunications Journal*, vol. 4, no. 2, pp. 29–36, June 2012.

[13] G. Lencse and S. Répás, "Performance analysis and comparison of different DNS64 implementations for Linux, OpenBSD and FreeBSD", in Proc. *IEEE 27th Internat. Conf. on Advanced Information Networking and Applications (AINA 2013)*, Barcelona, Spain, 2013, pp. 877-884. DOI: 10.1109/AINA.2013.80

[14] G. Lencse and S. Répás, "Improving the performance and security of the TOTD DNS64 implementation", *Journal of Computer Science and Technology*, ISSN: 1666-6038, vol. 14, no. 1, pp. 9–15. Apr. 2014.

[15] G. Lencse, "Test program for the performance analysis of DNS64 servers", *Internat. J. of Adv. in Telecommun., Electrotechn., Signals and Systems*, vol. 4, no. 3, pp. 60–65. Sep. 2015. DOI: 10.11601/ijates.v4i3.121

[16] A. G. Soós, "MTD64: Multi-Threaded DNS64 server" source code, [Online]. Available: https://github.com/Yoso89/MTD64

[17] G. Lencse, "dns64perf2" source code, [Online]. Available: http://www.hit.bme.hu/~lencse/dns64perf2

[18] M. Georgescu and G. Lencse, "Benchmarking methodology for IPv6 transition technologies", Internet Draft, IETF BMWG, July 7, 2016, [Online]. Available: https://tools.ietf.org/html/draft-ietf-bmwg-ipv6-tran-tech-benchmarking-02

[19] P. J. Denning, "The working set model for program behavior", *Communications of the ACM*, vol. 11, no. 5, pp. 323–333, May 1968. DOI: 10.1145/363095.363141

Gábor Lencse received his MSc in electrical engineering and computer systems at the Technical University of Budapest in 1994, and his PhD in 2001.

He has been working for the Department of Telecommunications, Széchenyi István University in Győr since 1997. He teaches computer networks, and the Linux operating system. Now, he is an Associate Professor. He is responsible for the specialization of the information and communication technology of the BSc level electrical engineering education. He is a founding and also core member of the Multidisciplinary Doctoral School of Engineering Sciences, Széchenyi István University. The area of his research includes discrete-event simulation methodology, performance analysis of computer networks and IPv6 transition technologies. He has been working part time for the Department of Networked Systems and Services, Budapest University of Technology and Economics (the former Technical University of Budapest) since 2005. There he teaches computer architectures and computer networks.

Dr. Lencse is a member of IEEE, IEEE Communications Society and IEICE (Institute of Electronics, Information and Communication Engineers, Japan).

Power-Efficiency Comparison of Spectrum-Efficient Optical Networks

Sridhar Iyer

***Abstract*—With steady traffic volume growth in the core networks, it is predicted that the future optical network communication will be constrained mainly by the power consumption. Hence, for future internet sustainability, it will be a mandate to ensure power-efficiency in the optical networks. Two paradigms known to support both, the traffic heterogeneity and high bandwidth requests are the: (i) next generation flexible (or elastic) orthogonal frequency division multiplexing (OFDM) based networks which provide flexible bandwidth allocation per wavelength, and (ii) currently deployed mixed-line-rate (MLR) based networks which provision the co-existence of 10/40/100 Gbps on varied wavelengths within the same fiber. In this work, the power-efficiency of an OFDM, and a MLR based network has been compared for which, a mixed integer linear program (MILP) model has been formulated considering deterministic traffic between every network source-destination pair. The simulation results show that in regard to power-efficiency, the OFDM based network outperforms the MLR based network.**

***Keywords*—Elastic optical networks, mixed line rate optical networks, MILP, power-efficiency, spectrum-efficiency.**

I. Introduction

For satisfying request(s) of the various heterogeneous services having different applications and varied bandwidth requirements, the legacy 10 Gbps optical transport networks have been upgraded to the 40 and/or 100Gbps networks via the adoption of a mixed line rate (MLR) strategy [1]. MLR networks are spectrum-efficient as they provision the co-existence of 10/40/100 Gbps on varied wavelengths within the same fiber, and further, decrease the overall transmission cost owing to volume discount of the high bit-rate transponders [2]. However, the MLR based networks follow the ITU-T defined fixed-grid which necessitates the admission of all the channels within a fixed 50 GHz channel spacing [2], which may (i) not be adequate for high speed channels, and (ii) under-utilize spectrum for low bit-rate requests. Hence, for pursuing technologies for future networks, flexi-grid systems need to be adopted which can adjust the bandwidth utilization as per the demands, and also provision long transmission range (TR) and high spectral-efficiency (SE) [3, 4].

Recent studies have identified Orthogonal Frequency-Division Multiplexing (OFDM) as the technology to enable the flexi-grid system based networks [5, 6]. In OFDM, several orthogonal carriers (individual carrier is referred to as a subcarrier) are modulated and the composite signal is then carried over an individual wavelength, via a fiber, and further, many such wavelengths are multiplexed within the fiber. Further, in an OFDM based flexi-grid network (i) the ITU-T defined standardized granularity of 12.5 GHz [6] is followed, (ii) on the basis of requirement(s), wider channels are created by combining the spectrum units (also called as slots), and (ii) use of multiple subcarriers ensures that the wavelength capacity can be zoned into finer granularities, hence provisioning increased flexibility in capacity allocation to the heterogeneous demands. Such elastic networks make use of the flexible transceivers (referred to as Bandwidth Variable Transponders (BVTs) in this study) which allows many demand serving options by making a decision on the modulation format, bit-rate, and/or spectrum, and making a choice which provides adequate TR performance. Hence, any BVT with a cost c, r Gbps of transmission rate tuning, and using the spectrum slot(s) of bandwidth b and guardband g, leads to p amount of power consumed in order to transmit with a satisfactory quality of transmission (QoT), for l km of distance [7].

Further, compared to MLR networks, in OFDM based networks, based on the various scenarios, the overall power incurred is different, which can be explained as follows: let there occur a 100 Gbps demand between two nodes *a*-*b* of the network. To satisfy such a demand, there may exist(s) multiple paths which are connected via the fiber links between the two network nodes *a*-*b*. Also, it may occur that the demand (i) is set up using a transparent (i.e., an all-optical channel (wavelength)) resulting in minimum network cost, or (ii) at the increased load values, owing to the signal reach constraint (which restricts high bit-rate signal(s) to traverse only a short distance before the regeneration requirement), there is no end-to-end transparent route, and hence, between the multiple channels, the demand will require splitting up. Further, the used channels may traverse via the same or through different fibers, and therefore, varied overall network power will be incurred. Hence, in the complete network with many requests, and the (i) wavelength-continuity constraint, (ii) capacity constraint, and (iii) maximum subcarrier constraint [3, 4], the optimization problem of minimizing

Manuscript received November 7, 2016, revised December 12, 2016

Sridhar Iyer is with Department of ECE, Jain College of Engineering, T S. Nagar Hunchanatti Cross- Machhe, Belagavi, Karnataka, India - 590014; e-mail: sridhariyer1983@gmail.com.

doi: 10.11601/ijates.v5i3.221

power consumption is challenging.

In this work, we compare the power efficiency of OFDM and MLR based networks. We propose and formulate a mixed integer linear program (MILP) model that minimizes power consumption of a specific network with *a-priori* traffic requests. The traffic is assumed to be deterministic (static) specified by a traffic matrix containing forecasted mean traffic between various source-destination (*s-d*) pairs. It must be noted that for the comparisons, we have not considered the single line rate (SLR) based networks, as existing studies have already established that under most traffic load values, the MLR networks are power-efficient compared to the SLR networks [2, 8, 9].

Rest of the paper is structured as follows: In Section II, we detail the problem formulation and the power model used in the study. Section III presents and discusses the various obtained simulation results. Finally, in Section IV, we conclude the study.

II. Problem Formulation

A. MILP Model

In this sub-section we detail the developed MILP mathematical model for power-optimization in an OFDM-based optical network, which is as follows:

Input parameters:

$G(V,E)$: Network topology comprising of a set of *V* nodes and a set of *E* links;

$T=[\Lambda_{s-d}]$: Matrix consisting of the traffic having the total Gbps requests of Λ_{s-d} between an *s-d* pair;

R: Rate for an individual subcarrier;

C_{TP}: Transponder power cost (fixed);

C_S: Individual subcarrier cost (fixed);

C_A: In-line amplifier cost;

A_{mn}: On a fiber, the amplifier numbers over the link with nodes *m* and *n*. For a span distance *L* = 80 km between adjacent amplifiers (EDFAs), the amount of EDFAs for the link of a fiber is given as $A_{mn}=[L_{mn}/L-1]+2$; where,

L_{mn} denotes length of span of the fiber between *m* and *n*.

C_p: Power cost of electronic processing (per Gbps) cost i.e., cost of Optical-Electrical-Optical (OEO) conversion.

W: Maximum amount(s) of the wavelength(s) on a link $\lambda \in \{1, 2, ...W\}$;

l_{mn}: Link (physical) between *m* and *n*;

P_{mn}: Lightpath(s) set passing through the link l_{mn}.

Variables:

$L_{ij\lambda}$: Variable (binary) referring to lightpath(s) number(s) over wavelength λ over link *i- j*;

T_{ij}^{sd}: Variable (integer) referring to the traffic volume from *s* to *d* routed over link *i- j*.

OF_{mn}: Variable (integer) referring to the number of optical fibers over a physical link (*m, n*).

D_j: Variable (integer) which denotes the data amount that is carried by the lightpaths ending at node *j*.

$S_{ij\lambda}^{k}$: Variable (binary) denoting whether k^{th} subcarrier in wavelength λ is utilized over the path between nodes *i- j*.

Problem formulation:

Minimize overall network power which is mathematically given as follows:

$$\sum_{\lambda}\sum_{ij}\sum_{k} S_{ij\lambda}^{k}\cdot C_s+\sum_{\lambda}\sum_{ij} T_{ij\lambda}\cdot C_{TP}+\sum_{m,n} C_A\cdot A_{mn}\cdot OF_{mn} +\sum_{j} D_j\cdot C_p \quad (1)$$

The objective function in (1) consists of power due to the (i) BVTs, which in turn consists of a variable and a fixed power consumption (detailed in sub-section *2.2*), (ii) fiber amplifiers in the network, and (ii) electronic processing used for setting up the multi-hop connections. Further, the objective function in (1) is constrained by

(i) the capacity constraint requiring the amount of subcarriers which are set up over the total wavelengths on a path to support the flow of aggregate traffic on that route, given as

$$R\sum_{\lambda}\sum_{k} S_{ij\lambda}^{k} \geq \sum_{s,d} T_{ij}^{sd} \quad \forall(i,j) \quad (2)$$

$$\sum_{\lambda}\sum_{k} S_{ij\lambda}^{k} \leq W \quad \forall(i,j,k) \quad (3)$$

(i) the constraint to avoid wavelength clash, given as

$$\sum_{i,j\in P_{mn}} X_{ij\lambda} \leq OF_{mn} \quad \forall(m,n),\forall\lambda \quad (4)$$

(ii) the conservation of traffic flow on each path, given as

$$\sum_{i} T_{ij}^{sd}-\sum_{i} T_{ji}^{sd}=\begin{cases}\Lambda_{sd} & \text{for } s=j\\ -\Lambda_{sd} & \text{for } d=j\\ 0 & \text{otherwise}\end{cases} \quad \forall(i,j)\forall(s,d) \quad (5)$$

(iii) the total of flows ending at node *j* i.e., sum traffic at every node requiring electronic processing, given as

$$E_j=\sum_{s,d}\sum_{i} T_{ij}^{sd} \quad \forall i\neq s,\forall j\neq d \quad (6)$$

(iv) the constraints which signify whether, at least, there occurs utilization of one subcarrier for specific path *i-j* and wavelength λ, which results in lightpath liting up for that specific path-wavelength combination, given as

$$L_{ij\lambda} \geq \frac{\sum_{k} S_{ij\lambda}^{k}}{M} \quad \forall i,j,\lambda \quad (7)$$

$$L_{ij\lambda} \leq S_{ij\lambda}^{k} \quad \forall i,j,\lambda \quad (8)$$

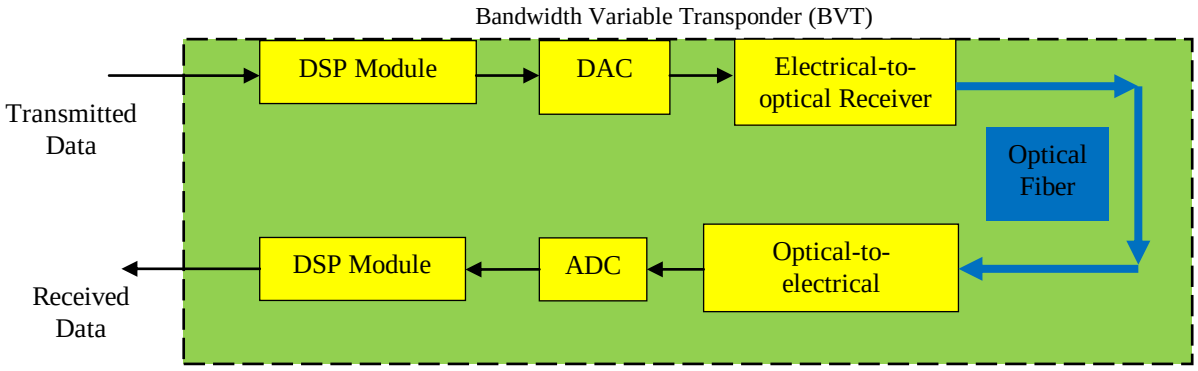

Fig.1. Architecture of a Bandwidth Variable Transponder.

B. *Power Model*

In our study, as shown in (1), the BVT power model consists of a (i) variable (dynamic) part, depending on the subcarrier(s) number(s) allocated for every lightpath, and (ii) fixed (static) part, accounting for power of the transponder.

Further, fixed part of the BVT is the major power consumer, whereas, variable part of the BVT alters with the accommodation of flexible bandwidth when various subcarrier(s) number(s) are modulated at the appropriate level(s). The BVT model of our study, shown in Fig. 1, consists of (i) two digital signal processing (DSP) modules, (ii) one digital-to-analog (DAC) module, (iii) one analog-to-digital convertors (ADC) module, and (iv) optical transmitters and receivers i.e., optical-to-electrical (transmitters) and electrical-to-optical (receivers) modules.

According to the studies in [10-13], the power consumed by BVTs supporting a maximum bandwidth of 100 Gbps can be gauged by utilizing the power consumption values of the following modules: (i) DSP: approximately 50-70 W, (ii) DAC/ADC, and (iii) optical transmitters and receivers. From the studies in [10, 11], the variable power consumption of a BVT is: 180 mW/Gbps of the bandwidth, approximately. Hence, as per the combined figures from [10-13], the aggregate power consumed by a BVT supporting a maximum bandwidth of 100 Gbps is approximately in the 120-140 W range. Further, the power consumed by the 10/40/100 Gbps transponders is 40 W, 100 W, and 210 W [14-16], respectively.

In our simulations, we have compared the MLR and OFDM based networks with a BVT power consumption which is fixed, and is given by the following equation

$$P_{BVT} = P_{DSP} + P_{ADC} + P_{DAC}, \quad (9)$$

Hence, from (9), we obtain the BVT power consumption with fixed values of 120 W, 140 W, and 160 W. Further, we also use a value of 192 W which is chosen so that the aggregate network power consumption can be compared for the case when, a 100 Gbps transponder and a BVT with utmost 100 Gbps bandwidth, incur the same power consumption. The aforementioned implies that power consumption of the BVT for the operation at 100 Gbps is $[(192)\times(180\,mW\times 100)] = 210W$. The normalized consumed power values are hence summarized in Table I.

TABLE I NORMALIZED POWER COST OF VARIOUS COMPONENTS.

Component	Normalized Power Cost			
	10 Gbps	40 Gbps	100 Gbps	OFDM
Transponder	1	2.7	5.8	M + 0.005*x*, where M = 3.5,3.8, 4.1, 5.3 *x* = bandwidth in Gbps
Amplifier	0.25 per fiber [8]			
OEO Processing	0.5*x*, where *x* = bandwidth in Gbps [8]			

It must be noted that the power consumption values of BVTs are as per the recently available data, and also, to the best of our knowledge, BVTs for long distance optical communication are not yet commercialized. Hence, in our study, we assume a BVT with utmost power consumption, which at full load, provisions the same power consumption as a single carrier transponder at the same bandwidth. The aforementioned assumption exploits the ability of BVT's power consumption adjustment with bandwidth, which corresponds to the variable part of the consumed power. Therefore, as an example, to support a demand of 40 Gbps, (i) as a worst case scenario, a 100 Gbps BVT as per our values has $[5.3+(0.005\times 40)] = 5.5\,units$ of normalized power consumption (see Table 1), whereas (ii) for the case of a single carrier, a 100 Gbps transponder incurs $5.5\,units$. We intend to capture the aforementioned particular scenario in our study.

III. SIMULATION RESULTS AND DISCUSSION

The formulated MILP is solved for the NSFnet backbone network topology shown in Fig. 2 and its corresponding traffic demand matrix shown in Table II [1]. To model traffic loads with higher values, the base traffic matrix mentioned Table II is scaled by appropriate constant values.

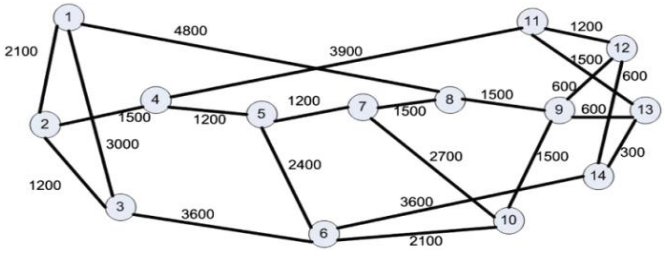

Fig.2. NSFNet topology (link lengths in km).

TABLE II TRAFFIC MATRIX FOR NSFNET NETWORK (EACH ENTRY IN GBPS).

Node	1	2	3	4	5	6	7	8	9	10	11	12	13	14
1	0	2	1	1	1	4	1	1	2	1	1	1	1	1
2	2	0	2	1	8	2	1	5	3	5	1	5	1	4
3	1	2	0	2	3	2	11	20	5	2	1	1	1	2
4	1	1	2	0	1	1	2	1	2	2	1	2	1	2
5	1	8	3	1	0	3	3	7	3	3	1	5	2	5
6	4	2	2	1	3	0	2	1	2	2	1	1	1	2
7	1	1	11	2	3	2	0	9	4	20	1	8	1	4
8	1	5	20	1	7	1	9	0	27	7	2	3	2	4
9	2	3	5	2	3	2	4	27	0	75	2	9	3	1
10	1	5	2	2	3	2	20	7	75	0	1	1	2	1
11	1	1	1	1	1	1	1	2	2	1	0	2	1	61
12	1	5	1	2	5	1	8	3	9	1	2	0	1	81
13	1	1	1	1	2	1	1	2	3	2	1	1	0	2
14	1	4	2	2	5	2	4	4	1	1	61	81	2	0

The number of available wavelengths (W) is assumed to be 16 wavelengths per link, and 16-QAM modulation format is assumed for every subcarrier. The OEO (electronic) processing and EDFAs power consumptions are as specified in [8]. From the study in [17], it is known that with an overhead of less than 10% for the cyclic prefix, at 100 Gbps rate of data, the least size of FFT corresponds to 2048. Hence, with assumption of the use of a standard single-mode fiber (SSMF) and a 1000 km tolerance for chromatic dispersion, a 3.9 ns length of cyclic prefix is used in the simulations so as to achieve a 10 % symbol overhead comprising of overheads such as, training symbol, FEC, Ethernet, and phase-noise compensation. For the MLR based fixed-grid network, we use the MILP formulation from [8] to minimize the power consumption. Further, compared to a similar bandwidth OFDM signal, for the MLR based network, each 10/40/100 Gbps transponder has the same TR. For conducting the simulations, we have used the ILOG CPLEX on an Intel Core 2 Duo machine which has a 2.0 GHz processor with 4 GB memory and the Ubuntu operating system, with which, each run of the MILP takes approximately 1-2 hours.

Fig. 3 compares the normalized power cost for an OFDM and a MLR based network. It can be seen from the figure that for various load values, an OFDM based network is highly power efficient compared to a MLR based network. It is also seen that for high values of traffic load, compared to the MLR based network, the saving(s) in power increases for an OFDM based network since the spectral resources are less over-provisioned.

In Fig. 4, for various BVT(s) and MLR transponder power consumption values, the variation of aggregate normalized power cost with the traffic load is shown. It can be seen from the figure that, with the BVT fixed power costs till 160 W, for all traffic loads, OFDM is more power efficient compared to MLR. However, when BVT fixed power consumption is 192 W (i.e., when the OFDM BVT and the MLR transponder power consumptions are similar for a bandwidth of 100 Gbps), and the traffic load(s) is low (i.e. for 5 and 10 Tbps), OFDM based network is seen to be power inefficient compared to the MLR based network. However, as the traffic load increases, OFDM based network demonstrates more power efficiency even for similar maximum power consumption of the OFDM BVT and the MLR transponder.

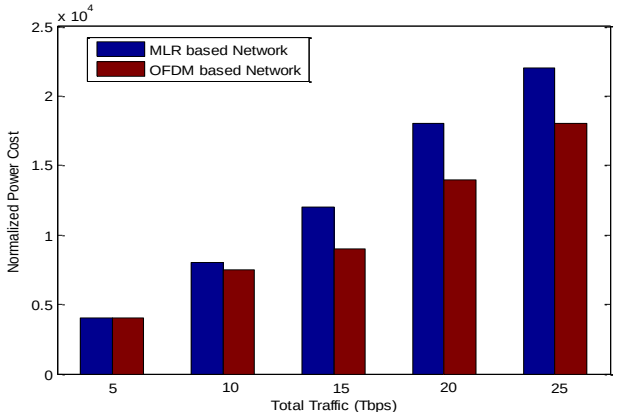

Fig.3. Comparison of normalized power cost for an OFDM and a MLR based network.

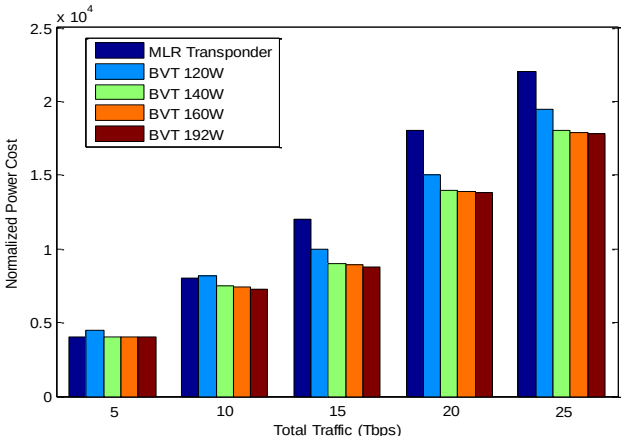

Fig.4. Aggregate normalized power cost versus transponder power consumption for an OFDM and a MLR based network.

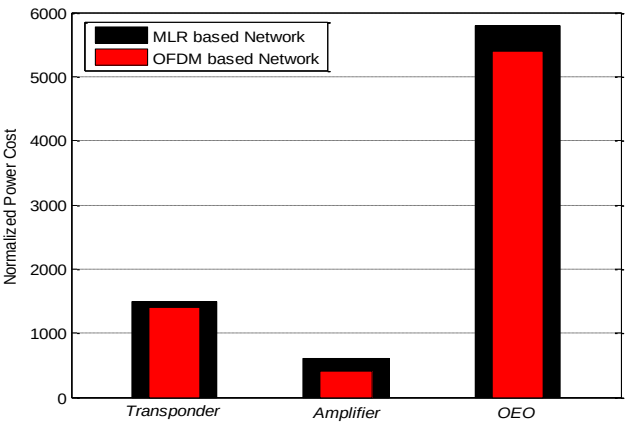

Fig.5. Normalized power cost for various components in an OFDM and a MLR based network for 20 Tbps traffic load.

In Fig. 5, we show the power consumed by various components when the total network traffic is 20 Tbps. From the figure it is seen the maximum network cost is incurred owing to the intermediate nodes of the *s–d* connections, whose establishment occurs over many i.e., multiple-hop lightpath(s) path(s), which requires OEO conversion (i.e. electronic processing). Also, compared to an MLR based network, owing to the higher spectral efficiency of OFDM based networks, the per fiber bandwidth packing is highly efficient, and hence, less power is exhausted on the BVTs and the EDFAs.

IV. CONCLUSION

In the current work, we conducted a power-efficiency comparison of an OFDM and a MLR based network for which, we formulated a MILP model with a specific mean traffic for every network source-destination pair. The simulation results show that in regard to power-efficiency, OFDM based network outperforms MLR based network.

It must be noted that the related planning problems using the MILPs are NP-hard, and hence, searching for the absolute optimums is time consuming. However, as an initial investigation, our primary focus in the current study has been to compare the power-efficiency in OFDM and MLR based networks. However, as a future work, we will aim to develop and use heuristic algorithms for power-efficiency comparison in fixed- and flexi-grid networks.

REFERENCES

[1] A. Nag, M. Tornatore, and B. Mukherjee, "Optical network design with mixed line rates and multiple modulation formats," *IEEE/OSA Journal of Lightwave Technology*, vol. 28, no. 4, pp. 466–475, Feb. 2010.

[2] S.P. Singh, S. Sengar, R. Bajpai, and S. Iyer, "Next- Generation Variable-Line-Rate Optical WDM Networks: Issues and Challenges", *Journal of Optical Communication, De Gruyter*, vol. 34, no. 1, pp. 331–350, 2013.

[3] M. Jinno, B. Kozicki, H. Takara, A. Watanabe, Y. Sone, T. Tanaka, and A. Hirano, "Distance-adaptive spectrum resource allocation in spectrum-sliced elastic optical path network", *IEEE Communications Magazine*, vol. 48, no. 8, pp. 138-145, 2009.

[4] Jinno, M., Takara, H., Kozicki, B., Tsukishima, Y., Sone, Y., Matsuoka, S.: 'Spectrum-efficient and scalable elastic optical path network: Architecture, benefits, and enabling technologies', *IEEE Communications Magazine*, vol. 47, no. 11, pp. 66–73, 2009.

[5] O. Gerstel, M. Jinno, A. Lord, S.J. Yoo, "Elastic Optical Networking: A New Dawn for the Optical Layer", *IEEE Communications Magazine*, vol. 50, no. 2, pp. S12-S20, 2012.

[6] A. Napoli *et al*. "Next Generation Elastic Optical Networks: The Vision of the European Research Project IDEALIST", *IEEE Communications Magazine*, vol. 53, no. 2, pp. 152-162, 2015.

[7] H. Khodakarami, B. Gopalakrishna Pillai, B. Sedighi, and W. Shieh, "Flexible optical networks: An energy efficiency perspective", *IEEE/OSA Journal of Lightwave Technology*, vol. 32, no. 21, pp. 3356–3367, 2014.

[8] P. Chowdhury, M. Tornatore, A. Nag, E. Ip, T. Wang, and B. Mukherjee, "On the design of energy-efficient Mixed-Line-Rate (MLR) optical networks," *IEEE/OSA Journal of Lightwave Technology*, vol. 30, no. 1, pp. 130–139, Jan. 2012.

[9] S. Iyer, and S.P. Singh, "Spectral and Power-Efficiency Investigation in Single and Multi-Line-Rate Optical Wavelength Division Multiplexed (WDM) Networks", *Photonic Network Communication*, Springer (Online First), 2016. Available: http://link.springer.com/article/10.1007/s11107-016- 0618-3

[10] R. Tucker, "Green optical communications—Part I: Energy limitations in transport", *IEEE Journal on Selected Topics in Quantum Electronics*, vol. 17, no. 2, pp. 245–260, 2011.

[11] R. Bouziane *et al*. "Design studies for an ASIC implementation of an optical OFDM transceiver", in *Proc. of IEEE ECOC*, pp. 1–3, 2010.

[12] I. Dedic, "High-speed CMOS DSP and data converters", in *Proc. Conference on Optical Fiber Communication, collocated National Fiber Optic Engineers Conference (OFC/NFOEC) , Workshop, Transmission Subsystems and Network Elements*, Paper OTuN1, 2011.

[13] I. Dedic, "56Gs/s ADC enabling 100GbE", in *Proc. Conference on Optical Fiber Communication, collocated National Fiber Optic Engineers Conference (OFC/NFOEC)*, pp.1–3, 2010.

[14] F. Idzikowski, "Power consumption of network elements in IP over WDM networks", *Tech. Rep.*, TU Berlin, Germany, 2009.

[15] Transmode TM-series data sheet. 2016. Available: http://www.transmode.com/.

[16] IDEALIST Project. Elastic Optical Network Architecture: Reference scenario, cost and planning. Deliverable D1.1. 2013. Available:http://cordis.europa.eu/docs/projects/cnect/9/317999/080/deliverables/001-D11ElasticOpticalNetworkArchitecture.doc.

[17] S. Jansen, I. Morita, K. Forozesh, S. Randel, D. van den Borne, and H. Tanaka, "Optical OFDM, a hype or is it for real?", in *Proc. IEEE ECOC*, pp. 49–52, 2008.

Sridhar Iyer received the B.E. degree in Electronics and Telecommunications Engineering from Don Bosco Institute of Technology, University of Mumbai, India in 2005, M.S degree in Electrical and Communication Engineering from Klipsch school of Electrical and Computer Engineering, New Mexico State University, Las Cruces, New Mexico, U.S.A in 2008, and the Ph.D. degree from Delhi University, India in 2017. He worked as an Assistant Professor in the Department of ECE, NIIT University, India between 2012-2014, and in Christ University, Faculty of Engineering, Department of ECE, India between 2014-2016. Currently he is an Associate Professor in the Department of ECE, Jain College of Engineering, India. His major area of research is efficient design of fixed-grid and flexi-grid optical networks.

A Novel Application of CWMP: An Operator-grade Management Platform for IoT

Martin Stusek, Pavel Masek, Krystof Zeman, Jiri Pokorny, Dominik Kovac, Petr Cika, and Franz Kröpfl

***Abstract*—The aggressive expansion of emerging smart devices connected to the Internet infrastructure is nowadays considered as one of the most challenging components of the Internet of Things (IoT) vision. As a particular segment of IoT, the smart home gateways, also named Machine-Type Communication Gateway (MTCG), become an important direction for industry including telecommunication operators. In most cases, the MTCG acts as a bridge between connected smart objects and the public network (Internet). As a consequence of the IoT domain expansion, the separate configuration of each individual Machine-to-Machine (M2M) device is not feasible anymore due to steadily growing numbers of M2M nodes. To perform this task, several novel technologies have recently been introduced. However, legacy protocols and mechanisms for remote network management still retain a certain application potential for IoT. Accordingly, we have investigated the protocol TR-069 with a particular focus on its usability for MTCG. To this end, the software module (bundle) based on the TR-069 for remote configuration and management of MTCG, as well as for controlling the end smart devices, has been developed. We believe that our implementation (available as open source on GitHub) can serve as an important building block for efficient management of future IoT devices. Therefore, TR-069 protocol constitutes a proven and standardized technology and could be easily deployed by most of the network and service providers today. Authors would like to recall that this paper represents extended version of their previously published work at TSP 2016 conference.**

***Keywords*—M2M, MTCG, OSGi framework, TR-069, Remote management**

I. Introduction

Today, Internet of Things (IoT) offers efficient means for interconnection of highly heterogeneous entities and networks, thus bringing a variety of communication patterns, including Human-to-Human (H2H), Human-to-Machine (H2M), and Machine-to-Machine (M2M) communications. IoT in general empowers the industry to develop new technology in unprecedentedly large numbers. New findings from the leading telecommunication players, such as Juniper [1] and Cisco [2], reveal that global retail revenue from smart wearable devices (as one of the IoT segments) will triple by 2016, therefore reaching $53.2 billion by 2019, as compared to the $4.5 billion at the end of 2015. The market over the following five years is expected to be substantially driven by the sales of smart devices, named MTCD (Machine-type Communication Devices) – an important component of this group is represented by smart home gateways, also known as MTCG (Machine-type Communication Gateway) [3], [4].

Presently, the MTCGs become more intelligent and provide new functions for smart data collection and visualization on end-user interfaces. In the light of the recent development in the IoT domain, the MTCG is capable of offering much more than conventional local networking features inside residential buildings [5]. Many devices acting as MTCD, that is, based on different communication technologies (IEEE 802.15.1, 6LoWPAN, ZigBee, Wireless M-BUS, etc.), are currently employing MTCG as an aggregation node providing access to the public network (Internet) [6], [7]. Inspired by these developments, we have recently introduced the concept of multi-purpose Smart Home Gateway (SH-GW) within our outgoing project under the title SyMPHOnY [8].

In this work, we aim at enabling remote configuration for devices in the role of SH-GWs by continuing our line of research [9]. Despite the fact that IoT is changing the conventional communication paradigm in many ways [10], some principles are remaining unchanged; therefore, many legacy technologies can be applied to IoT as well. Following this thinking, we have been investigating the protocol TR-069, well-known by network operators to maintain the Customer Premises Equipment (CPE), as a promising candidate for remote configuration of the IoT nodes, see Fig.1 and Fig.2 where the number of installed TR-069-enabled CPE is shown – with respect to device type and region. To this end, we have developed a SH-GW demonstrator, where the TR-069 is implemented as an extension of OSGi frameworks which are commonly used as the primary middleware layer for smart home gateways shipped by telecommunication operators. In other words, by using the TR-069 on MTCGs, service providers and telecom operators are able to manage and control not only the gateway but also the devices behind (e.g., energy meters, motion sensors, etc.) [11]. This important use case raises many research questions related to the configuration of various devices sets, the remote access capabilities, as well as the choice of cryptographic mechanisms used for data transmission. In this extended version of our previous work [9], we have focused our attention to address most of these issues. Namely, the description of (i) procedures and requirements, and (ii) application logic while using the TR-069 protocol in created setup is given in detail.

The rest of this paper is organized as follows. Section II is devoted to describing the operation principles of TR-069 protocol. Further, in Section III, a detailed description of our developed software implementation for OSGi frameworks together with a practical scenario accounting for all mentioned issues are offered. Finally, the lessons learned during our system development are summarized in the concluding

Manuscript received September 17, 2016; revised December 21, 2016.

M. Stusek, P. Masek, K. Zeman, J. Pokorny, D. Kovac, and P. Cika are with Department of Telecommunications, Brno University of Technology, Brno, Czech Republic (e-mails: martinstusek@phd.feec.vutbr.cz, masekpavel@feec.vutbr.cz, krystof.zeman@phd.feec.vutbr.cz, pokorny.jiri@phd.feec.vutbr.cz, kovacd@feec.vutbr.cz, cika@feec.vutbr.cz).

F. Kröpfl is with Telekom Austria Group, Austria (e-mail: Franz.Kroepfl@telekomaustria.com).

The described research was supported by the National Sustainability Program under grant LO1401. For the research, infrastructure of the SIX Center was used. Authors would like to thank to Telekom Austria Group for access to SIP infrastructure and insight into M2M and its real-life usage.

Section IV.

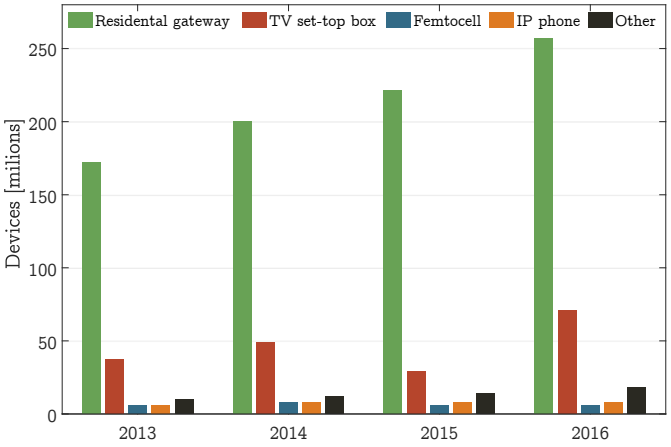

Fig. 1: Number of installed TR-069-enabled CPE by type.

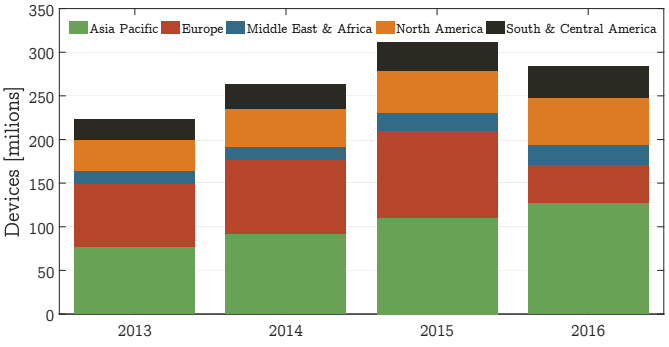

Fig. 2: Number of installed TR-069-enabled CPE by region.

II. Remote Network Configuration Using TR-069

As mentioned in the introduction, the need for remote configuration and management of network nodes brings new challenges to the IoT domain. Fueled by large numbers of M2M devices, the service providers require to control all of the devices in efficient and centralized way. For this purpose, several application layer protocols for remote management of end-user devices have already been introduced by different working groups and standardization bodies [12]. As a well-known and widely used representative, the TR-069 protocol is often utilized by telecom operators [3]. In this section, the functional architecture blocks of TR-069 are described with the emphasis on future implementation as a bundle in OSGi framework.

A. Protocol Architecture

TR-069 represents a protocol for encrypted remote self-configuration of CPE from the side of ACS (Auto-Configuration Server). The overall architecture of TR-069 ecosystem is depicted in Fig. 3.

The key element of TR-069 protocol is ACS server that provides information to one or more CPE according to a number of criteria. This mechanism allows for offering a default set of parameters and, furthermore, introduces a possibility of adding

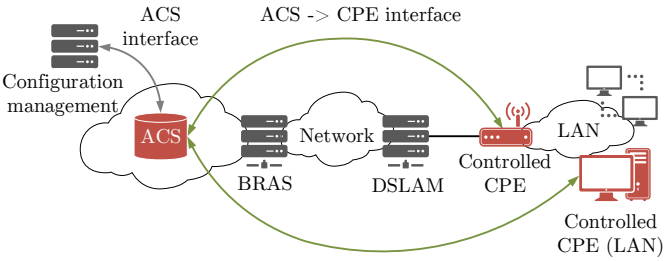

Fig. 3: Architecture of TR-069 ecosystem

new features according to the manufacturer's requirements. Parameters of the connected CPEs are available during the initial connection setup as well as the regular transmission as requests (e.g., providing information about CPE from ACS based on asynchronous, server-initialized[1] connection).

TABLE I: Protocol Layer Summary [12]

Protocol	Description
CPE/ACS Application	The application uses the CPE WAN management protocol for the CPE and ACS, respectively. It is defined locally but is not a part of the CPE WAN.
RPC Methods	The specific RPC methods are defined by the CPE WAN Management Protocol. This includes the definition of the CPE parameters accessible by the ACS using the parameter-related RPC methods.
SSL/TLS	Standard Internet transport layer security protocols – SSL 3.0 or TLS 1.0 are used.
SOAP	A standard XML-based syntax is used to encode remote procedure calls via the SOAP 1.1 protocol.
HTTP	Standard HTTP 1.1.
TCP/IP	Standard TCP/IP.

One of the most important tasks for remote configuration is to allow secure communication for sensitive data like e.g., encryption keys. TR-069 provides tools to download new software / firmware from the ACS server using digital signatures – to verify the integrity of downloaded files at the side of CPE [13]. Further, TR-069 defines a set of parameters that can be used for connection / service diagnostics [12].

1) Protocol Components: The TR-069 protocol architecture includes several unique components comparing to other *dedicated* IoT management protocols (e.g., the RPC (Remote Procedures Calling), see Section II-A3). In addition, TR-069 uses standard protocols, such as SOAP (Simple Object Access Protocol), HTTP (Hypertext Transfer Protocol), SSL / TLS (Secure Sockets Layer / Transport Layer Security), and TCP / IP (Transmission Control Protocol / Internet Protocol) [12]. The overview of complementary protocols acting on different layers is given in Table I.

On top of the supported protocols, TR-069 defines several device types, where each device may be described by a data model containing information about the parameters and

[1]In TR-069 terminology, the connection is called server-initialized, even though the communication is started at the CPE side. This is due to the fact that there is a need for appropriate connection setup of the CPE devices residing in local network where Network Address Translation (NAT) is used.

provided functions for a selected device. Supported TR-069 data models are shown in Table II (highlighted rows stand for the data models implemented in this work).

TABLE II: Data Models [14]

Data model	Compliant device
TR-064 and TR-133	LAN CPE devices
TR-068 and TR-124	Gateway modems
TR-098	Internet gateway device data model for TR-069
TR-104	Provisioning parameters for VoIP CPE
TR-106	Data model template for TR-069-enabled devices
TR-110	Reference model for VoIP configuration
TR-111	Applying TR-069 to remote management of home networking
TR-122	ATA devices
TR-126	Triple-Play QoE (Quality of Experience) requirements
TR-128 and WT-123	TR-069 testing support
TR-131	ACS Northbound interface requirements
TR-135	Data model for a TR-069 enabled STB
TR 140	TR-069 data model for storage service-enabled devices
TR-142	Framework for TR-069-enabled Passive Optical Network (PON) devices
TR-143	Enabling network throughput performance tests and statistical monitoring
TR-157	Component objects for CWMP (UPnP/DLNA device support)
TR-181	Device data model for TR-069
TR-196	Femto access point service data model

2) Security Mechanisms: The TR-069 protocol is designed to ensure the adequate level of security. Therefore, it includes methods for protection against manipulation during the transactions between the ACS server and the end-device (CPE). Further, the security algorithms using multiple levels of authentication are implemented by means of SSL/TLS for communication between the ACS and the CPE [12].

3) Architectural Components: The RPC defines a list of parameters and methods that have to be included at the end-device (CPE) in order to construct and send the TR-069 requests. In the following text, a summary of the most important components is given [12]:

- **Parameters** – RPC method specification defines a generic mechanism allowing the ACS server to read or write parameters for the CPE configuration, and to monitor CPE status and statistics. Each parameter has a name-value structure. The name identifies a particular parameter and has a hierarchical structure similar to the conventional directory listing ones (each level is separated by "." (dot)). The value of a parameter may be one of several defined data types.
- **File Transfers** – In TR-069, the mechanism enabling file download or (optionally) upload is implemented in order to perform tasks, e.g., CPE firmware upgrade or download of vendor-specific configuration files. When the session between ACS and CPE is initiated, the data transmission is performed utilizing HTTP or (preferably) HTTPS. Other protocols, including FTP and TFTP, are supported as well, but used less frequently.
- **CPE Connection Notifications** – TR-069 defines a mechanism allowing CPE to notify the corresponding ACS about various conditions – to ensure that the frequency of CPE-ACS communication remains optimal.
- **Asynchronous ACS-Initiated Notifications** – An important aspect of auto-configuration service is the ability of the ACS server to notify the remote CPE about configuration changes asynchronously. It allows the auto-configuration mechanism to be utilized for services requiring real-time management of the CPE.

4) Procedures and requirements: Protocol TR-069 defines required procedures which are necessary for (i) finding ACS, (ii) establishing a connection or (iii) creating of a session.

- **Finding ACS** – Following methods can be used to get the address of the server:
  - (i) Using DNS (Domain Name System) to get the IP address of the server from URL (Uniform Resource Locator) which is located in CPE.
  - (ii) It is possible to use the part of IP model for automatic configuration, that means using DHCP (Dynamic Host Configuration Protocol) whose messages contain the URL of the server. After that, using the DNS gets the CPE IP address of the server.
  - (iii) CPE can contain a default ACS address which is used if no other URL is defined.
- **Establishing connection** – After successfully getting the address, the connection can be established by CPE or ACS. If NAT (Network Address Translation) is used, connection can be established only from CPE side.
  - Establishing connection from CPE: End device can establish connection anytime it knows the ACS address but it is mandatory to establish connection in these cases:
    - First connection of CPE into the network and first configuration.
    - Device startup.
    - After an interval defined in settings.
    - When a method requires it.
    - Change of ACS address.
    - After any change of parameters.

    To protect the auto-configuration server from congestion, every CPE has a defined maximum value of messages informing the server of parameter changes.
  - Establishing connection from ACS: In this case it can be accomplished with mechanism of announcement of connection request. This parameter is mandatory on CPE side and recommended on ACS side. Establishing a connection from side of the server is possible only when the CPE address is public. In other case only the client can establish a connection.
- **RPC message requirements** – List of methods which are defined in the layer of remote call is shown in Table III.
- **Session management** – All sessions must start with an information message from CPE that contains an initialization HTTP message. That serves for setting up com-

TABLE III: RPC message requirements

Method name	CPE side	ACS side
CPE methods	Answers	Call
GetRPCMethods	Mandatory	Optional
SetParameterValues	Mandatory	Mandatory
GetParameterValues	Mandatory	Mandatory
GetParameterNames	Mandatory	Mandatory
SetParameterAttributes	Mandatory	Optional
GetParameterAttributes	Mandatory	Optional
AddObject	Mandatory	Optional
DeleteObject	Mandatory	Optional
Reboot	Mandatory	Optional
Download	Mandatory	Mandatory
Upload	Optional	Optional
FactoryReset	Optional	Optional
GetQueuedTransfers	Optional	Optional
ScheduleInform	Optional	Optional
SetVouchers	Optional	Optional
GetOptions	Optional	Optional
Server methods	Call	Answers
GetRPCMethods	Optional	Mandatory
Inform	Mandatory	Mandatory
TransferComplete	Mandatory	Mandatory
RequestDownload	Optional	Optional
Kicked	Mandatory	Optional

munication limits and coding at client's side. A session is terminated if server or client do not have to send any more requests or answers to a request. There can be only one existing session at a time. Both, ACS and CPE must handle session (initialization, incoming/outgoing requests, session termination) according to TR-069 standard. In text below set of basic session commitments required by TR-069 is given.

- CPE - Session Initiation: CPE can initialize a session only in case parameters available through its interface are locked. The reason is to protect parameters from change from a different source. This lock can remain active until the end of the session.
- CPE - Incoming requests: End device responds to requests in order in which they have been received. To prevent a deadlock, CPE does not wait for confirmation of previous request from server before it sends another request.
- CPE - Outgoing requests: When CPE has some requests for the server, it may send them in any order with respect to responses being sent from CPE to ACS.
- CPE - Session Termination: Client has to terminate a session when the following conditions are met:
  1) Server has no other requests.
  2) CPE has no other requests.
  3) Client received all unfinished requests from the server.
  4) Client sent all requests to ACS.

  CPE must terminate a session if it has not received any answer from the server in more than 30 seconds. If these conditions are not met, client must continue the session. In case of unexpected session termination, session initiation must start from the beginning.
- ACS - Session Initiation: After receiving the initial Inform request from CPE, the server must respond with the Inform response.
- ACS - Outgoing requests: When the server has requests to send, it may send them with respect to responses sent by ACS to CPE. If the ACS has more than one request to send or there are responses left to send, the ACS must send at least one request or response to CPE. Empty HTTP response is only allowed if ACS has no more requests or no responses to send.
- ACS - Session Termination: If the connection has been established by CPE, then it is also responsible for the session termination. ACS may consider to terminate the session when all the following conditions are met:
  1) CPE has no more requests.
  2) ACS has no more requests.
  3) CPE has sent all remaining responses to ACS.
  4) ACS has received all remaining requests from CPE.

  If the above conditions have not been met and ACS has not received any response from CPE in the past 30 seconds, ACS may consider to terminate the session.

III. Our Implemented Solution

To increase the impact of our recent research [8], [15] and as well as to extend it, we have developed the *TR-069 bundle* as an universal software package for any OSGi framework [15]. In case of this particular work, we have tested this bundle together with the OSGi Knopflerfish framework [16]. The motivation to focus on the OSGi platforms follows from the fact that today's MTCGs are mostly built with pre-configured operating systems, wherever OSGi framework is used [8]. Further in this section, the key parts of the created TR-069 bundle are described.

A. Application Logic

Remote configuration of the network node consists of two building blocks: (i) ACS server and (ii) TR-069 client; the application logic is depicted in Fig. 5. Our solution is based on an open source implementation of ACS called GenieACS [17], which combines modern technologies including Mongo DB, Node.js, and Redis server. Proposed TR-069 client follows the communication logic from modus TR-069 project – originally developed in Orange Labs [21]. Modus TR-069 implements the OSGi standards [19], [20] and uses the Knopflerfish framework as a runtime environment. Comparison of available TR-069 clients is shown in Table IV. In modus TR-069 architecture, each TR-069 RPC method is implemented as a separated bundle, see Fig. 4. This approach brings modularity into implementation of the TR-069 RPC methods –

new method can be easily added as new bundle. Further, bundle must import *RPC Method Mng Service* which serves as interface between bundle and *TR69 Client API*. Mentioned TR69 Client API bundle is used as a core part of the system and enables communication between bundles and external applications. Except *RPC Method Mng Service*, modus TR-069 contains following key elements:

- **OSGi Bundle** – this service allows modus TR-069 to control (install/uninstall or start/stop) other bundles launched within OSGi framework.
- **Data Model Bundle** – defines data model used in communication between ACS and CPE. In this work, TR-106 model (Internet Gateway Device) takes place.
- **File Persist Bundle** – stores obtained configuration data into system memory for subsequent use.
- **Server Com Bundle** – this service acts as a server which controls all communication (initialization, maintaining, etc.) between ACS and CPE. Also, bundle provides FTP, TFTP and HTTP service for file downloading over the TR-069 protocol.

TABLE IV: Comparison of TR-069 CWMP client implementations [18]

	RPC CPE metody	EasyCwmp	netcwmp	freecwmp	cwmpclient	open-tr069	modus-tr069
Mandatory	GetRPCMethods						
	SetParameterValues						
	GetParameterValues						
	SetParameterAttributes						
	GetParameterAttributes						
	GetParameterNames						
	AddObject						
	DeleteObject						
	Reboot						
	Download						
Optional	FactoryReset						
	ScheduleInform						
	Upload						
	GetQueuedTransfers						
	SetVouchers						
	GetOptions						

Further, obtained data is processed and visualized by the following packages: (i) Item, (ii) Core, (iii) TR069 Parser, and (iv) WebConsole.

B. Communication Logic

The application data structure is defined in *Item bundle*, see Fig. 5. This package is utilized only as a library without its own activator defining standard format of messages exchanged between the bundles. For this reason, it is necessary to import this package in each bundle communicating with Core one. As a provider of Items service (register all available items, e.g., smart meters), *Core bundle* is used. Each item is addressed by the serial number as the unique device identifier. The selected data structure, the ConcurrentHashMap, guarantees thread-save access. On the top of it, Core bundle must be started as first since it acts as an activator and control process for all others.

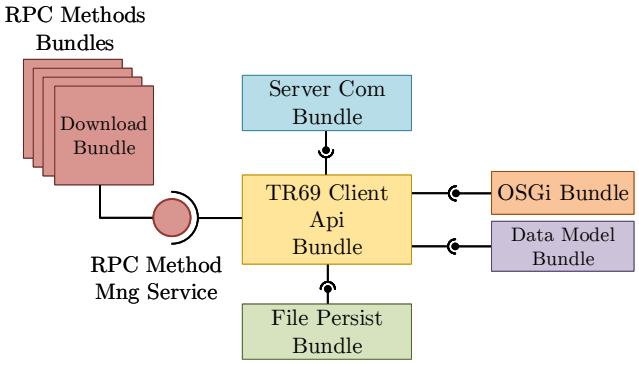

Fig. 4: Modus TR-069 Architecture

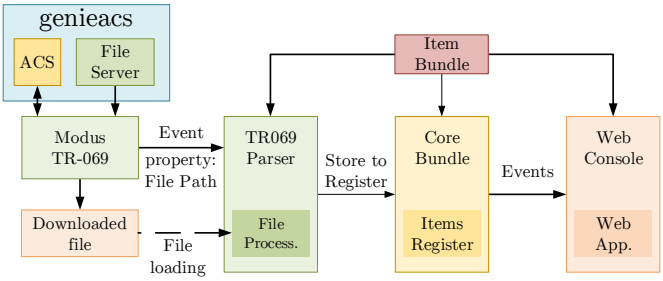

Fig. 5: Location of entities in case of using TR-069 protocol.

The main advantage of using the described model is the possibility to add new bundles (packages) to OSGi framework without the need to modify the source code in Core bundle. The only condition to be fulfilled for a new bundle is an import of Items service. This logic provides a possibility for the one way communication between all bundles and Core bundle. To resolve this issue, we have used OSGi Event Admin service allowing the backward communication between Core bundle and other packages. In this case, Core bundle is used as a source of the OSGi events that other packages are listening to, see Fig. 6. Individual events are distinguished with a dedicated array called *event topic*. Payload of each event starts by word *property* which contains one or more Item objects.

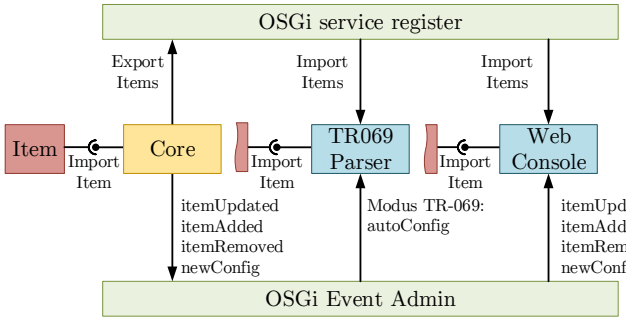

Fig. 6: Communication between Core bundle and other bundles within the OSGi Knopflerfish framework.

C. TR-069 Parser

Device configuration is carried out by the received configuration file processing – file structures may differ based on

the agreed terms between ACS and CPE(s). Therefore, it is not necessary to know the file structure during its download phase, but on the other hand, it is crucial to be aware of such structure when processing on MTCG. This method is a default option for remote configuration of the network devices for telecommunication operators – we have performed the test of our solution in cooperation with Telekom Austria Group (TAG) company.

Since client of Modus TR-069 was not developed for direct cooperation with other systems, it was necessary to modify it to make the cooperation possible. Once the new configuration file has been downloaded, the TR-069 creates an event, which contains the path to this new configuration. The bundle TR069 Parser listens for this event and processes the downloaded configuration file and loads the configuration into the system.

The implemented TR-069 communication procedure is shown in Fig. 7. TR-069 protocol is used for the new configuration file notification – represented in TR-069 terminology by TR-069 configuration files and defined by number '3' as FileType array. Developed TR-069 client allows to use HTTP or FTP as transport protocol. Further, downloaded file is processed by *TR-069 Parser bundle*. Note that in this phase of the development, it supports neither secure connection nor authentication to the ACS required by some telecom providers.

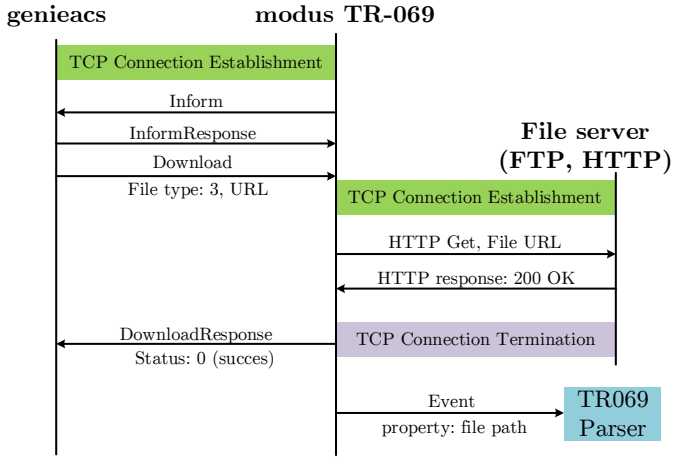

Fig. 7: Obtaining configuration file using implemented TR-069 protocol.

D. Tested scenario

Proposed scenarios were tested in the first phase within created local communication network. Further, the real communication infrastructure provided by Telekom Austria Group was used. Client side was realized by IP router NEC RGG200LV (based on the ARM (Acorn RISC Machine) architecture) with implemented JAVA OSGi framework – equipped with modus TR-069 client and our created application. CPE logic implementation was devoted from root node called InternetGatewayDevice, defined in TR-098 data model. Rest of the parameters used at the side of CPE were defined in DeviceInfo node, namely: (i) Manufacturer, (ii) SerialNumber, (iii) SoftwareVersion, and (iv) HardwareVersion.

First part of *configuration update* consists from file upload to ACS server. In this step, the CPE which will receive configuration update could be defined together by the parameters mentioned in previous paragraph (as an unique identifier for target (specific) device or for whole group of devices with same parameters). After successful file upload, ACS server sends notification update (Download procedure) for selected devices. These devices parse incoming message and create second communication channel to file server. In our particular scenario, unencrypted HTTP application protocol was used for data transfers. Content of transferred file is independent on TR-069 protocol. In this work, JSON (JavaScript Object Notation) file is used. File structure is considered in (i) core section of created application, and (ii) in TR069 Parser bundle.

E. Console Output

In some cases, it is not possible to display the list of running events in the system console (e.g., when OSGi framework runs as a daemon in the background). Therefore, we have created a specialized *WebConsole bundle* working as a web service and displaying system events in a web console. Communication between the bundle and the web service is realized by WebSocket protocol which is an elementary part of HTML 5. WebConsole bundle operates as OSGi EventHandler listening to all OSGi events utilized within the SyMPHOnY project, see Fig. 5. Each event is processed and the payload part is sent to the web services, and, finally displayed, see Fig. 8 where communication between ACS and CPE is shown.

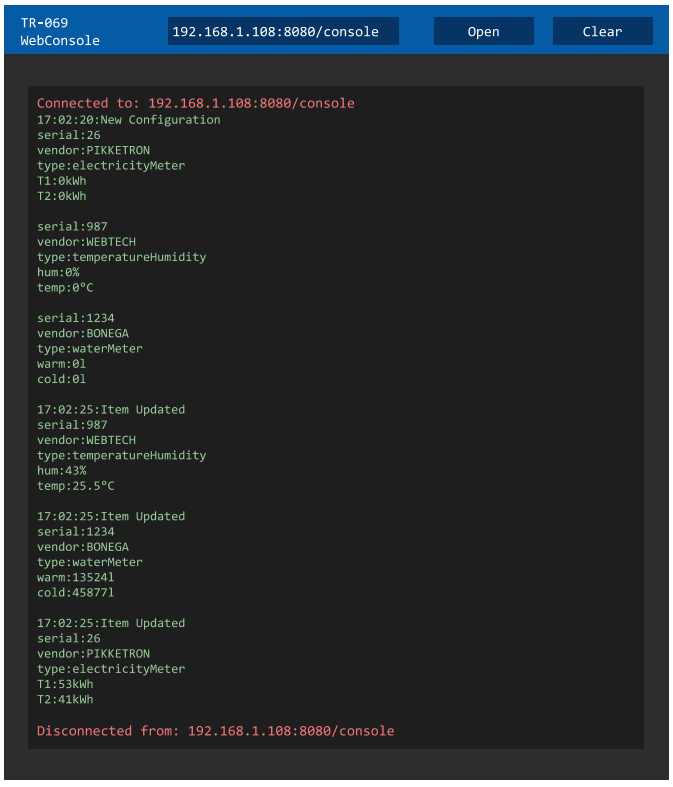

Fig. 8: Console output of captured communication between ACS and CPE.

IV. Concluding Thoughts

Within the proposed logic for the remote configuration of IoT devices acting as MTCG (and MTCD devices connected to MTCG), our implementation of TR-069 protocol has demonstrated the functionality of communication between the ACS server and the end-device (CPE) in a real network.

We have successfully tested the developed solution in cooperation with Telekom Austria Group. As we aimed our solution to be universal for various types of MTCG devices, we have constructed TR-069 bundle to be compliant with the well-known OSGi frameworks. As mentioned in Section III-C, the developed TR-069 implementation in its current version does not support secure connection and authentication to the ACS. Therefore, as a next step, we are planning to implement this functionality in our TR-069 bundle.

Our main and most essential learning while working with the TR-069 protocol is such that the structure of the configuration file is not static. Following the specifics of the concrete mobile network (ACS server configuration), the configuration files may differ. In our trial, we have utilized the JSON structure [22] implemented in live A1 cellular network.

At the end of this paper, we recall that this manuscript represents extended version of our previous work – originally presented at TSP 2016 conference [9].

References

[1] M. S. Whitcup and K. LaMattina, *Juniper What is Inhibiting Growth in the Medical Device Wearable Market?* Available from: http://bit.ly/1Dfffbf, September 2014.

[2] Cisco, *Cisco Visual Networking Index: Global Mobile Data Traffic Forecast Update, 2014-2019*, February 2015.

[3] P. Masek, J. Hosek, D. Kovac, F. Kropfl, *M2M Gateway: The Centrepiece of Future Home.* in Proc. of 6th International Congress on Ultra Modern Telecommunications and Control Systems and Workshops (ICUMT). St. Petersburg, Russia. pp. 286–293. 2014.

[4] M. Gerasimenko, V. Petrov, O. Galinina, S. Andreev, Y. Koucheryavy, *Energy and delay analysis of LTE-advanced RACH performance under MTC overload.* Globecom Workshops (GC Wkshps), IEEE. pp. 1632–1637. 2012.

[5] P. Masek, K. Zeman, Z. Kuder, J. Hosek, S. Andreev, R. Fujdiak, F. Kropfl, *Wireless M-BUS: An Attractive M2M Technology for 5G-Grade Home Automation.* in Proc. of EAI International Conference on CYber physiCaL systems, iOt and sensors Networks (CYCLONE). pp. 1–12. ISBN: 978-1-4673-9282-2. 2015.

[6] N. Himayat, S.-P. Yeh, A. Y Panah, S. Talwar, M. Gerasimenko, S. Andreev, Y. Koucheryavy, *Multi-radio heterogeneous networks: Architectures and performance.* in Proc. of International Conference on Computing, Networking and Communications (ICNC). pp. 252–258. 2014.

[7] O. Galinina, S. Andreev, M. Gerasimenko, Y. Koucheryavy, N. Himayat, S.-P. Yeh, S. Talwar, *Capturing spatial randomness of heterogeneous cellular/WLAN deployments with dynamic traffic.* Journal on Selected Areas in Communications. vol. 32. issue 6. pp. 1083–1099. 2014.

[8] GitHub: SyMPHOnY (Smart Multi-Purpose Home Gateway). Available from: https://github.com/SyMPHOnY-/Smart-Home-Gateway/wiki/

[9] M. Stusek, P. Masek, D. Kovac, A. Ometov, J. Hosek, F. Kropfl, S. Andreev, *Remote Management of Inteligent Devices: Using TR-069 Protocol in IoT.* in Proc. of the 39th International Conference on Telecommunication and Signal Processing, TSP 2016. Vienna, Austria. pp. 1–5. ISBN: 978-1-5090-1287-9. 2016.

[10] A. Ometov, S. Andreev, A. Turlikov, Y. Koucheryavy, *Characterizing the effect of packet losses in current WLAN Deployments.* in Proc. of 13th International Conference on ITS Telecommunications (ITST). pp. 331–336. IEEE. 2013.

[11] S. Andreev, P. Gonchukov, N. Himayat, Y. Koucheryavy, A. Turlikov, *Energy efficient communications for future broadband cellular networks.* Computer Communications, Volume 35, Issue 14, pp. 1662–1671. 2012.

[12] J. Bernstein, T. Spets, *CPE WAN Management Protocol.* DSL Forum, Tech. Rep. TR-069. 2004.

[13] D. Dasgupta, S. Saha, A. Negatu, *Techniques for validation and controlled execution of processes, codes and data: A survey,* in Proc. of International Conference on Security and Cryptography (SECRYPT). pp. 1–9. 2010.

[14] Incognito, *Broadband Forum TR-069 standards support.* [online]. Available from: http://bit.ly/1OdCsjM/

[15] M. Stusek, J. Hosek, D. Kovac, P. Masek, P. Cika, J. Masek, F. Kropfl, *Performance Analysis of the OSGi-based IoT Frameworks on Restricted Devices as Enablers for Connected-Home.* in Proc. of 7th International Congress on Ultra Modern Telecommunications and Control Systems and Workshops (ICUMT). Brno, Czech Republic. pp. 211–216. ISBN: 978-1-4673-9282-2. 2015.

[16] Knopflerfish, *Open Source OSGi SDK.* [Online]. Available from: http://www.knopflerfish.org/

[17] GenieACS, *Smart, fast TR-069 ACS.* [online]. Available from: https://genieacs.com/

[18] A. Stack. TR-069 cwmp client implementation: open sources comparison. In: *Stackoverflow* [online]. 2014. Available from: http://bit.ly/1PTzzWS

[19] OSGi, *OSGi Alliance.* [Online]. Available from: http://www.osgi.org/

[20] R. Hall, K. Pauls, S. McCulloch, D. Savage, *OSGi in action: creating modular applications in Java.* Greenwich [Conn.]: Manning. 548 p. ISBN: 19-339-8891-6. 2012.

[21] France Telecom, *Modus TR069.* [online]. Available from: http://modus-tr-069.sourceforge.net/

[22] A. Greenspan, L. Cameron, *Monetize the Internet of Things: JSON turns a flood of data into business actions and results.* 2015 [online]. Available from: http://bit.ly/1He09Vu/

ISSN 1805-5443